UNIVERZITA KARLOVA
PŘÍRODOVĚDECKÁ FAKULTA
KATEDRA BUNĚČNÉ BIOLOGIE

Biologie
Buněčná a vývojová biologie - Fyziologie buňky


Bc. Anna Nováková

# Horizontal transfer of mitochondria and its role in carcinogenesis

# Horizontální transfer mitochondrií a jeho význam v karcinogenezi

Diplomová práce

Vedoucí práce/Školitel: Prof. Ing. Jiří Neužil, CSc.

Praha 2019

Prohlášení:
Prohlašuji, že jsem tuto diplomovou práci zpracovala samostatně pod vedením prof. Jiřího Neužila a že jsem uvedla všechny použité informační zdroje a literaturu. Tato práce ani její podstatná část nebyla předložena k získání jiného nebo stejného akademického titulu.

V Praze, dne

Podpis: . . . . . .

## Poděkování

Ráda bych poděkovala prof. Ing. Jiřímu Neužilovi, CSc. za příležitost být součástí jeho laboratoře a podílet se na fascinujícím výzkumu stejně jako za trpělivost při vedení mé diplomové práce. Za odborné vedení mé práce, nekonečnou trpělivost, velkou pomoc a psychickou podporu bych také chtěla poděkovat Jaromíře Kovářové, Ph.D. Za jedinečnou pomoc při zpracování výsledků i revizi práce patří můj dík také RNDr. Soně Hubáčkové, PhD. a Mgr. Zuzaně Nahácké. Mgr. Marii Olšinové, PhD. a Mgr. Markétě Dalecké z IMCF Biocev děkuji za odbornou pomoc při experimentech a následném zpracování dat.

Za cenné rady, pomoc a skvělou atmosféru na pracovišti děkuji všem členům kolektivu Laboratoře molekulární terapie Biotechnologického ústavu AV ČR.

Velký dík patří hlavně mému manželovi, dceři a mé rodině za psychickou i finanční podporu po čas studia vysoké školy i ve zbytku života.

# Abstract

Mitochondria are essential organelles as they produce most ATP to support cellular activities, synthesize critical metabolic factors and are involved in lipid and phospholipid metabolism as well as calcium signalling. The oxidative phosphorylation (OXPHOS) system, present at the inner mitochondrial membrane, plays role in regulation of cellular metabolism and survival of cancer cells. Recent studies show importance of OXPHOS in growth of cancer cells via regulation of the *de novo* pyrimidine synthesis pathway. Dihydroorotate dehydrogenase (DHODH), a flavoprotein localized in the inner mitochondrial membrane, converts dihydroorotate (DHO) to orotate within the *de novo* pyrimidine synthesis pathway, generating electrons that are transferred, via redox-cycling of ubiquinone, to complex III (CIII) of respiratory chain. Since DHODH is functionally linked to CIII activity, impairment of respiration results in reduced activity of DHODH and pyrimidine synthesis. Therefore, mitochondrial damage or mutation in mitochondrial DNA (mtDNA) leads to decreased respiration, cancer cell proliferation and delay of tumour growth.

As a compensation for damaged mitochondria, horizontal transfer of functional mitochondria from donor somatic cells to the mitochondria-damaged tumour cells was demonstrated. This mitochondrial renewal leads to tumour progression dependent on respiration recovery. *In vivo* transfer of mitochondria from donor cells to mtDNA-damaged tumour cells has been described in mouse models of melanoma and mammary tumours. It can be mediated by different mechanisms including extracellular microvesicles, cytoplasmic fusion or gap junctions. Another mechanism, described *in vitro* on the model of 4T1 breast cancer cells and B16 melanoma cells, is to transfer mitochondria through highly sensitive *de novo* formed nanotube structures between cells, representing complex networks described as tunnelling nanotubes (TNT).

Using tumour cells with depleted mitochondria (rho0 cells) this work confirmed the essential role of mitochondrial transfer from donor cells in respiration recovery and tumour formation initiation. This work also clarifies the role of TNTs in the horizontal mitochondrial transfer as well as the properties of such way of transfer.



**Key words:** cancer, cancer metabolism, mitochondria, dihydroorotate dehydrogenase, mitochondrial transfer, tunnelling nanotubes

# Abstrakt

Mitochondrie jsou buněčné organely, které produkují většinu ATP nutného pro správné fungování řady dějů v buňce. Syntetizují důležité metabolické faktory a podílejí se na metabolismu lipidů a fosfolipidů, stejně jako na signalizaci vápníku. Systém oxidační fosforylace (OXPHOS), lokalizovaný na vnitřní mitochondriální membráně, hraje klíčovou roli v regulaci buněčného metabolismu a přežití nádorových buněk. Nedávné studie dokazují význam systému OXPHOS při růstu nádorových buněk prostřednictvím jeho propojení s *de novo* syntézou pyrimidinů.

Enzym dihydroorotátdehydrogenáza (DHODH), flavoprotein lokalizovaný ve vnitřní mitochondriální membráně, přeměňuje dihydroorotát (DHO) na orotát v rámci *de novo* pyrimidinové syntézy. Tímto způsobem jsou generovány elektrony, které se přenášejí prostřednictvím oxidačně-redukčního koloběhu ubichinonu na komplex III (CIII) dýchacího řetězce. DHODH je tedy funkčně spojena s aktivitou CIII, a proto snížení schopnosti buněčné respirace vede ke snížení aktivity DHODH a snížené syntéze pyrimidinů. Poškození mitochondrií nebo mutace v mitochondriální DNA (mtDNA) mají proto za následek sníženou schopnost respirace, snižuje se také proliferace nádorových buněk a dochází ke zpoždění růstu nádoru.

Nedávno byl však prokázán horizontální přenos funkčních mitochondrií z dárcovských somatických buněk do nádorových buněk s poškozenými mitochondriemi, ve kterých tak došlo k obnovení mitochondriálních funkcí. Tato obnova vede k progresi nádoru v závislosti na obnovení schopnosti buněčné respirace. *In vivo* byl přenos mitochondrií z dárcovských buněk do nádorových buněk s poškozenou mtDNA popsán na myších modelech melanomu a karcinomu prsu. Mitochondriální přenos může být zprostředkován různými mechanismy, včetně přenosu extracelulárních mikrovesikulů, cytoplazmatické fúze nebo mezerového spojení. Dalším mechanismem, popsaným *in vitro* na modelu buněk karcinomu prsu 4T1 a melanomových buněk B16, je přenos mitochondrií prostřednictvím vysoce citlivých nanotrubicových struktur tvořených de novo mezi buňkami, představujících komplexní sítě popsané jako tunelovací nanotrubice (TNT).

Za použití nádorových buněk s depletovanými mitochondriemi (rho0 buněk), potvrdila tato práce zásadní úlohu mitochondriálního přenosu z dárcovských buněk při obnově respirace a vzniku nádoru. Tato práce také objasňuje úlohu TNT v horizontálním mitochondriálním přenosu a některé vlastnosti takového způsobu přenosu.

**Klíčová slova:** rakovina, metabolismus rakovinných buněk, mitochondrie, mitochondriální přenos, dihydroorotátdehydrogenáza, spojovací nanovlákna

# Contents

# List of used abbreviations

| | |
|---|---|
| 2DG | 2-deoxyglucose |
| 6TG | 6-thioguanine |
| A549 | alveolar adenocarcinoma cell line |
| AcCoA | Acetyl Coenzym A |
| AMF | autocrine motility factor |
| AMPK | AMP-activated protein kinase |
| ANT | adenine nucleotide translocator |
| ASCT2/SN2 | glutamine transporter |
| ATP | adenosine triphosphate |
| B cell | B lymphocytes |
| BCA | bicinchoninic acid |
| BEAS-2B | human bronchial epithelial cell line |
| BFP | blue fluorescent protein |
| BMDC | bone marrow derived cells |
| Breg | regulatory B lymphocyte |
| CAD | carbamoyl-phosphate synthetase 2 |
| CAF | cancer associated fibroblast |
| CCL5 | chemokine ligand 5 |
| COPD | chronic obstructive pulmonary disease |
| CoQ | Coenzyme Q |
| CSF1 | colony-stimulating factor |
| CSF1R | colony-stimulating factor receptor |
| CT | computed tomography |
| CTVT | canine transmissible venereal tumour |
| Cx43 | connexin 43 |
| DHO | dihydroorotase |
| DHODH | dihydroorotate dehydrogenase |
| DMEM | Dulbecco's Modified \| Eagle's Medium |
| dMiro | Drosophila ortholog of Miro1 |
| DMSO | dimethyl sulfoxide |
| DNA | deoxyribonucleic acid |
| DP | double positive |
| EAA | essential amino acids |
| ECM | extracellular matrix |
| EDTA | ethylenediaminetetraacetic acid |
| EGF | epidermal growth factor |
| EGFR | epidermal growth factor receptor |
| EMT | epithelial mesenchymal transition |
| ER | endoplasmatic reticulum |
| ERK | extracellular signal-regulated kinases |
| EtBr | ethidium bromide |
| ETC | electrone transporting chain |
| F2,6P2 | fructose-2,6-bisphosphate |
| FBS | foetal bovine serum |
| FDG | 18F-fluorodeoxyglucose |
| GA | Golgi apparatus |
| GAPD | glyceraldehyde-3-phosphate dehydrogenase |
| GBM | glioblastoma multiforme |
| GFP | green fluorecent protein |
| GLS1 | glutaminase 1 |
| GLUT1 | glucose transporter 1 |
| GPI | glycosylphosphatidylinositol |
| H2052 | pleural sarcomatoid mesothelioma |
| hBMSC | human bone marrow cell line |
| HEK293 | human embryonic kidney cell line |
| HIF1 | hypoxia-inducible factor 1 |
| HK2 | hexokinase 2 |
| HMEC | primary mammary epithelial cell line |
| H-Meso | pleural biphasic mesothelioma cell line |
| HUVEC | umbilical vein endothelial cell line |
| IF | immunofluorescence |
| IF-gamma | interferon gamma |
| iPSC-MSC | human-induced pluripotent MSC |
| KC | Krebs cycle |
| KIF5 | kinesin-related protein 5 |
| LAT1 | neutral amino acid transporter |
| LDHA | lactate dehydrogenase A |
| LP9 | peritoneal mesothelial cell line |
| LSCC | lung squamous cell carcinoma cell line |
| MAE | malic enzyme |
| MAPK | mitogen-activated protein kinase |
| mBMSC | mouse bone marrow MSC |
| MCF-7 | breast cancer cell |
| MSC | mesenchymal stem cell |
| MCT4 | monocarboxylate transporter 4 |

| | |
|---|---|
| MDA-MB | breast cancer cell line |
| MDSC | myeloid-derived suppressor cells |
| Met5A | mesothelial cell line |
| Milton | motor-adaptor protein |
| MIP | maximal intensity projection |
| Miro1 | mitochondrial Rho GTPase 1 |
| Miro2 | mitochondrial Rho GTPase 2 |
| MSTO-211H | pleural biphasic mesothelioma cell line |
| MT | microtubule |
| mtDNA | mitochondrial DNA |
| mTOR | mammalian target of rapamycin |
| MVB | multivesicular body |
| NAD+/NADH | nicotinamide adenine dinucleotide |
| NGS | next generation sequencing |
| NK | natural killers |
| OMM | outer mitochondrial membrane |
| OVCAR-3 | human ovarian carcinoma cell line |
| OXPHOS | oxidative phosphorylation |
| PBS | phosphate-buffered saline |
| PC12 | rat pheochromocytoma cell line |
| PDMS | polydimethylsiloxane |
| PET | positron emission tomography |
| PFA | paraformaldehyde |
| PI3K | phosphatidylinositol-3-kinase |
| PKM2 | pyruvate kinase M2 |
| PLL | poly-L-lysine |
| PRPS2 | phosphoribosyl pyrophosphate synthetase 2 |
| rho0 (ρ0) | mtDNA depleted cells |
| RhoT1 | mitochondrial Rho GTPase 1 |
| ROS | reactive oxygen species |
| RPE | retinal pigment epithelium |
| RPTEC | primary renal proximal tubule epithelial cells |
| RT4 | bladder papilloma cell line |
| RTK | receptor tyrosine kinase |
| SKOV-3 | ovarian cancer cell line |
| STAT3 | signal transducer and activator of transcription 3 |
| STED | stimulated emission depletion |
| s.c. | subcutaneously |
| T cell | T lymphocyte |
| T24 | bladder carcinoma cell line |
| TAM | tumour associated macrophage |
| TAN | tumour associated neutrophile |
| TFAM | mitochondrial transcription factor A |
| Th | helper T lymphocyte |
| TME | tumour microenvironment |
| TNT | tunnelling nanotube |
| TOM20 | mitochondrial import receptor subunit |
| TPP | thiamine pyrophosphate |
| Trak1 | trafficking kinesin protein 1 |
| Trak2 | trafficking kinesin protein 2 |
| Treg | regulatory T lymphocyte |
| USI | ultrasonic Imaging |
| UV | ultraviolet |
| VADC | voltage-dependent anion channel |
| VAMT | pleural sarcomatoid mesothelioma cell line |
| VEGF | vascular Endothelial Growth Factor |

# 1. Introduction

## 1.1. Cancer metabolism

### 1.1.1. Deregulated cellular energetics as a hallmark of cancer

Cancer occurs as a result of uncontrolled proliferation of cell accompanied by many transcriptional, signalling and metabolic changes. Hanahan and Weinberg proposed ten hallmarks of cancer depicted in Figure 1.1, which help to understand the development of tumours and subsequent life strategy of cancer cells. Among others, one of the newly formulated hallmarks of cancer is the deregulation of cellular energetics. (Hanahan and Weinberg 2000, Hanahan and Weinberg 2011)

The uncontrollable growth and proliferation of cancer cells are characteristic and essential for all neoplastic diseases. These adjustments of life strategy of cancer cells require the changes in metabolism, to ensure enough fuel for emerging tumour. Nutrients that are used in catabolic processes to maintain cell viability, as well as in anabolic processes to create new biomass, are harvested by tumour cells from their surroundings. (Giampazolias and Tait 2016, Pavlova and Thompson 2016)

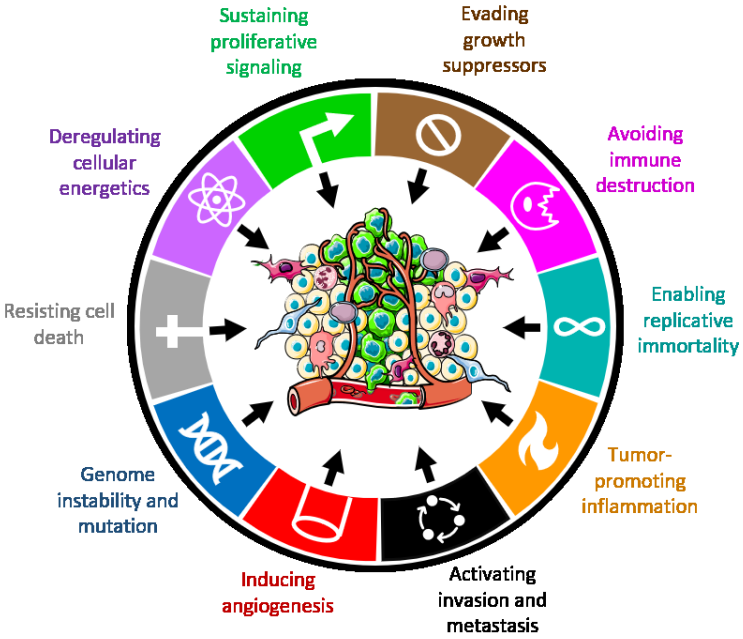


***FIGURE 1.1: A schematic representation of ten hallmarks of cancer.*** *(Hanahan and Weinberg 2011)*

For metabolism of differentiated tissues, at a standard oxygen level, the flow from glucose to pyruvate and from pyruvate to the final products ($CO_2$ and $H_2O$) is tightly

coupled. Under conditions of reduced oxygen supply, the lactate fermentation allows for reoxidation of NADH for glycolysis. In differentiated tissues the so-called Pasteur effect takes place, where fermentation is lower under aerobic and higher under anaerobic conditions. However, this effect is disturbed in tumour cells, where lactate production is high even in the presence of oxygen, and the coupling of glucose to pyruvate and pyruvate to final products generally declines.

These abnormalities in the cancer metabolism were characterized first almost a century ago by Otto Warburg. In his work he described that cancer cells use primarily aerobic glycolysis to generate energy. Thereby the cancer cells are able to reprogram their metabolism and to use the process of glycolysis to synthesize energy in the form of adenosine triphosphate (ATP) instead of oxidative phosphorylation, even in the presence of sufficient oxygen. On the basis of his discoveries, Otto Warburg formulated the hypothesis that the primary cause of the onset of neoplastic diseases should be mutations in mtDNA resulting in the replacement of respiration by aerobic glycolysis (Koppenol, Bounds and Dang 2011). This assumption is however valid rather under exceptional circumstances, when specific mitochondrial genes such as genes for succinate dehydrogenase or fumarate hydratase are mutated (Baysal et al. 2000, Tomlinson et al. 2002). Comparison of the efficiency of differentiated tissue metabolism and tumour tissue metabolism with respect to ATP production is represented in Figure 1.2.

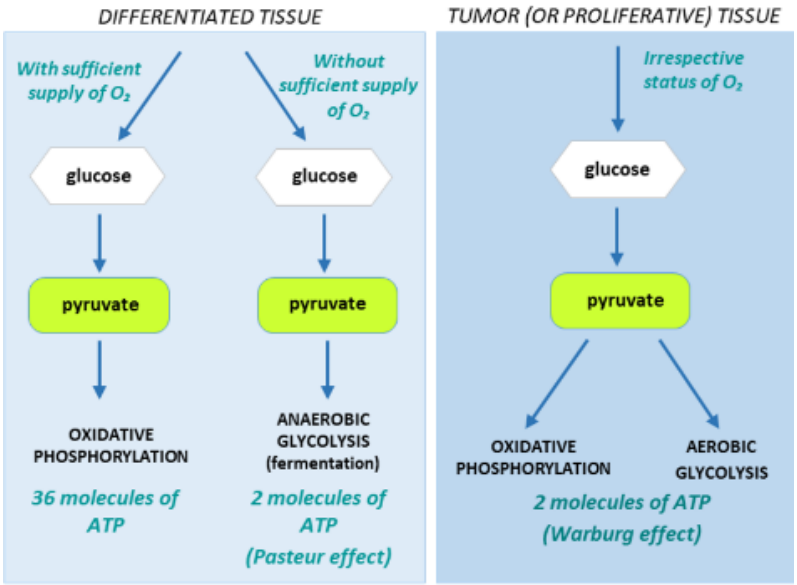


***FIGURE 1.2: Diagram of the efficiency of differentiated tissue metabolism compared to tumour tissue metabolism with respect to ATP production.*** *Figure adapted from Vander Heiden, Cantley and Thompson, 2009.*

The metabolism of glucose and glutamine in normal cells is very efficient. Primary end products ($CO_2$, $H_2O$, and ammonia) are generated while the maximum yield of ATP per mole of glucose or glutamine is achieved. On the other hand, the metabolism of glucose and glutamine in tumour cells is very uneconomical. The primary end products are apart from $CO_2$ and $H_2O$, also lactate, pyruvate, alanine, and aspartate and there is low yield of ATP per mole of glucose or glutamine achieved in cancer cells.

This evokes a question, why the ATP production through glycolysis should be more beneficial for cancer cells than eighteen times more efficient energy production through the process of oxidative phosphorylation. Reprogrammed cancer cells are able to divert the glycolytic metabolism intermediates into different synthetic pathways and thus be more effective in the production of a new biomass, i.e. in growth and proliferation. That's why "Warburgian metabolism" can be found in highly proliferating cells including embryonic stem cells (Vander Heiden, Cantley and Thompson 2009, Hsu and Sabatini 2008, Kondoh et al. 2007).

Due to anaerobic glycolysis, glucose uptake via glucose transporter GLUT1 in tumours is increased. This phenomenon is visualized and documented by non-invasive positron emission tomography (PET), which is used to diagnose the neoplastic diseases as well as to analyse the effectiveness of its treatment. PET involves in administering radioactive fluorine-labelled glucose analogue ($^{18}$F-fluorodeoxyglucose, FDG) to patients, and subsequent tomographic visualization of sites where glucose in the body is preferentially consumed and metabolized as shown in Figure 1.3 (Vander Heiden et al. 2009, Som et al. 1980, Almuhaideb, Papathanasiou and Bomanji 2011).

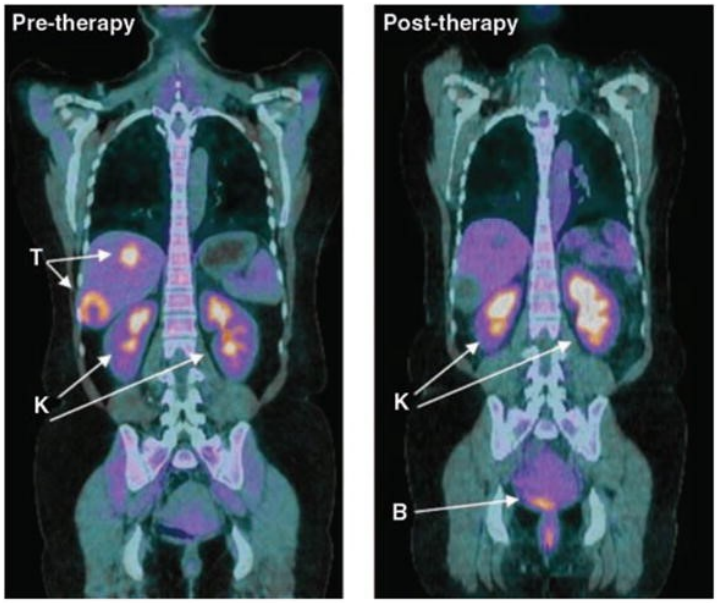


***FIGURE 1.3: Tumour visualized using positron emission tomography $^{18}$F-fluorodeoxyglucose.*** *Fused images of FDG-PET and computed tomography (CT) visualization of decreased metabolism of glucose in a patient with malignant sarcoma before and after therapy. Excess FDG is excreted in the urine, and therefore the kidneys (K) and bladder (B) are also visualized as labelled as well as the tumour (T) in the pre-therapy image [Image courtesy of A. D. Van den Abbeele, Dana-Farber Cancer Institute, Boston] (Vander Heiden et al. 2009).*

Cancer cells, due to their rapid proliferation, accumulate changes in metabolism to ensure a steady supply of nutrients. According to the work of Pavlova and Thompson, these changes can be divided into three groups shown in Figure 1.4, where the first group comprise changes affecting the nutrients uptake. Second and third group then represents re-programming of intracellular metabolism and long-term metabolite-directed changes leading to the changes in cell functions and their behaviour in tumour microenvironment, respectively (Pavlova and Thompson 2016).

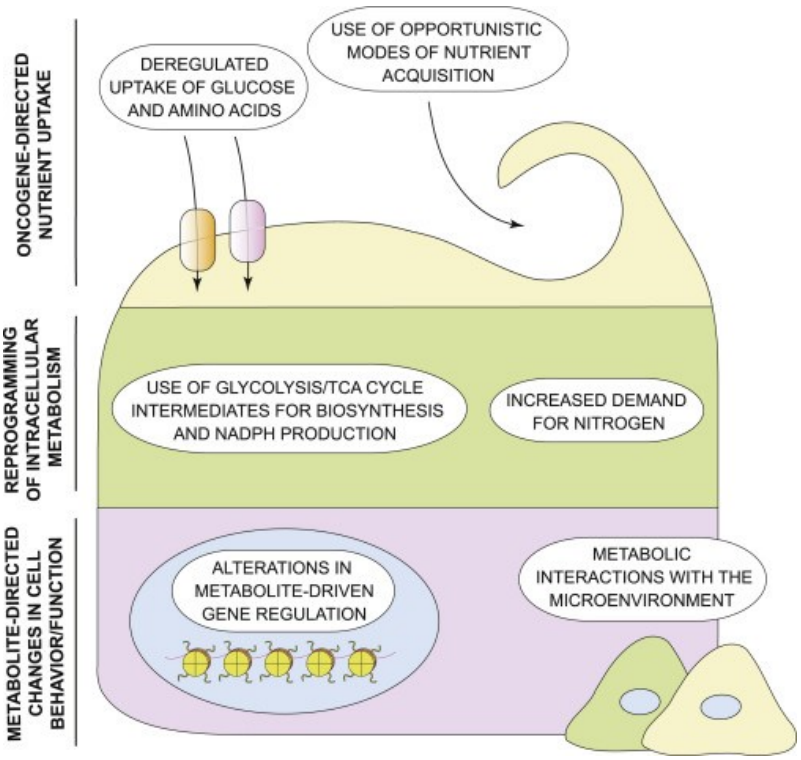


***FIGURE 1.4: Emerging hallmarks of cancer metabolism*** *(Pavlova and Thompson 2016).*

### 1.1.2. Nutrients uptake deregulations in cancer cells

As mentioned above, glucose and glutamine are two essential nutrients necessary for biosynthesis in mammalian cells. *In vivo*, within the progressive tumour growth, cancer cells are forced to deal with a lack of nutrients and oxygen induced by insufficient vascular supply to a growing tumour. Therefore, they have to reprogram themselves and increase glucose and glutamine uptake together with using the intermediates of glycolysis and the Krebs cycle (KC) for biosynthesis. In the absence of free amino acids, cancer cells are able to obtain them by micropinocytosis of extracellular proteins. Other possible ways of obtaining nutrients alternatively are living cell entosis or apoptotic body phagocytosis. The reprogramming of cancer cells takes place via the signalling of growth factors, which is directly affected by metabolism and secondary affects transcription and translation.

### 1.1.3. Multi-functional roles of glycolytic enzymes

Oncogenic signalization reprograms directly the enzymes of glycolysis. Hexokinase 2, which phosphorylates glucose in the first step of glycolysis and produces glucose-6-phosphate (G6P) was determined as a cancer's double-edged sword (Mathupala, Ko and Pedersen 2006). This enzyme is usually active only during embryonic

development and is reactivated in tumour cells. It is capable to extensively increase glycolysis partially by its localization on the mitochondrial membrane, where it transfers ATP from the inner space of mitochondria directly from voltage anion dependent channel (VADC). Thanks to its location in proximity with VADC and ANT, HK2 prevents access of pro-apoptotic proteins and formation of the mitochondrial transition pore, and thus prevents apoptosis (Pastorino, Shulga and Hoek 2002, Majewski et al. 2004, Rathmell et al. 2003, Pastorino and Hoek 2003, Danial et al. 2003).

The intracellular metabolic enzyme glucose-6-phosphate isomerase (GPI) becomes an extracellular signalling molecule during evolution. GPI expression is induced by cMyc and HIF-1 and is increased in many cancers (Pusapati et al. 2016, Semenza 2013, de Padua et al. 2017). In addition to its glycolytic function – isomerizing glucose-6-phosphate to fructose-6-phosphate intracellularly, it can also be secreted as autocrine motility factor (AMF). Upon binding to its receptor GPI, it affects the activity of the small GTPases Rac and Rho regulating the cytoskeleton assembly, which results in increased invasiveness of cancer cells (Gallardo-Pérez et al. 2014). GPI also directly and indirectly promotes angiogenesis in the tumour microenvironment and inhibits apoptosis via both MAPK and PI3K pathways (Yanagawa et al. 2004, Niinaka et al. 1998, Watanabe et al. 1996).

Enolase 1 (ENO1) converts 2-phosphoglycerate to phosphoenolpyruvate and plays a role as a plasminogen receptor. Plasmin activator anneals to the plasmin activator receptor, converting plasminogen to plasmin, which in turn activates matrix metalloproteases and various forms of growth factors (Subramanian and Miller 2000, Feo et al. 2000, Kumari and Malla 2015). This leads to increased motility and invasiveness of cancer cells. The expression of enolase is regulated at multiple levels – i.e. nuclear factor kappa B (NFκB) and hypoxia-inducible factor-1α (HIF-1α) are involved in the transcriptional activation of ENO1 and also activation of the Src and MEK/ERK signalling pathways upregulates the ENO1 expression. The possibility that other factors might regulate ENO1 expression during tumorigenesis remains to be investigated (Zhan et al. 2015).

Pyruvate kinase M2 (PKM2) is a less active isoform of the terminal glycolytic enzyme pyruvate kinase. Its expression is increased and facilitates lactate production in cancer cells. Modulation of PKM2 catalytic activity also regulates the synthesis of DNA and lipids that are required for cell proliferation, and of NADPH

that is required for redox homeostasis. (Ward and Thompson 2012, Li, Zheng and Lu 2016, Luo and Semenza 2012, Dong et al. 2016).

Glyceraldehyde phosphate dehydrogenase (GAPD) participates in the $NAD^+$/NADH balance in the cell and also participates in transcriptional regulation and in cell death via the SIAH1-GAPDH cascade. Its expression is highly dependent on the proliferative state of the cell and can also be regulated by transcription factors, such as HIF-1 and p53. When cancer cells resist apoptosis, the increased level of GAPDH inhibits cell death by simultaneously increasing ATP levels through glycolysis and stimulating autophagy-mediated clearance of permeabilized mitochondria. (Colell, Green and Ricci 2009)

(Dastoor and Dreyer 2001, Chuang, Hough and Senatorov 2005, Zheng, Roeder and Luo 2003). The enzyme lactate dehydrogenase plays key role in oxidation of NADH to $NAD^+$, while reducing pyruvate to lactate. Moreover, it is also involved in transcriptional regulation as a component of OCA-S a trans-activator complex of histone H2B, whose components are associated with cancer metastasis (Zheng et al. 2003).

### 1.1.4. Key mutations responsible for changing metabolism of cancer cells

To meet the requirements for rapid ATP formation, mutations of protooncogenes and tumour suppressor genes occur in cancer cells. The products of these mutations drive or regulate various signalling pathways and at least some of them act in mitochondria. In total, ~1.6% of the 22,000 functional genes in the human genome show recurrent somatic mutations in cancer (Futreal et al. 2004). Figure 1.5 depicts the scheme of connections between several metabolic pathways and key components of signalling pathways, that could be influenced or mutated within metabolic reprogramming in cancer cells.

#### Activation of protooncogenes

The most common events in the process of cancer cell transformation besides changes in p53 expression, include changes in ERK, PI3K or AMPK signalling cascades and p53 or Myc signalling pathways (Galluzzi et al. 2010).

The above-mentioned PI3K, Myc and HIF-1 proteins enhance the expression of glucose transporters and in addition with p53 increase the activity of enzymes that control the limiting steps of glycolysis – hexokinase (HK), phosphofructokinase, or lactate dehydrogenase (LDH). At the same time the association of HK with ANT and

VDAC attenuate the OXPHOS due the constitutive activation of PI3K-LKB1 pathway and inhibits ATP synthase by a sharp decrease in ADP levels that are consumed by substrate phosphorylation in glycolysis (Wallace 2005, Mathupala et al. 2006).

The mammalian target of rapamycin (mTOR) signalling pathway is activated in cancer cells to contribute to the metabolic turnover. It affects the biosynthesis of lipids and proteins, mRNA translation and ribosome biogenesis. Moreover, mTOR plays a role of important activator of HIF1, regulating the survival of cancer cells in hypoxic conditions (Guertin and Sabatini 2007, LoRusso 2016). AMPK, repressing the mTOR signalling, is often attenuated in cancer cells to avoid subsequent stress responses (Shackelford and Shaw 2009).

### Inactivation of p53

p53 is inactivated or mutated in more than half of neoplasms. The loss of p53 in tumour cells causes increased glycolysis, reduced pyruvate oxidation and decreased ATP production by oxidative phosphorylation. p53 inhibits aerobic glycolysis in several pathways (Liu et al. 2015). Interestingly, it has been reported that mutant p53 proteins and wild-type p53 proteins often regulate the same cellular biological processes with opposite effects. The wild-type p53 activity inhibits cytochrome oxidase and increases production of F2,6P2, which both result in inhibition of glycolysis (Zheng 2012, Maddocks and Vousden 2011). It also reduces pyruvate dehydrogenase (PDK2) kinase expression and thereby activates the pyruvate dehydrogenase complex, which reduces the requirement for ATP formation during glycolysis (Amelio and Melino 2015). On the other hand, mutant p53 promotes glycolysis through distinct mechanisms. It induces the mevalonate pathway, which participates in a regulation of lipids metabolism. Furthermore, the mutant p53 activates RhoA/ROCK signalling pathway that stimulates GLUT1 translocation to the plasmatic membrane and therefore increases glycolysis and supports the Warburg effect in cancer cells (Zhang et al. 2013b).

p53 has been extensively studied in last decades and many functions of wild-type p53, such as cell cycle arrest, apoptosis, and senescence have been discovered. However, some aspects of the role of mutant p53 in cancer metabolism regulation remain partly unclear as well as how different forms of mutant p53 impact upon tumour metabolism. Metabolic regulation of cancer cells via the p53 protein remains a highly dynamic area of research.

## Activation of HIF-1

HIF-1 is expressed in many types of neoplastic diseases mainly as a response to hypoxia in rapidly growing and poorly vascularized tumours. HIF-1 increases aerobic glycolysis and therefore supports the Warburg effect. Increased activity of HIF-1 induces the same effects as the loss of the p53 function, i.e. enhanced glycolysis and glucose uptake via increased expression of the GLUT1 transporter or decreased oxidation of pyruvate and ATP production in OXPHOS (Chan et al. 2011). HIF-1 increases expression of aldolase, enolase, PDK1 and PDK3 as well as the expression of LDHA and the lactate transporter MCT4, which is used as a marker of aerobic glycolysis in glycolytic cells (Kitajima and Miyazaki 2013, Kroemer and Pouyssegur 2008).

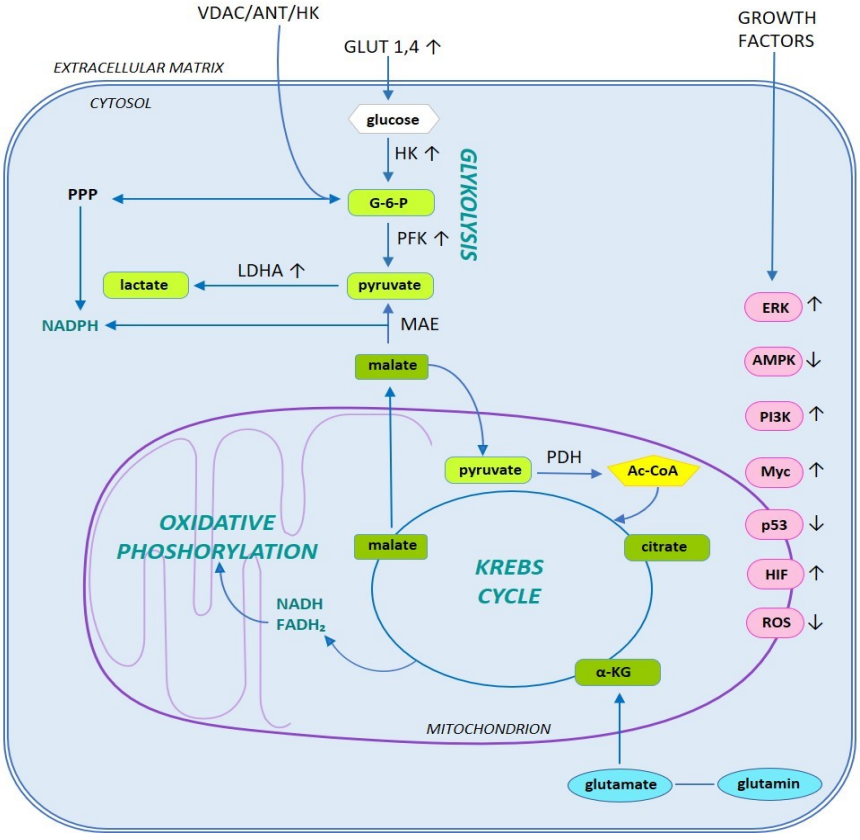


***FIGURE 1.5: Scheme of connection between several metabolic pathways and molecular mechanisms of cancer-specific metabolic reprogramming.***

*α-KG (α-ketoglutarate), AcCoA (acetyl coenzyme A), AMPK (AMP activated protein kinase), ANT (nucleotide transporter), ERK (extracellular signal-activated kinases), G-6-P (glucose-6-phosphate), GLUT1, GLUT4 (glucose transporters), HK (hexokinase), LDHA (lactate dehydrogenase A), MAE (malic enzyme), Myc (tumour suppressor, myelocytomatosis oncogene), p53 (tumour suppressor p53), HIF-1 (hypoxia-induced factor 1), PDH (pyruvate dehydrogenase), PDK (pyruvate dehydrogenase kinase), PFK (phosphofructokinase), PI3K (phosphatidylinositol-3-kinase), PPP (pentose phosphate pathway), ROS (reactive oxygen radicals), VDAC (voltage-mediated anion transporter).*

## 1.2. Role oxidative phosphorylation in cancer metabolism

Current advances in research of neoplastic diseases have improved our understanding of why metabolic reprogramming occurs in cancer cells. However, it is clear that one metabolic setting cannot be generalized to define the metabolism of all cells within the tumour. Therefore, functional mitochondria are indispensable for proliferation and survival of cancer cells (Jose, Bellance and Rossignol 2011).

According to recent results emphasizing the relevance of mitochondria and OXPHOS in the tumour microenvironment, mitochondria are able to drive the metabolic turnover, act on the immune system, affect proliferative potential and cell survival as well as influence the processes of angiogenesis and metastases (Galluzzi et al. 2010, Tan et al. 2015, Gentric, Mieulet and Mechta-Grigoriou 2017).

### 1.2.1. Mitochondria and oxidative phosphorylation

Mitochondria are double membrane organelles, that play a key role in a wide range of cellular processes from energy production and generation of reactive oxygen species, through regulation of biosynthetic pathways to cell death. There is a system of OXPHOS localized in the mitochondrial inner membrane (MIM), which is the principal feature of mitochondria. This system consists of an electron-transporting chain (ETC), which is composed of four complexes (CI-CIV) and linked the fifth complex - ATP synthase. In a multi-step process, within the four complexes of respiratory chain, electrons produced in the Krebs cycle utilize oxygen to water. During the gradual transfer of electrons to the final acceptor oxygen, an electrostatic and proton gradient is formed by means of the complexes (except from complex II) on the MIM. This gradient, also referred to as mitochondrial membrane potential ($\Delta\Psi m$, i), is the driving force of ATP synthase that produces ATP from ADP and inorganic phosphate. To produce ATP, the OXPHOS system must be linked to adenosine nucleotide translocases (ANT1-3 in mammals) and a phosphate transporter, that mediate the transfer of ATP / ADP and phosphates across the MIM.

The OXPHOS system is necessary for the production of ATP in non-proliferating post-mitotic somatic cells. Compared to proliferating cells having an active Krebs cycle, which is accompanied by efficient antioxidant defense to OXPHOS-derived ROS, non-proliferating cells have a higher level of respiration.

Proliferating cells, which include e.g. cells in the embryonic development as well as cancer cells, acquire a significant part of the necessary ATP from glycolysis, and therefore OXPHOS function is not as critical for them as for non-proliferating cells.

### 1.2.2. DHODH pathway

If nutrients such as aspartate or pyruvate become limiting, OXPHOS inhibition may also interfere with the anabolic pathways such as nucleotide synthesis. Pyrimidines are synthesized *de novo* from simple precursors in a six-step pathway, where the fourth and rate-limiting enzyme dihydroorotate dehydrogenase (DHODH) is localized in the MIM. *De novo* synthesis of pyrimidines is associated with respiration through the redox cycle of coenzyme Q. In this cycle, the oxidized form of coenzyme Q (CoQ) – ubiquinone is reduced to ubiquinol by electrons produced during conversion of dihydroorotate (DHO) to orotate by DHODH. Complex III then reoxidizes ubiquinol back to ubiquinone by transfer of electrons to cytochrome c. (Löffler et al. 2005). Functional respiration is therefore necessary for the activity of DHODH and pyrimidine synthesis.

Deleterious mutations in mtDNA lead to inhibition of tumour formation (Park et al. 2009). Tumour cells with depleted mtDNA (rho0 cells) have non-functional OXPHOS as a result of lack of the mitochondria-encoded subunits and inability to assemble the functional respiratory complexes. It was proven that these cells are able to restore the mitochondrial functions by transferring whole mitochondria from the stroma when injected into mice (Bajzikova et al. 2019, Dong et al. 2017, Tan et al. 2015). Bajzíková et. al show that DHODH-driven pyrimidine biosynthesis renewal after respiration recovery, rather than OXPHOS-mediated ATP production, is essential for initiation of tumorigenesis. Intriguingly, reactivation of CoQ redox-cycling alone the using alternative oxidase (AOX) as an acceptor of electrons from reduced CoQ, is sufficient to drive DHODH and to allow cancer cells to form tumours (Bajzikova et al. 2019). The comparison of the linkage of *de novo* pyrimidines synthesis to ETC is shown in Figure 1.6.

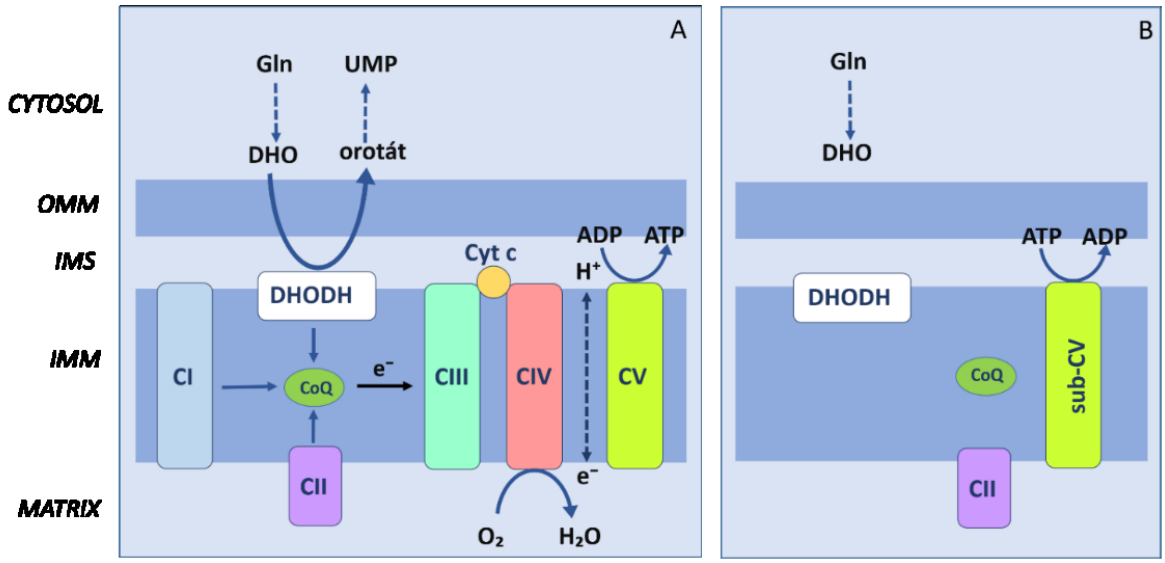


***FIGURE 1.6: Schematic representation of the linkage of de novo pyrimidines synthesis to ETC.*** *Parental cells with mtDNA (A), derived mtDNA depleted rho0 cells (B), adapted from Bajzikova et al., 2019.*

## 1.3. Tumour microenvironment (TME)

A tumour is a highly complex tissue with a wide variety of different cell types including supporting stromal cells, stem cells, immune cells and many others cell types, as is shown in Figure 1.7. The biology of tumours can no longer be understood simply by enumerating the traits of the cancer cells but must encompass the contributions of the "tumour microenvironment" for induction of tumorigenesis. (Hanahan and Weinberg 2011)

### 1.3.1. Stromal cells in the tumour microenvironment

#### Bone marrow-derived cells (BMDCs)

Tumour-associated macrophages (TAMs) are a prototype of bone marrow-derived cells (BMDCs), whose presence in the tumour microenvironment was found in most experimental mouse models of tumours as well as in human tumours and are connected with a poor prognosis (Qian and Pollard 2010, Pollard 2004, Bingle, Brown and Lewis 2002). Their role is mostly tumour-promoting, showing the ability to modify the behaviour of tumour cells. The bidirectional interaction between TAM and TME forms a response to conditions in a specific region of the tumour, for example, by accumulating TAM in hypoxic or necrotic areas due to the release of hypoxia-induced chemoattractants (Murdoch, Giannoudis and Lewis 2004, White et al. 2004, Mantovani et al. 2006). TAMs subsequently contribute to angiogenesis (Lin

et al. 2006, Zumsteg and Christofori 2009). Moreover, TAMs play an important role in invasiveness and migration of cancer cells (Condeelis and Pollard 2006), since TAMs produce the epidermal growth factor (EGF), thereby increasing the invasiveness and migration of EGF receptor expressing EGFR (EGFR) cancer cells. On the other hand, cancer cells expressing CSF1 acting on TAM that express CSF1R. Together it induces a paracrine loop-driven co-migration and invasion of both cell types towards blood vessels. (Lin et al. 2001, Achkova and Maher 2016, Dwyer, Greenland and Pixley 2017).

Adipocytes can participate in interactions with cancer cells in some types of tumours. For example in intra-abdominal tumours they support the growth of malignant cells through the transport of fatty acids, that promotes nutrient supply and actively help to recruit cancer cells through adipokine secretion (Vona-Davis and Gibson 2013, Nieman et al. 2011).

There is evidence of various tumour-promoting functions of tumour associated neutrophils (TANs) in the tumour microenvironment including promotion of growth of the primary tumours and angiogenesis or increasing of ECM degradation and enhanced development of circulating tumour cells (Hurt et al. 2017, Nozawa, Chiu and Hanahan 2006, De Larco, Wuertz and Furcht 2004, Erler et al. 2009). On the other hand, tumour-suppressing effects were described after immunological or cytokine activation (Hicks et al. 2006, Colombo et al. 1992).

Increased levels of inhibitory immune myeloid cell-derived suppressor cells (MDSCs) have been observed in various types of tumours in mice and humans. MDSCs are able to inhibit $CD8^+$ T lymphocytes, induce $T_{reg}$ lymphocytes or contribute to the formation of the TAM phenotype, which suggests their tumour-promoting potential (Sinha et al. 2007, Porta, Sica and Riboldi 2018).

### Tumour blood supply

The angiogenic signals produced by cancer and TME cells during hypoxia activates angiogenesis and stimulates branching of the blood vessels to form a new vascular supply for the tumour. The most important angiogenic factor produced by cancer cells is vascular endothelial growth factor (VEGF), but in higher stages of tumours it can be replaced by other angiogenic factors i.e. platelet-derived endothelial cell growth factor (PD-ECGF), transforming growth factor (TGF)-β, angiogenin and others (Pang and Poon 2006) . Tumour vasculature is almost always heterogeneous

and disordered. Vascular leakage increases the interstitial fluid pressure and irregular blood flow resulting in increased oxygenation and nutrient distribution in TME (Carmeliet and Jain 2011, Mittal, Ebos and Rini 2014).

Pericytes provide structural support to endothelial cells in blood vessels. Tumours with low occurrence of pericytes show a poor prognosis associated with higher tumour cell invasiveness and metastasis. Tumour vasculature coverage could therefore act as a key negative regulator of metastasis (Balkwill, Capasso and Hagemann 2012, Cooke et al. 2012).

### Cancer associated fibroblasts (CAFs)

Cancer associated fibroblasts (CAFs) may originate from multiple precursors i.e. smooth muscle cells, endothelial cells or MSCs. They produce a number of growth factors that are mitogenic for tumour cells, induce the epithelial-mesenchymal transition (EMT) and contribute to the immunosuppressive microenvironment by producing chemoattractants recruiting other types of stromal cells to the TME. Fibroblasts also contribute to the TME composition by their secretion of ECM components and ECM re-modelling enzymes (Balkwill et al. 2012, Erez et al. 2010, Farhood, Najafi and Mortezaee 2019).

### Cells of the immune system

Tumour-associated B lymphocytes are found primarily at the periphery of invasive tumours and lymph nodes adjacent to tumours (Sarvaria, Madrigal and Saudemont 2017). Regulatory B lymphocytes ($B_{reg}$) have been found to have tumour-promoting impact in some cancer types e.g. ovarian cancer, non-small lung carcinoma and cervical cancer (Schioppa et al. 2011, Olkhanud et al. 2011, Sarvaria et al. 2017). Some studies point to poor prognosis after the inhibition of cytotoxic T lymphocytes by B cells (Qin et al. 1998). However, in some types of breast (Coronella et al. 2001) or ovarian carcinomas (Milne et al. 2009) B cells infiltration into the tumour microenvironment is associated with a good prognosis

Infiltration with $CD4^+$ T lymphocytes, e.g. helper $T_H2$ lymphocytes, recruit B cells and $T_H17$ cells into the tumour and activate their secretion of pro-inflammatory cytokines, which could enhance chronic inflammation and tumorigenesis (Fridman et al. 2012, Becht et al. 2016, Balkwill et al. 2012, Anderson, Stromnes and Greenberg 2017). Beside $T_H2$ cells, high level of regulatory T lymphocytes ($T_{reg}$) in

the tumour microenvironment is associated with worse prognosis in many cancer types i.e. breast (Bates et al. 2006), ovarian (Curiel et al. 2004) or pancreatic cancer (Hiraoka et al. 2006).

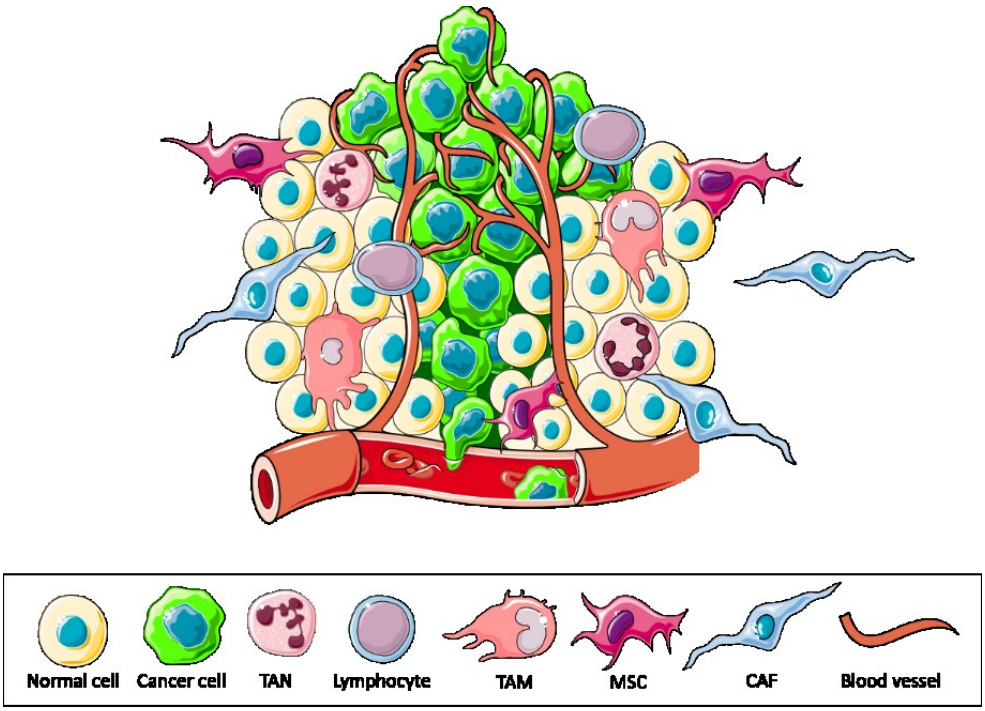


***FIGURE 1.7: Components of tumour microenvironment.*** *The cancer cells are in primary tumours surrounded by complex tumour microenvironment within bone-marrow derived cells as tumour associated macrophages (TAMs) or mesenchymal stem cells, endothelial cells and tumour associated fibroblasts (CAFs). Adapted from Joyce and Pollard, 2009.*

### 1.3.2. Mesenchymal stem cells (MSCs)

Although MSCs belong to the group of bone marrow-derived cells, they have unique role in mitochondrial transfer into cancer cells. As was written above, these adherent multipotent cells can be found mainly in the bone marrow although their origin is not hematopoietic. MSCs are able to differentiate into various cell types of mesenchymal cells i.e. along the osteogenic, adipogenic and chondrogenic lineages, which is very important for tissue damage reparations. Thanks to self-renewal potential, MSCs keep their multipotency also after cell division. MSCs can be isolated from the bone marrow but are present also in other tissues such as skeletal muscle, umbilical cord, amniotic fluid, foetal liver and adipose tissue (Guan and Chen 2013, Jin et al. 2013). MSCs are frequently found in stromal niches of various tumours (Nwabo Kamdje et al. 2017).

Due to their ability to repair tissues and protect transformed cells from chemotherapy MSCs play an important role in the tumour microenvironment in all stages of tumour development including metastatic expansion. Through the secretion of various cytokines and growth factors such as CCL5, TGF-β, IL-6, IL-10, VEGF, MMP, SDF-1 or Neuregulin1, the MSCs are able to modulate immune reaction and facilitate neovascularization processes and angiogenesis, which are the key aspects for subsequent tumour growth and invasiveness (Zhang et al. 2013a, Han et al. 2014, Donnelly et al. 2014, Kucerova et al. 2014, Nwabo Kamdje et al. 2011).

There are several pieces of evidence that MSCs are able to differentiate into CAFs both *in vitro* after long-term cultivation in tumour cell-conditioned medium via a TGFβ1/Smad3-dependent mechanism (Yu et al. 2014, Mishra et al. 2008, Sugihara et al. 2015) and *in vivo*, where the MSCs derived CAFs promote metastases in advanced solid tumours (Margolin et al. 2015, Hong et al. 2015, Mühlethaler-Mottet et al. 2015, Liao et al. 2015).

MSCs are able to trans-differentiate. Trans-differentiation is the process of cell fusion of both cancer cells and other components of the tumour microenvironment, which results in tissue remodelling and tumour stroma formation. Trans-differentiation of MSCs has been reported, for example, in human melanoma (Kucerova et al. 2014), breast or ovarian carcinoma (Yang, Otte and Hass 2015), lung carcinoma (Wei et al. 2014) and others. Positive and negative effect of TME by MSCs is shown in Figure 1.8.

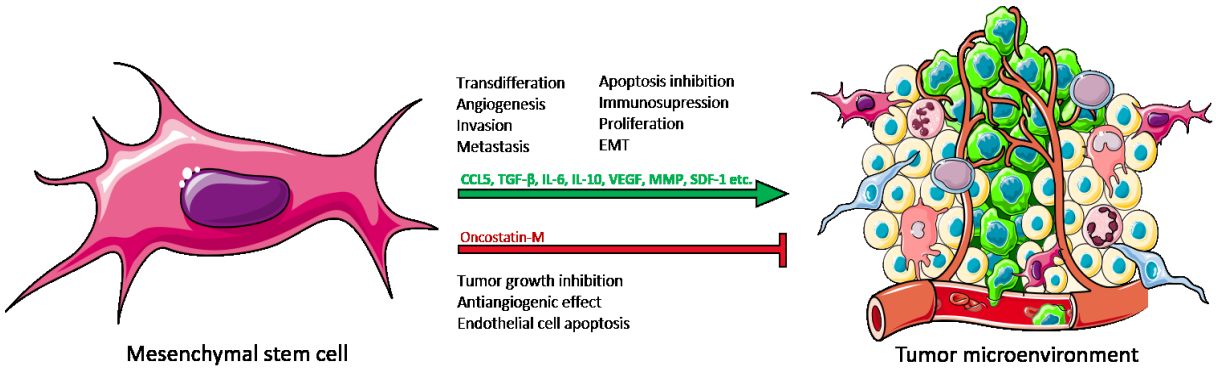


***Figure 1.8: Positive and negative effects of MSCs in TME.***
*MSCs have a number of tumour-promoting functions through which they modulate tumour cells or cells of the tumour microenvironment. Various factors produced by MSCs, which positively affect tumour growth are depicted in green. On the other hand, also tumour-suppressive effects of MSCs were described. Adapted from Barcellos-de-Souza et al., 2013.*

However, several studies describe anti-neoplastic properties of MSCs in e.g. Kaposi's sarcoma or non-Hodgkin's lymphomas (Khakoo et al. 2006, Secchiero et al. 2010) as well as induction of apoptosis in endothelial cells of newly formed vessels (Secchiero et al. 2010, Otsu et al. 2009). *In vivo* experiments using co-injection of glioma cells and MSCs caused reduce tumour volume and its vascularization (Ho et al. 2013). Wang et al. showed, that MSCs inhibit tumour growth *in vivo* and proliferation and migration of lung adenocarcinoma *in vitro* through oncostatin-M secretion (Wang et al. 2012, Barcellos-de-Souza et al. 2013).

Similarly, as for immune cells, tumour-promoting or tumour-suppressing role of MSCs depends on TME, which modulates the function of MSCs means of properties such as cell type composition, hypoxia, pH or inflammation.

## 1.4. Intercellular communication

Intercellular communication usually introduces one of the classic ways in which the transmission of information between cells is mediated. Communication with the environment, besides proper nutrient intake, is one of the indispensable conditions for cell survival (Vander Heiden et al. 2009). Traditional ways of intercellular communication include direct interactions by cell-to-cell contact, interactions of receptors with soluble ligands, vesicle transfer, or transmission through gap junctions. Cancer cells are able to activate their surrounding microenvironment by secreting cytokines, growth factors and proteases, which can act in cascades of autocrine and paracrine signalling, indicated in Figure 1.9. This signalling disrupts homeostasis of healthy surrounding tissue and induces angiogenesis and inflammation. Angiogenesis is necessary for both, the growth of the tumour and for progression of tumour from pre-malignant into malignant stage. At the same time, the cancer cells can initiate secretion of ECM components supporting migration an invasiveness of cancer cells and reduce the expression of protease inhibitors a well as upregulate expression of serine proteases and matrix metalloproteases that degrade and rebuild the ECM. All these components, together with the tumour-derived growth factors, affect fibroblasts in the tumour microenvironment and activate them. (Mueller and Fusenig 2004, Brücher and Jamall 2014).

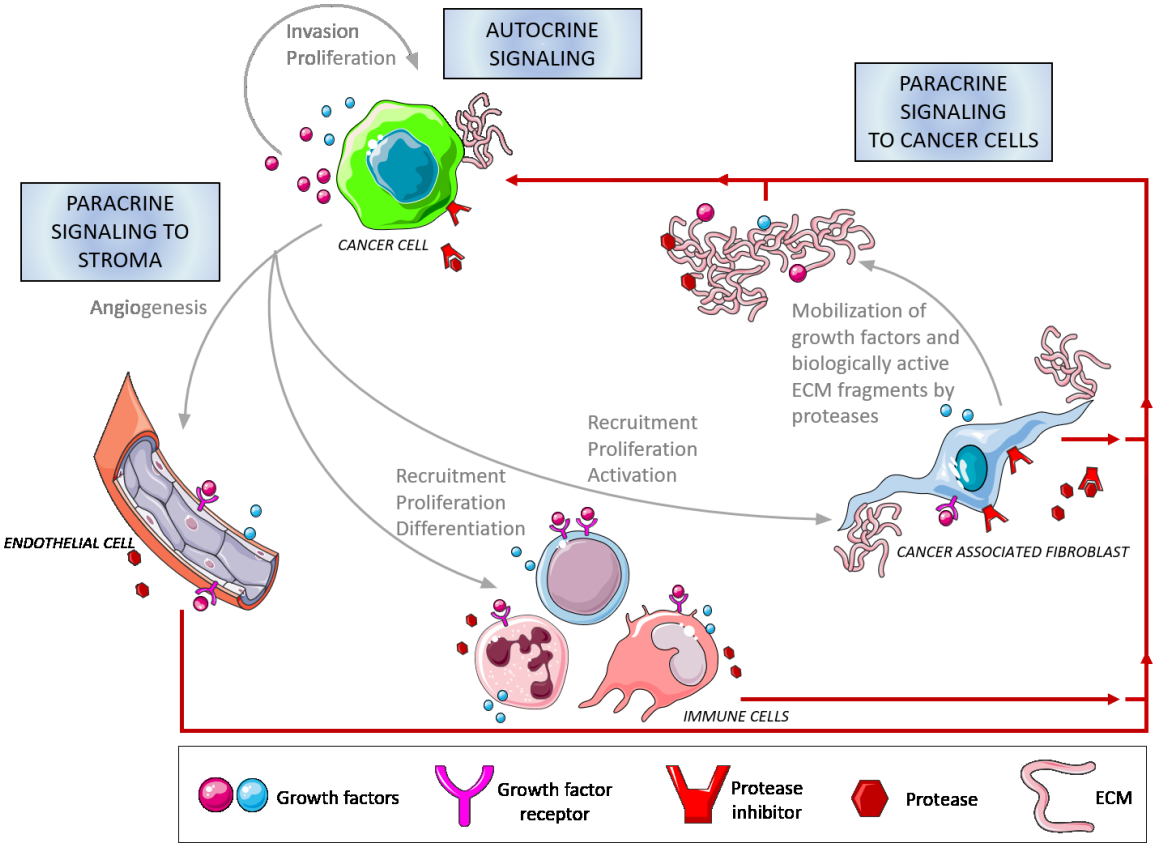


***Figure 1.9: Crosstalk between cancer cells and tumour microenvironment.*** *Cancer cells are able to activate the surrounding stromal environment in autocrine and paracrine manners by secreting growth factors and proteases. This signalling results in cancer cells migration, angiogenesis and activation of the cells of immune system and cancer associated fibroblasts. Adapted from Mueller and Fusenig, 2004.*

A special type of communication of cells is the exchange of whole organelles. This type of communication corresponds to adaptation to external stress and improves the ability of tumour cells to survive.

Intercellular transfer of organelles has been described in many different cell types of both human and rodents origin, differentiated and multipotent cells, malignant and benign tumours and can be realized by different mechanisms including cellular fusion, transport of microvesicles, formation of exosomes and apoptotic bodies, transfer via gap junctions or through tunnelling nanotubes (TNTs) as shown in Figure 1.10 (Torralba, Baixauli and Sánchez-Madrid 2016). In all cases, transfer of organelles includes their active transport via the cytoskeletal system in the cell, which is of high ATP demand. (Spees et al. 2006, Gurke et al. 2008).

Beside strictly unidirectional transfer from one cell type to the other (Koyanagi et al. 2005), bidirectional transfer between the two type of cells has been reported, too

(He et al. 2011, Yasuda et al. 2011). The model of primary human proximal tubular epithelial cells (RPTEC) shows bidirectional transfer not only for organelles but also for many cargo vesicles (Domhan et al. 2011) as well as for small ions as calcium, this was observed in human retinal pigment epithelial (RPE) cells, human neuroblastoma SH-SY5Y cells and human embryonic kidney HEK 293 cells (Smith, Shuai and Parker 2011, Wittig et al. 2012).

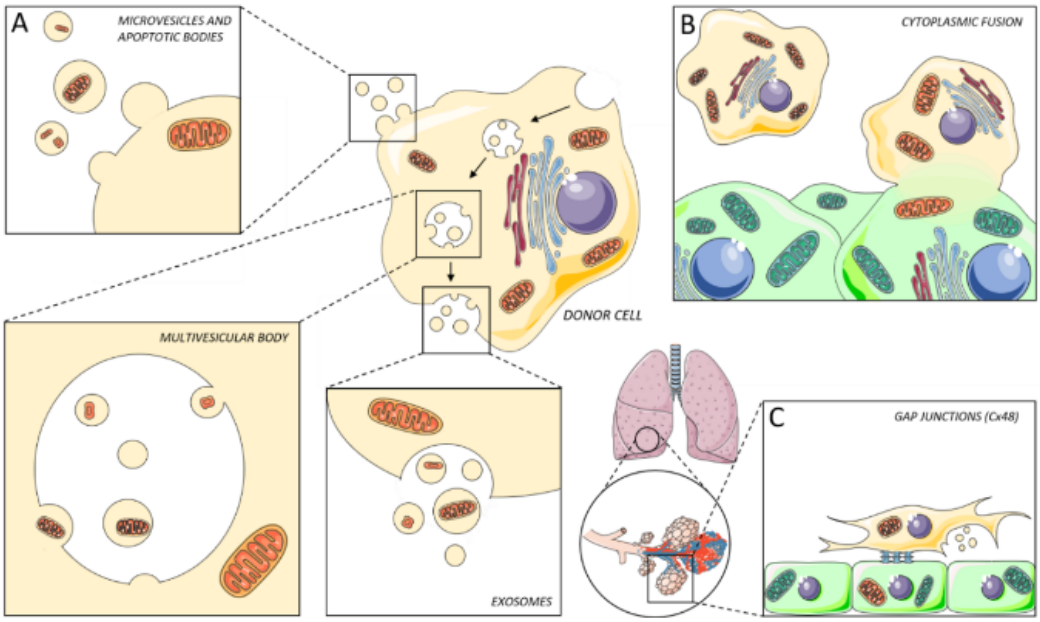


***Figure 1.10: Cellular mechanisms of intercellular mitochondrial transfer.***
*Mitochondria can be transferred by various mechanisms. First of them is the exchange of various extracellular vesicles such as exosomes, various microvesicles and apoptotic bodies or multivesicular body (MVB). These extracellular vesicles contain whole mitochondria or their fragments – depicted in yellow and orange (Torralba et al. 2016, Phinney et al. 2015) (A). Another way of the transfer is cellular fusion, when two independent cells fuse their plasmatic membranes and share their content including organelles and other cytosolic compounds, while the nuclei remain intact after the fusion (Oh et al. 2003) (B). In alveolar cells the mitochondrial transfer from BMSCs was detected after LPS treatment. The treatment increased connexin 43 expression in alveolar cells, that facilitates the attachment of BMSCs and formation of gap junctional channels, microvesicles and tunnelling nanotubes for mitochondrial transfer (Islam et al. 2012, Torralba et al. 2016)(C). Figure adapted from Torralba et al., 2016.*

## 1.5. Mitochondrial transfer *in vitro* between mammalian cells

Transfer of mitochondria between cells results in their incorporation into the endogenous mitochondrial network in the recipient cells, which can influent cellular metabolism. This has significant implication for the pathology of mitochondria leading to enhancement of neoplastic diseases as a result of reprograming of signalling and metabolic pathways (Torralba et al. 2016).

### 1.5.1. Intercellular transfer from MSCs to tumour cell lines

Progenitor stem cells, present in almost every tissue, have the propensity to repair possible tissue damage or to replace depleted cells. These cells can be also supported by MSCs. The stem cells differentiate in the region of damage to replace the injured cells and produce various growth factors to communicate with their neighbourhood. Due to these characteristics are MSCs often used for *in vitro* studies investigating mitochondrial transfer to cells with mitochondrial dysfunctions (Prockop, Gregory and Spees 2003).

The first evidence of mitochondrial transfer was documented by Spees et al. between MSCs and fibroblasts which were cultivated with adenocarcinomic human alveolar basal epithelial cells with depleted mtDNA (A549 rho0). The A549 rho0 cells were prepared by long-term cultivation with low concentration of ethidium bromide (EtBr). Upon co-cultivation with MSCs or fibroblasts, A549 rho0 cells acquired functional mitochondria and restored aerobic respiration (Spees et al. 2006). Other studies subsequently described mitochondrial transfer between MSCs and various types of breast cancer cells (MCF-7, MDA-MB) or ovarian cancer cells (OVCAR-3, SKOV-3). Except the transfer between two different cell types – heterocellular transfer, also homocellular transfer between cells of one type was observed (Pasquier et al. 2013, Caicedo et al. 2015). The study on rho0 variant of human osteosarcoma cell line (143B) rho0 cells showed, that the extent of mitochondrial disruption the potential recipient cells is very, such that there was no mitochondrial transfer from MSCs to rho0 cells after partial damage of mitochondria (Cho et al. 2012). In another study, Wharton's jelly-derived MSCs, a stem cells isolated from postpartum umbilical cord, were used for co-culture studies with 143B rho0 cells. The results showed that rho0 cells, which received functional mtDNA, recovered the ability to respire and to restore their normal cellular behaviour (Lin et al. 2015).

### 1.5.2. Intercellular transfer between tumour cells

As mentioned above, the transfer of mitochondria exists not only between healthy and cancer cells but cancer cells can also transfer mitochondria to each other (Pasquier et al. 2013). The mitochondrial transfer was observed between various mesothelioma cell lines (MSTO-211H, VAMT, H-Meso) as well as between non-malignant mesothelial LP9 and Met5A cells, but interestingly there was no evidence of transfer when mesothelial and mesothelioma cells were co-cultured (Lou et al. 2012). Another piece of evidence of transfer via TNTs is from the study with human lung squamous cell carcinoma cells (LSCC), where the TNTs were observed not only as a phenomenon of *in vitro* cell culture but also and more importantly in tissue sections (Antanavičiūtė et al. 2014). Using an *in vitro* bladder cancer cell co-culture model, Lu et al. demonstrated heterocellular mitochondrial transfer between two cancer cell lines. Formation of TNT and uni-directional transfer of mitochondria occurred between highly invasive T24 cells and less invasive RT4 cells. This spontaneous intercellular mitochondria trafficking between the cell types was followed by increased Akt activation, mTOR signalling, and invasiveness of RT4-Mito-T24 cancer cells, that originated by transferring of mitochondria from T24 to R24 cells (Lu et al. 2017). Another model for mitochondrial transfer represents PC12 cell line derived from a pheochromocytoma of the rat adrenal medulla. There is evidence of the transfer between un-treated PC12 and UV-treated PC12 cells in the co-culture, where UV-treated PC12 cells received healthy mitochondria from their un-treated counterparts. (Wang and Gerdes 2015b, Bukoreshtliev et al. 2009, Rustom et al. 2004).

### 1.5.3. Intercellular transfer between non-cancerous cells

There are examples of intercellular mitochondrial transfer between non-cancerous cells. In addition to neoplastic diseases, heart disorders such heart attack and ischemia are the most common cause of death in developed countries. Therefore, intercellular transfer of mitochondria seems to be a possible way of the therapeutic modality in this context. The donation of functional mitochondria from MSCs to cardiomyocytes with dysfunctional or damaged mitochondria leads to the restoration of mitochondrial function and improves the condition of the affected cells (Plotnikov et al. 2008, He et al. 2011, Acquistapace et al. 2011, Oh et al. 2003).

Liu et al. simulated ischemic reperfusion in human umbilical vein endothelial cells (HUVEC) by cultivation of cells under the reduced oxygen supply. Subsequent co-cultivation with MSCs with both functional and damaged mitochondria revealed, that unlike damaged MSCs, co-cultivation with healthy MSCs restored mitochondrial function in HUVEC cells indicating the regenerative potential of mitochondrial transfer (Liu et al. 2014).

Rats exposed to cigarette smoke as well as human bronchial epithelial cells (BEAS-2B) are *in vivo* and *in vitro* models of chronic obstructive pulmonary disease (COPD), a disease expressing mitochondrial disfunction. Co-cultivation of BEAS-2B with human-induced pluripotent stem cell-derived MSCs (iPSC-MSCs) or grafting of adult bone marrow MSCs (BM-MSCs) into rat, respectively, result in renewal of damaged mitochondria in recipient cells and attenuate lung damage caused by cigarette smoke (Li et al. 2014).

Similarly, mitochondrial transfer between primary human RPTEC and human mammary epithelial cells (HMEC) (Domhan et al. 2011) or MSCs and rat renal tubular cells (Plotnikov et al. 2010) was detected.

## 1.6. Mitochondrial transfer between mammalian cells *in vivo*

Occurrence of intercellular mitochondrial trafficking *in vivo* is rare. Anyway, there are several studies showing mitochondrial trafficking under pathophysiological conditions.

Phylogenetic and sequencing studies on the canine transmissible venereal tumour (CTVT) demonstrate that cumulative damage of mitochondrial DNA lead to periodic transfer of mitochondria from host animals into the cancer cells (Strakova et al. 2016, Rebbeck, Leroi and Burt 2011). Islam et al. reported mitochondrial transfer in a mouse model of acute lung injury. The mice were exposed to endotoxin - lipopolysaccharide (LPS) and subsequently grafted with mouse or human bone marrow-derived MSCs. After alveolar attachment, BMSCs transferred their mitochondria to the alveolar epithelium. Connexin 43 (Cx43), expressed on all structures including microvesicles, nanotubes and gap junctional channels, was found as a crucial factor affecting the alveolar attachment of BMSCs, which helps to transport functional mitochondria into the alveolar cells, as presented in Figure 1.10 – C (Islam et al. 2012, Sinha et al. 2016).

## 1.7. Tunnelling nanotubes (TNTs)

Many publications describe mitochondrial transfer via TNTs as the major mechanism by which this organelle exchange takes place (Pasquier et al. 2013, Lou et al. 2012, Antanavičiūtė et al. 2014, Wang and Gerdes 2015a, Koyanagi et al. 2005, Domhan et al. 2011, He et al. 2011, Liu et al. 2014, Islam et al. 2012). Moreover, TNTs can transport various vesicles as early endosomes, endoplasmic reticulum (ER), Golgi apparatus (GA) or lysosomes (Smith et al. 2011, Wang et al. 2011, Osswald et al. 2015, Rustom et al. 2004) as well as ions ($Ca^{2+}$) or small molecules as miRNAs. Furthermore, TNTs transfer pathogens like bacteria, viruses and prions, that results in spreading of the pathologies (Onfelt et al. 2006, Hashimoto et al. 2016, Kumar et al. 2017, Gousset et al. 2009, Panasiuk et al. 2018, Jansens et al. 2017).

### 1.7.1. TNTs formation

There are two possible mechanisms of TNT formation (ref.). Both models require active cell motion and cytoskeleton remodelling. The first model – referred to as 'cell dislodgement' mechanism involves a membrane fusion between donor and recipient cells, that are in close contact. Their subsequent migration in opposite directions then prolong TNT between each other. The second model, known as the actin-driven mechanism, consist of extension of filopodia-like protrusion from one cell to distant cell, where the membrane fusion at the contact site gives rise to the TNT structure (Abounit, Delage and Zurzolo 2015, Ariazi et al. 2017, Hekmatshoar et al. 2018). As mentioned above, several studies report the key role of Cx43 in TNT production and attachment and subsequent mitochondrial transmission (Berridge et al. 2016, Osswald et al. 2015)

### 1.7.2. Role of cytoskeleton in TNTs formation

TNTs are thin transient plasma membrane extensions forming during the interphase of the cell cycle. They are very heterogeneous structures in terms of the length, width, longevity, the way of formation and the composition of the cytoskeletal components i.e. actin filaments, microtubules (MTs) and intermediate filaments (IFs). The content of cytoskeletal components varies depending on the properties of TNTs and the character of the cells involved in this intercellular linkage. The organization and position of all three cytoskeletal elements are expected to play crucial role in the effective transport of material via TNTs and in

the stability of TNTs (Ariazi et al. 2017, Resnik et al. 2018). These structures can span various lengths i.e. up to several hundreds of micrometres and diameter ranges from 50 to 1500 nm (Vignais et al. 2017, Hekmatshoar et al. 2018).

Interplay between IFs in donor and recipient cells is documented to have a key role in formation of TNTs connecting RT4 and T24 urothelial cell, squamous carcinoma cells and mesothelioma H2052, VAMT, and MSTO-211H cells (Sáenz-de-Santa-María et al. 2017, Veranic et al. 2008, Ady et al. 2014), while evidence about MT-IF interplay in TNTs is missing (Resnik et al. 2018). It is indisputable that actin filaments are essential for the formation and propagation of all TNTs, while MTs are present preferentially in TNTs of larger diameter and contribute to their stability and longevity (Osteikoetxea-Molnár et al. 2016, Jansens et al. 2017, Panasiuk et al. 2018, D'Aloia et al. 2018).

Present work assumes that there are actin filaments and MTs inside the TNTs and that both of these cytoskeletal elements are important as highways for motor proteins, which transport their cargos between the two connected cells.

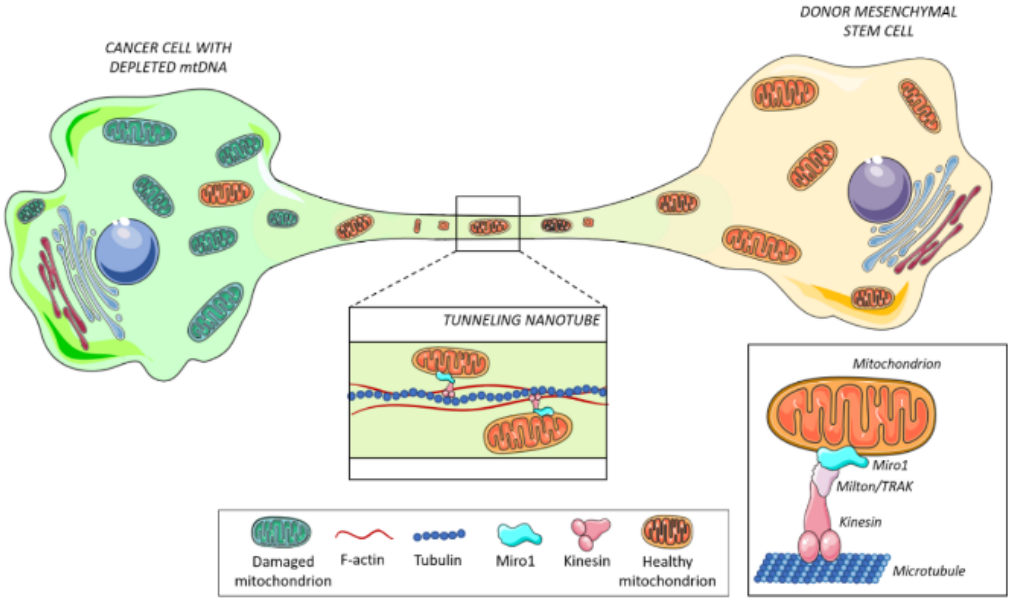


***Figure 1.11: Schematic representation of mitochondrial transfer via the intercellular TNT link.*** *Moving through tunnelling nanotubes appears to be a relevant way of transferring mitochondria with mtDNA into a cell with disrupted mtDNA. This process is driven by protein motors kinesin-1 and dynein, which carry cargo in the anterograde and retrograde directions. For one-way intercellular movement of mitochondria by TNTs, kinesin appears to be more appropriate. The mitochondrial load is attached via adapter proteins Miro1 (or Miro2) and miltons (Trak1 and Trak2 in humans) (Lovas and Wang 2013, Torralba et al. 2016, Ahmad et al. 2014). Adapted from Torralba et al., 2016.*

### 1.7.3. Miro1 protein as a regulator of intercellular mitochondrial transfer

From all cytoskeletal compartments, transfer on MTs is the most well described. The process of transferring mitochondria through TNT is driven by the motor protein kinesin-1. It has been shown that kinesin-1 shifts the cargo along the fibre in the anterograde direction, from minus to plus end of the microtubule. In the opposite, retrograde direction, dynein probably acts as a molecular motor. The mitochondria are then attached to the kinesin via the adapter proteins Miro1, see Figure 1.11 (MacAskill and Kittler 2010, Guo et al. 2005, Glater et al. 2006, Fransson, Ruusala and Aspenström 2006).

Primary structure of Miro proteins, shown in Figure 1.12, contains two GTPase domains as well as two helix-loop-helix structural EF domains, which protrude into the cytosol and are responsible for $Ca^{2+}$ binding. Except these domains, Miro protein has a carboxy-terminal transmembrane domain, which anchor the outer mitochondrial membrane (OMM) (Peters et al. 2018).

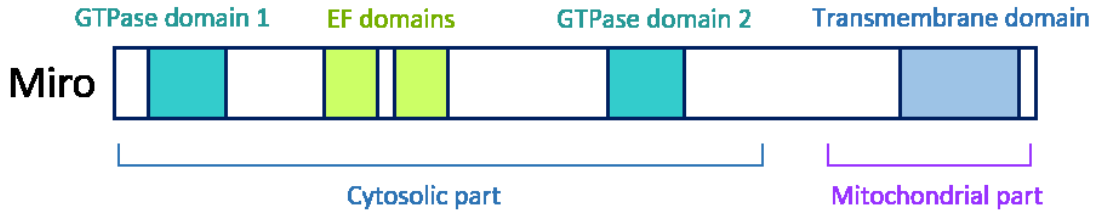


***Figure 1.12: Primary structure of Miro proteins.*** *Figure adapted from Stephen et al. 2015.*

Miro1 is an essential protein in mitochondrial transport in both *in vitro* and *in vivo* models. Co-cultivation of epithelial cells with MSCs show increased mitochondrial transfer in MSCs with Miro1 overexpression in contrast to decreased efficacy of mitochondria transfer in co-culture with Miro1 knockdown MSCs. In mouse model of allergic airway inflammation with inhibited complex I respiratory chain using rotenone, grafting of MSCs with overexpressed Miro1 has been associated with higher therapeutic efficacy (Ahmad et al. 2014).

Another study confirmed the key role of Miro1 in mitochondrial transfer using *in vitro* model of ischemia in astrocytes and in PC12 cells with mitochondria damaged by EtBr. Increased mitochondrial transfer through TNTs was occurred in both models showed increased frequency of mitochondrial transfer and subsequent restoration of neuronal function after intravenous injection of MSCs overexpressing Miro1 (Babenko et al. 2018).

### 1.7.4. The mechanism of mitochondrial transport

As mentioned above, the transport of mitochondria along microtubules is mediated by the engine proteins kinesin and dynein, which transfer mitochondria through many adapter proteins. In a study on Drosophila, dMiro was found to interact directly with Milton protein and form a protein complex that regulates mitochondrial transport (Guo et al. 2005).

Later, mammalian orthologs of the Milton protein, called TRAK 1 and TRAK2 (or also OIP106 and OIP98/Grif-1), which are able to form complexes with two mammalian orthologs of dMiro (Miro1 and Miro2), have also been identified (Brickley et al. 2005). Unlike drosophila, TRAK1 and TRAK2 do not appear to be specific factors for mitochondria transmission in the cells, although they participate in regulation of transfer of other cargos as endosomes (Webber, Li and Chin 2008, Kirk, Chin and Li 2006).

It was shown that mitochondrial transfer is dependent on the cytosolic levels of calcium in both neuronal and non-neuronal cells. It was shown, that resting physiological concentration of $Ca^{2+}$ (50-100 nM) is responsible for maximal mitochondrial motility, whereas total suppression of the mitochondrial activity occurs in 1 µM $Ca^{2+}$ concentration (Yi, Weaver and Hajnóczky 2004). The EF domains of Miro protein are calcium sensors, that are able to mediate calcium-dependent inhibition of mitochondrial transfer (Macaskill et al. 2009, Wang and Schwarz 2009, Saotome et al. 2008).

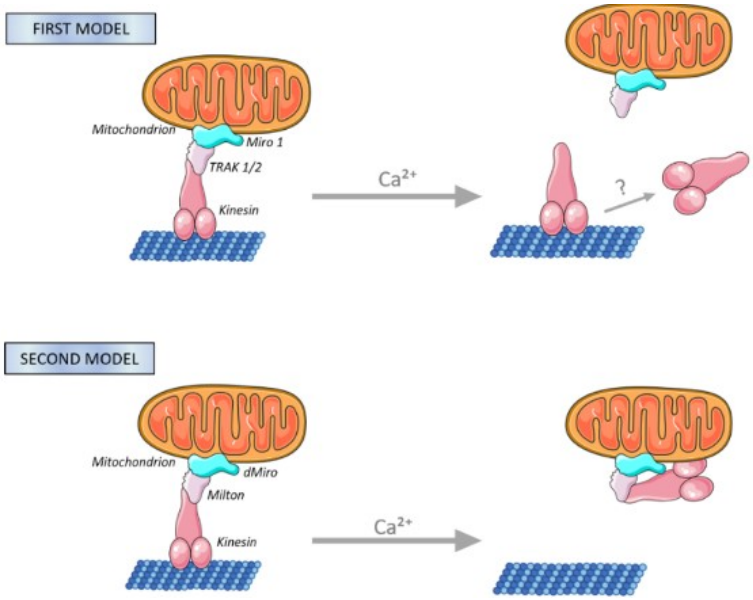


***Figure 1.13: Two models of the mechanism of mitochondrial stopping.*** *Figure adapted from MacAskill and Kittler, 2010.*

Two models of the mechanism of this inhibition were described, as is shown in Figure 1.13. The first model shows disruption of Miro1 and kinesin interaction after calcium binding. This results in detachment of mitochondrion from the transport machinery and leads to motors inactivation (Macaskill et al. 2009). The second model observed in Drosophila presumes, that high level of calcium blocks kinesin connection to microtubules and binds it directly to dMiro protein linked to mitochondria, which results to uncoupling mitochondria from the microtubule transport pathway (Wang and Schwarz 2009, MacAskill and Kittler 2010). However, the exact mechanism of mitochondria movement regulation remains unclear.

# 2. Aims

*QUESTION 1*

Is there a link between OXPHOS and initiation of tumorigenesis?

*AIM 1.1*

To investigate the tumour formation ability of mtDNA deficient murine metastatic melanoma (B16) and murine metastatic breast carcinoma (4T1) cells.

*AIM 1.2*

To examine metabolic state of B16 a 4T1 sub-lines with different mtDNA levels.

*AIM 1.3*

To characterize the influence of mitochondrial transfer in B16 and 4T1 sub-lines.

*QUESTION 2*

Is mtDNA transfer in B16 and 4T1 cells realized via the transport of intact mitochondria mediated by TNTs?

*AIM 2.1*

To verify the transfer of intact mitochondria *in vivo*.

*AIM 2.2*

To investigate intercellular transfer of mitochondria via TNTs.

# 3. Material

## 3.1. Chemicals

| Chemical | Supplier | Catalog number |
|---|---|---|
| ***Cell culture*** | | |
| Dimethylsulfoxide (DMSO) | Sigma | D2650 |
| Ethidium bromide (EtBr) | Sigma | E1510 |
| Ethylenediaminetetraacetic acid (EDTA) | Sigma | E7889 |
| FluoroBrite™ DMEM Medium | TermoFisher | A1896702 |
| Isopropanol | Penta | 17500 |
| Poly-L-lysine solution | Sigma | P4707 |
| Trypsin/EDTA (0,25 % w/v) | Sigma | T4049 |

## 3.2. Media

| Chemical | Supplier | Catalog number |
|---|---|---|
| ***Complete growth RPMI medium for 4T1 sub-lines culturing*** | | |
| D(+)-Glucose | Roth | HN06.3 |
| FBS (10 % w/v) | Sigma | F7524 |
| Penicilin G (sodium salt) (100 U/ml) | Sigma | P3032 |
| RPMI-1640 Medium | Sigma | R8758 |
| Sodium pyruvate (1 mg/ml) | Sigma | P8574 |
| Streptomycin (sulfate) (100 µg/ml) | Sigma | S9137 |
| Uridin (0,05 mg/ml) | Sigma | U3750 |
| ***Complete growth DMEM medium for B16 sub-lines culturing*** | | |
| D(+)-Glucose | Roth | HN06.3 |
| DMEM (Dulbecco's modified Eagle medium) | Sigma | D6429 |
| FBS (10 % w/v) | Sigma | F7524 |
| Penicilin G (sodium salt) (100 U/ml) | Sigma | P3032 |
| Sodium pyruvate (1 mg/ml) | Sigma | P8574 |
| Streptomycin (sulfate) (100 µg/ml) | Sigma | S9137 |
| Uridin (0,05 mg/ml) | Sigma | U3750 |
| ***Complete growth MesenCult medium for MSCs culturing*** | | |
| MesenCult™ basal medium (Mouse) | StemCell technologies | 05514 |
| MesenCult™ 10X supplement (Mouse) | StemCell technologies | 05515 |
| MesenPure™ | StemCell technologies | 05500 |
| Penicilin G (sodium salt) (100 U/ml) | Sigma | P3032 |
| Streptomycin (sulfate) (100 µg/ml) | Sigma | S9137 |

## 3.3. Antibodies and mounting media

| Chemical | Supplier | Catalog number |
|---|---|---|
| ***Primary antibodies*** | | |
| Anti-Alpha-tubulin | abcam | ab190573 |
| Anti-DNA mouse monoclonal | Progen | 61014 |
| Anti-Ki67 | abcam | ab15580 |
| Anti-TFAM rabbit polyclonal | abcam | ab131607 |
| Anti-TOM20 | Santa Cruz Biotechnology | sc11415 |
| ***Secondary antibodies*** | | |
| Abberior STAR 580 | Abberior Instruments | ST580 |
| Abberior STAR RED | Abberior Instruments | STRED |
| Alexa Fluor 488 goat anti-rabbit IgG | Life Technologies | A21245 |
| Alexa Fluor 555 goat anti-mouse IgM | Life Technologies | A21236 |
| Hoechst 33342 | Sigma | 14533 |
| ***Mounting media*** | | |
| Aberrior mount liquid | Abberior Instruments | MM-2009-2X15ML |
| VECTASHIELD® antifade mounting medium with DAPI | Vector laboratories | H-1200 |
| VECTASHIELD® antifade mounting medium | Vector laboratories | H-1000 |

## 3.4. Immunofluorescent dyes

| Chemical | Supplier | Catalog number |
|---|---|---|
| MitoTracker™ Orange CM-H2TMRos | ThermoFisher | M7511 |
| MitoTracker™ Deep Red FM | ThermoFisher | M22426 |
| SiR-tubulin kit | SpiroChrome | CHF420.00 |

## 3.5. Kits

| Chemical | Supplier | Catalog number |
|---|---|---|
| ***Photolitography*** | | |
| SYLGARD® 184 silicone elastomer kit | Sigma | 761036 |
| ***Cell Viability Assay*** | | |
| CellTiter-Glo® luminescent cell viability assay | Promega | G7570 |
| ***Total gDNA isolation*** | | |
| Wizard® genomic DNA purification kit | Promega | A1120 |
| ***Total protein concentration measurement*** | | |
| Pierce™ BCA protein assay kit | ThermoFisher | 23225 |
| ***NAD/NADH Assay*** | | |
| NAD/NADH-Glo™ assay | Promega | G9071 |

## 3.6. Buffers

| Chemical | Supplier | Catalog number |
|---|---|---|
| ***Isolation buffer for MSCs*** | | |
| FBS (10 % w/v) | Sigma | F7524 |
| Penicilin G (sodium salt) (100 U/ml) | Sigma | P3032 |
| Streptomycin (sulfate) (100 µg/ml) | Sigma | S9137 |
| PBS 1x | | |
| ***Wash buffer for immunofluorescence staining*** | | |
| Glycine | Serva | 23390.30 |
| TRITON™ X-100 | Sigma | T8787 |
| TWEEN® 20 | Sigma | P7949 |
| PBS 1x | | |
| ***Citrate buffer for antigen restoration (10mM, pH 6)*** | | |
| Citric acid 0,1M | Sigma | 251275 |
| Sodium citrate 0,1M | Sigma | 1613859 |
| Water | | |
| ***RIPA (Radio-immunoprecipitation assay) lysis buffer*** | | |
| EDTA 1mM | Sigma | E7889 |
| NP-40 1% | Sigma | 74385 |
| SDS 0,1% | Sigma | 436143 |
| Sodium deoxycholate 0,5% (w/v) | Sigma | D6750 |
| Sodium chloride 150mM | Serva | 39781.02 |
| Tris 50mM (pH 8) | Serva | 37190.03 |

## 3.7. Primers

| Name | Sequence 5´-XXX-3´ | |
|---|---|---|
| | Forward | Reverse |
| mMito1 | CTAGAAACCCCGAAACCAAA | CCAGCTATCACCAAGCTCGT |
| B2M1 | GCTGGGTAGCTCTAAACAATGTATTCA | CCATGTACTAACAAATGTCTAAAATGGT |

## 3.8. Enzymes

| Chemical | Supplier | Catalog number |
|---|---|---|
| DNase I | Roche | 11284932001 |
| Collagenase | Sigma | C7657 |

## 3.9. Experimental models

### 3.9.1. Cell lines

| Cell line | Supplier | Identifier |
|---|---|---|
| 4T1 | ATCC | CRL-2539 |
| B16 | ATCC | CRL-6323 |

### MSCs

Murine MSCs are multipotent stromal cells that are able to differentiate into a variety of cell types (osteoblasts, chondrocytes, myocytes and adipocytes). All cells were isolated from BALB/c$^{su9DsRed2}$ or C57BL/6J$^{su9DsRed2}$ mice.

### 4T1 sub-lines

4T1 is 6-thioguanine-resistant adherent murine cell line of an animal stage IV human breast cancer syngeneic with BALB/c mouse strain.

| Cell sub-line | Phenotype |
|---|---|
| 4T1 | parental cells with standard mtDNA content |
| 4T1 rho0 | cells with depleted mtDNA |
| 4T1 rho0 D5-D60 | cells with various mtDNA content derived from tumours |
| 4T1 rho0 GFP (LV) | GFP is expressed diffuse in cytoplasm |
| 4T1 rho0 pmGFP/nBFP | GFP is expressed in plasmatic membrane and BFP in nucleus |

### B16 sub-lines

B16 is adherent murine cell line of melanoma syngeneic with C57BL/6J mouse strain.

| Cell sub-line | Phenotype |
|---|---|
| B16 | parental cells with standard mtDNA content |
| B16 rho0 | cells with depleted mtDNA |
| B16 rho0 nBFP | BFP is expressed in nucleus |
| B16 rho0 DP | BFP is expressed in nucleus and transfered mitochondria espress dsRed protein |

## 3.9.2. Mice

Animal studies were performed according to the guidelines of the Czech Animal Ethics Committee and were approved by the respective local Animal Ethics Committee.

Transgenic mice expressing red fluorescent protein in somatic cell mitochondria (the CAG/su9-DsRed2 transgene) were generated in the Transgenic Unit of the Czech Centre for Phenogenomics, Institute of Molecular Genetics, Prague, Czech Republic, using a pronuclear injection from the construct provided by prof. Masaru Okabe (Osaka University, Japan) (Hasuwa et al. 2010) and C57BL/6N mice (Dong et al. 2017).

| Strain | Supplier | Identifier |
|---|---|---|
| C57BL/6 mice | Jackson Laboratories | C57BL/6 |
| Balb/c mice | Jackson Laboratories | Balb/c |

C57BL/6J mice were used as syngeneic host animals for grafting B16 sub-lines

C57BL/6N$^{su9DsRed2}$ mice were used for isolation of MSCs for co-cultures with B16 sub-lines

Balb/c mice were used as syngeneic host animals for grafting 4T1 sub-lines

Balb/c$^{su9DsRed2}$ mice were used for isolation of MSCs for co-cultures with 4T1 sub-lines

## 3.10. Instruments

| Instrument | Supplier |
|---|---|
| ***Cell culture*** | |
| Centrifuge 5415R | Eppendorf |
| Centrifuge 5804R | Eppendorf |
| Centrifuge MiniSpin Plus | Eppendorf |
| Flow box SafeFAST Classic 218 A | Schoeller |
| Incubator Sanyo CO2 | Schoeller |
| Water bath TW20 | Julabo GmbH |
| ***Microscopes*** | |
| Abberior STED 775 QUAD scanning microscope | Abberior Instruments |
| Confocal inverted microscope Leica SP8 SMD – FLIM | Leica Microsystems |
| Leica DMIL LED microscope | Leica Microsystems |
| Confocal microscope Leica TCS SP5 AOBS Tandem | Leica Microsystems |
| Nikon Eclipse E400 | Nikon |
| ***Other instruments*** | |
| Analytical scales | Mettler Toledo |
| Flowcytometer BD FACS Aria™ Fusion | BD Biosciences |
| HistoCore MULTICUT – Semi-automated rotary microtome | Leica Biosystems |
| Innovatis CASY® cell counter | Innovatis |
| Real Time PCR System Eco™ Illumnia | Illumnia |
| Tecan Infinitive M200 | Tecan |
| Ultrasound Vevo 770 | VisualSonics |
| ***Softwears*** | |
| Amira 6 | Fei Systems |
| Huygens professional version software 18.10 | Scientific Volume Imaging |
| ImageJ | Fiji |
| LAS v4.5 software | Leica Microsystems |
| Photoshop Adobe | Photoshop Adobe |
| Prism | GraphPad |

# 4. Methods

## 4.1. Cell culture

All manipulations with the cells were performed in the sterile atmosphere of laminar flow box and all used equipment was sterile, autoclaved or disposable.

All cell lines were grown in the incubator at 37°C under 5% CO2 atmosphere and 95% humidity. Cells were split according to their growth rate, usually when reached 80 - 90% confluence.

### 4.1.1. Cell freezing and thawing

The cells were frozen in cryovials in 10% DMSO in the standard medium and stored in liquid nitrogen. For thawing, the cells were removed from liquid nitrogen and immediately placed in the cryovials into a water bath of 37 °C. After thawing, the content of the cryovial was diluted in pre-warmed medium and centrifuged at 300x g for 5 min at room temperature. The supernatant was removed, and cells were resuspended in fresh culture medium.

### 4.1.2. Cell passage and counting

The medium was aspirated from the culture flasks, the cells were washed twice with PBS and then incubated for approximately 5 min with an appropriate volume of trypsin solution in PBS (0.25% w/v) in an incubator (37 °C / 5% CO2). After the incubation, trypsin was inactivated by addition of at least the same amount of the culture medium. The suspension was thoroughly resuspended and split or used for further purposes.

For microscopy, the cells were counted in the Bürker chamber, accordingly to the manufacturer´s.

### 4.1.3. Preparation and characterization of rho0 cells

Cells were deprived of mtDNA by cultivation of parental cells in presence of sub-lethal concentrations (50 ng/ml) of ethidium bromide (EtBr) for at least 3 months. After the EtBr treatment characterization of rho0 cells was performed by measuring respiration using the Oxygraph-2k respirometer. Compared to parental cells, rho0 cells are unable to respire using the ETC. Therefore, the level of transcripts encoded

by mitochondrial DNA using qPCR was determine in Rho0 cells, as is described in chapter 4.14 in detail.

### 4.1.4. Transfection of B16 cell lines

B16 and B16 rho0 cells were transfected with the pTagBFP-H2B vector, described in Figure 4.1, to prepare cells, that permanently express the blue fluorescent protein (BFP) in the nucleus. The vector 12B triggers a BFP tag that is bound to the H2B region in the plasmid. To transfect the plasmid into the cells, a FuGENE® HD Transfection Reagent was used. Subsequently the selection of non-transfected cells was done using G418-sulfate antibiotics (0,4 mg/ml for 14 days).

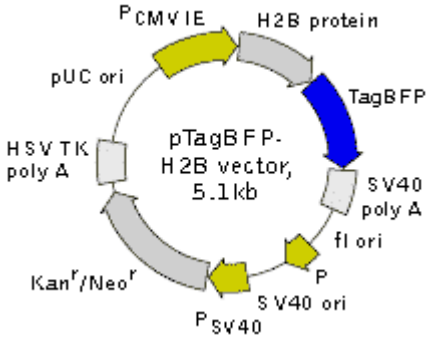


***FIGURE 4.1: The map of pTagBFP-H2B vector (Evrogen)*** *used for fluorescent labeling of histone H2B in live cells. (http://evrogen.com/vector-descriptions/pTagBFP-H2B/pTagBFP-H2B.pdf)*

## 4.2. Isolation and cultivation of MSCs

### 4.2.1. Isolation of mouse bone marrow MSCs

Mice up to 20 weeks of age were sacrificed by cervical dislocation and rinsed in 70% ethanol for disinfection. The skin from the hind and fore limbs were removed and the limbs were dissected. All the adherent tissues (muscles and tendons) were carefully cleaned from the bones using the scalpel. Clean tibiae, femora and humeri were kept in the isolation buffer for one hour. After incubation in the isolation buffer, bones were cut and the bone marrow was rinsed out with the complete MesenCult™ basal medium (Mouse) using a 5ml syringe with 23G 0,6 x 30mm needle and collected in the falcon tubes. The bone cavities were thoroughly washed at least three times until the bones changed their colour from red to white. Collected bone marrow was then centrifuged at 300x g for 5 min. The pellets were resuspended in

fresh complete MesenCult™ basal medium (Mouse) with the addition of MesenPure™ and seeded in T75 flasks containing 15 ml of media. The whole procedure of MSCs isolation is shown in Figure 4.2.

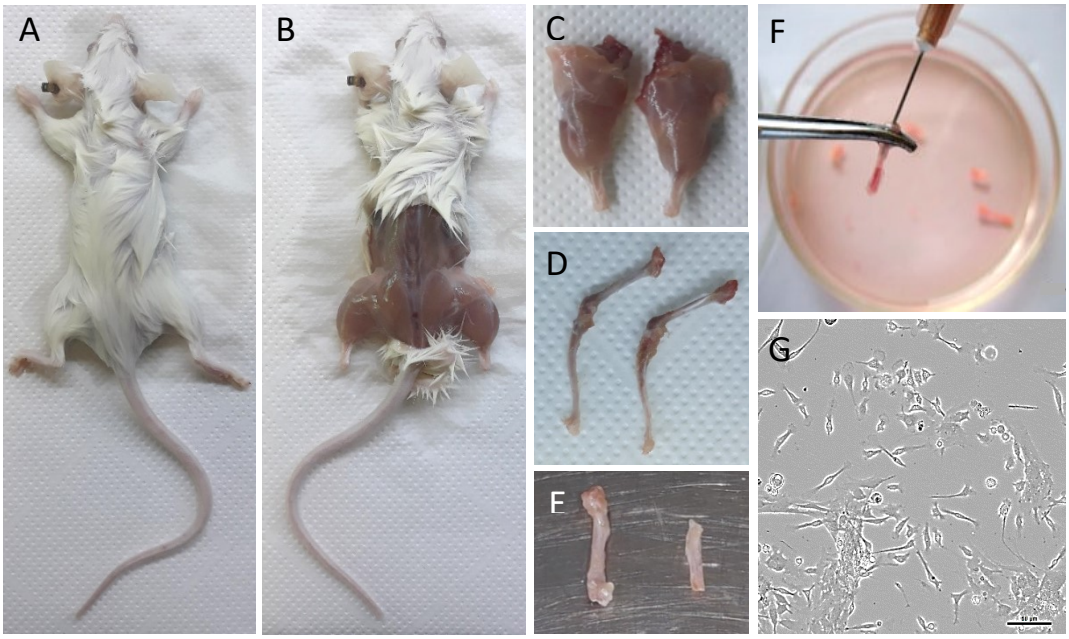


***FIGURE 4.2: Isolation and culture of MSCs from mouse compact bone.*** *A mouse disinfected by ethanol (A), skinning (B), isolated hind limbs (C), femora and humeri with removed adherent tissue (D), bones with and without joint heads (E), rinsing out of the bone marrow (F), established primary culture of MSCs (G).*

### 4.2.2. Cultivation of MSCs

The culture of isolated MSCs was kept in humified incubator (37 °C / 5% $CO_2$) for 4-7 days depending on the confluency. After obtaining a confluent culture in passage 0, all non-adherent cells were washed out from the flask with PBS. MSCs were then incubated for approximately 10 minutes with 0,25 % w/v solution of trypsin in PBS. After trypsinization 4 ml of the MesenCult™ basal medium (Mouse) was added and the cell suspension was plated at the 1:2 ratio into fresh T75 flasks and the cells were grown till confluence. The experiments were performed using MSCs between the third end ninth passage.

## 4.3. Tumour generation and isolation

The mice used for the grafting experiments were healthy, 10 weeks old animals with no sign of stress or discomfort. All animal procedures and experimental protocols were approved by the Animal Welfare Committee of the Czech Academy of Sciences.

### 4.3.1. Cancer cells injection

The cells were trypsinized and counted in the Bürker chamber according to protocol mentioned in sections 4.1.2. and 4.1.3. The mice were then grafted subcutaneously (s.c.) above the right hind limb with various cell lines at $5 \times 10^5$ cells per animal into groups of 5-6 mice.

### 4.3.2. Tumour isolation and primary culture establishment

At the end of experiment, the mice were sacrificed, and the pre-tumour lesions or tumours were removed under sterile conditions. The tumour tissue was mechanically, or even enzymatically disintegrated. The pre-tumour lesion derived from B16 rho0 cells was resected and digested enzymatically (collagenase (250 ng/ml) / DNase (50 ng/ml), 20 min, 37°C). 4T1 sub-lines were selected from tumour by treatment with 6-thioguanine (6TG) as described (Tan et al. 2015). The isolated cells were used to establish primary sub-lines for further study and were cultivated in the presence of 1 mM pyruvate and 50 mg/ml uridine.

## 4.4. Tumour growth evaluation

Tumour growth was monitored twice a week by ultrasound imaging using a Vevo 770 instruments (FUJIFILM VisualSonics). Mice were anesthetized by the isoflurane-oxygen inhalation and then maintained in the anaesthetic state on the heated platform. The area, where the tumour cells were grafted, was shaved, and tumours were scanned with RMV704 or RMV708 scan-heads at 25-55 MHz. The acquired data were further processed using specific software.

## 4.5. Preparation of samples for microscopy

### 4.5.1. Standard samples

#### Life-cell samples

Cells were seeded into Petri dishe with glass bottom and incubated overnight. The next day the Mitotracker or live-cell staining was applied, and the cells were observed in a microscope.

#### Fixed samples

Cells were seeded on high precision cover slips at the to reach the final density and grown overnight. The cells were washed twice with PBS and fixed for 10 minutes in

4% paraformaldehyde. Fixed cells were permeabilized by washing in Wash Buffer three times for 10 minutes. After permeabilization the cells, unspecific signal was blocked by incubated in 300 µl of the 5% normal goat serum (5% NGS) for 30 minutes. After washing with PBS cells were incubated overnight with primary antibodies.

The next day, cover slips were washed three times for 10 minutes in Wash Buffer and incubated for 1 hour in secondary antibodies. After incubation, cells were washed three times with PBS for 10 minutes, once with $H_2O$ and were left to dry in dark. Dry cover slips were mounted to the microscope slides 76x26x1mm with 4 µl of mounting media and fixed by sealing the edges with transparent nail polish.

#### Fixed samples of tissue sections for immunohistochemistry

Isolated tumour tissue was fixed and embedded in paraffin blocks. It was cut into 7µm sections on semi-automated rotary microtome (HistoCore MULTICUT, Leica Biosystems). The sections were deparaffined, rehydrated and the antigen were restored by heating in 10mM citrate buffer. Subsequently the samples were blocked with 10% NGS and labelled with Anti-Ki67 primary antibody. AlexaFluor 594 was used as a secondary antibody. Samples were mounted in VECTASHIELD® Antifade Mounting Medium with DAPI and the signal was detected on fluorescence microscope Nikon Eclipse E400.

## 4.6. Microfluidic PDMS stamp

### 4.6.1. Preparation of the PDMS stamp

Polydimethylsiloxane (PDMS) was prepared using a SYLGARD® 184 kit by mixing a silicone elastomer base (monomer) with a silicone elastomer curing agent. The reagents were mixed up carefully for at least 5 minutes. The arisen bubbles were drained by a brief centrifugation. The unpolymerized PDMS was applied on the master mold (Figure 4.3 – A) in line around the negative pattern as a barrier (Figure 4.3 – B). This barrier allowed to polymerize into the solid polymer on a hot plate prewarmed at 150 °C. The area defined by the barrier was evenly filled with the remaining PDMS. To remove any air bubbles left in the unpolymerized PDMS, it is necessary to place the whole form in a petri dish for 30 minutes to an hour in the desiccator (Figure 4.3 – C) and let the air bubbles disappear (Figure 4.3 – D). Subsequently, the master mould was transferred once again to the hot plate

prewarmed to 150 °C where the PDMS polymerized for about 5 minutes (Figure 4.3 – E). After cooling, the polymerized PDMS (Figure 4.3 – F) was transferred to a sterile petri dish in the flow box. The holes for pipetting the cells were made with the punch needle into the polymer at the points of inlets and outlets (Figure 4.3 – G). Finally, the individual chips were cut from the polymerized PDMS. The chip surface was hydrophilized by glow discharge plasma before use.

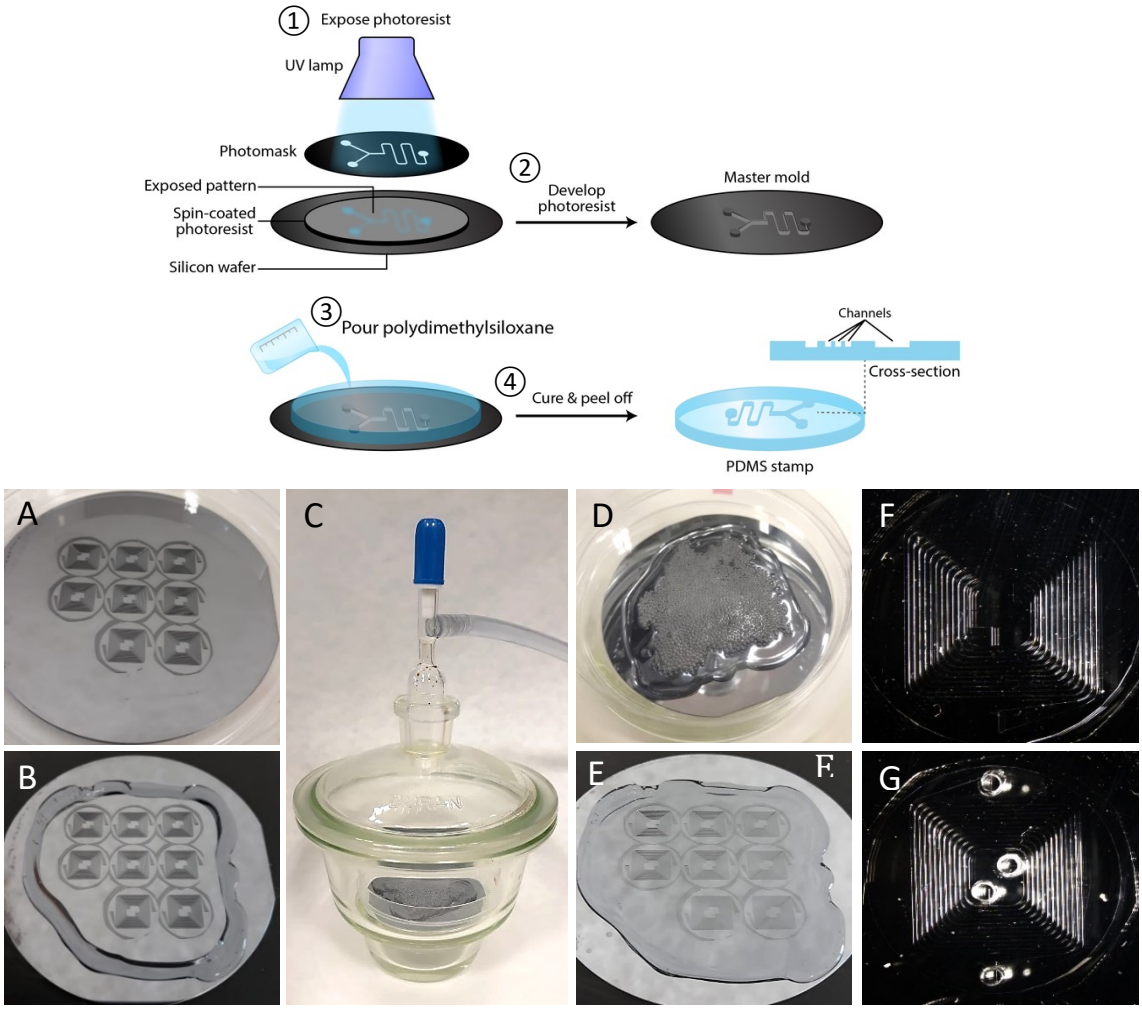


***Figure 4.3: Scheme of photolithography.*** *A reverse mould is created by shining a UV light through a mask, which cures a photosensitive epoxy resist below it (1). When the uncured photoresist is washed away, this leaves a master mould (2) with which a polydimethylsiloxane (PDMS) stamp is created (3,4). (http://biomechanicalregulation-lab.org/photolithography/)*

### 4.6.2. Preparation of co-culture samples for microscopy in PDMS stamp device

#### Life-cell samples

The petri dish was treated with poly-L-lysine for 10 minutes. After plasma discharge treatment, the PDMS stamp was attached to bottom of the petri dish and cells were pipetted into the microfluidic chip as was described in the section 4.4.2.1. The cells were incubated overnight in the chip. Next day the chip was removed and cells were observed using confocal microscope.

#### Fixed samples

The high precision cover slips were treated with poly-L-lysine for 10 minutes. After plasma discharge treatment the PDMS stamp was attached to the cover slip. Two cell lines were pipetted into different channels of microfluidic chip through the inlets. The cells were incubated in the microfluidic chip overnight. The next day the PDMS stamp was removed. After next 24 hours cells were fixed as described in the section 4.5.1.1.

## 4.7. Microscopy

Microscopy experiments were done in the Imaging Methods Core Facility in BIOCEV or Institute of Molecular Genetics (IMG) with a help of Mgr. Marie Olšinová PhD., Mgr. Ivan Novotný PhD., Mgr. Markéta Dalecká and most of all with help of Mgr. Jaromíra Kovářová PhD.

### 4.7.1. Confocal microscopy

All confocal images of B16 sub-lines were acquired using Leica TCS SP5 AOBS Tandem (Obj. HCX PL APO 63x/1,30 GLYC CORR. 37°C) confocal microscope equipped with the LAS AF software. Confocal images of the 4T1 sub-lines and co-cultures were acquired using Leica SP8 SMD-FLIM (objective: HC PL APO 63x/1.2 W Corr CS2) confocal inverted microscope.

### 4.7.2. Stimulated emission depletion (STED) microscopy

The B16 sub-lines samples were visualized using Leica TCS SP8 STED 3X microscope equipped with 660 nm STED depletion laser and fitted with the LAS X 64 bit package software with LAS AF SP8 Dye Finder, 3D visualization, deconvolution and co-localization module. The STED images of 4T1 sub-lines were acquired on Abberior STED 775 QUAD Scanning microscope equipped with Nikon

CFI Plan Apo Lambda objective (60x Oil, NA 1.40). The labelled proteins were illuminated by pulsed 561 nm and 640 nm lasers and depleted by pulsed 775 nm STED depletion laser of 2D donut.

### 4.7.3. Correlative light electron microscopy (CLEM) microscopy

The cells were seeded into gridded 35 mm dish with glass bottom (MatTek Corporation) and after 24 hours were labelled with MitoTracker (250 nM, 30 min) and SirTubulin (1:1000 diluted, 1 hour) and prefixed with a mix of PFA and glutaraldehyde. For light microscopy, confocal and DIC images were acquired using Leica SP8 SMD-FLIM (Obj. HC PL APO 63x/1.2 W Corr CS2) confocal inverted microscope. Whole specimens were viewed using the Tile Scan function, and the positions of TNTs connecting two cells were localized. The coordinates of the TNTs in the specimen were noted based on the grid of the MatTek dish. After light microscopy data acquisition, the cells were post-fixed with osmium tetroxide, then dehydrated in ethanol series and embedded in epoxy resin. Subsequently, the areas of interest have been identified according to the grid imprinted into the block and visualized by focused ion beam – scanning electron microscopy FIB-SEM. The FIB-SEM data were acquired using FIB-SEM DualBeam microscope FEI Helios NanoLab 660 G3 UC.

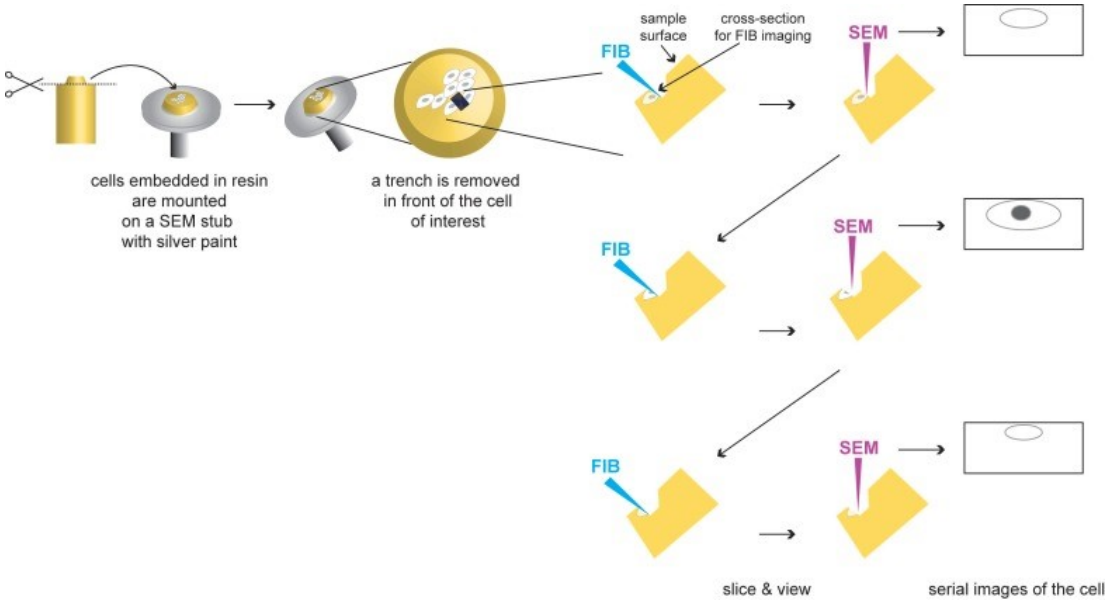


***Figure 4.4: Focused ion beam scanning electron microscopy (FIB-SEM).*** *Milling with a focused ion beam (blue) and imaging are performed within a dual-beam SEM (pink) (Romero-Brey and Bartenschlager 2015) .*

### 4.7.4. Microscopy images evaluation and post-processing

The confocal and STED images were stabilized for drift and deconvolved with Huygens Professional version software 17.04 (Scientific Volume Imaging) using Classic Maximum Likelihood Estimation algorithm and processed by FiJi ImageJ software. The CLEM/FIB-SEM data were analyzed using Amira 6 software.

## 4.8. Evaluation of mtDNA level

Total DNA was extracted using the Wizard® Genomic DNA Purification Kit (Promega). 50 ng of DNA was subsequently diluted in water to total volume 4.5 µl, and 0.5 µl of the combined 10 mM forward and reverse primers added (for mtDNA, mMito1 primers; for nDNA mB2M1 primers). Then 5 µl of 2xRT2 SYBR Green qPCR Mastermix (Qiagen) were added and the reaction was run on the Eco qPCR System (Illumina). The setting of Eco qPCR is described in (Bajzikova et al. 2019).

## 4.9. Evaluation of protein level

For the evaluation of protein level Pierce™ BCA Protein Assay (ThermoFisher) was used according to manufacturer´s protocol.

## 4.10. Evaluation of ATP level

ATP was determined in cells seeded at $10^4$ per well in 96-well plates in medium contained either 4.5 g/L glucose and 50 mM or no 2DG, which acts as it acts as a competitive inhibitor of glucose-6-phosphate production by glycolysis. The results were evaluated using a luciferase-based assay (CellTiter-Glo Luminescent Assay, Promega) and normalized to the total protein level in cell lysates assessed by the BCA method described above.

## 4.11. Evaluation of NADH/$NAD^+$ ratio

The 4T1 parental and rho0 cells were seeded at concentration 1.5 x $10^4$ per well in white-walled 96-well plates. The NADH/$NAD^+$ ratio was evaluated using the bioluminescent NADH/$NAD^+$ Glo Assay (Promega). Luminescence intensity was acquired with a Tecan Infinite M200 microplate reader.

## 4.12. Statistical analysis

Presented data are mean values ± SEM of at least three independent measurements provided in triplicates. In mouse experiments, groups of 5-6 animals were used. Two-way Anova was used for multiple comparisons where applicable, using GraphPad Prism software. Images from microscopy are representative of three independent experiments.

# 5. Results

## 5.1. Restoration of mtDNA in B16 rho0 cells mediated by the transfer of intact mitochondria

Tan et al. have shown in their work B16 rho0 cells, that were injected s.c. into syngeneic C57BL/6J mice formed tumours with a 2–3-week delay compared to parental B16 cells. Next generation sequencing confirmed the host origin of mtDNA in the primary tumour cells grown from the original rho0 cells. (Tan et al. 2015).

### 5.1.1. Stable Transfection of B16 rho0 cells

B16 and mtDNA deficient B16rho0 cells were stably transfected with the mammalian expression vector pTagBFP-H2B (Evrogen) encoding TagBFP-H2B fusion protein. The vector backbone contains among others the immediate early promoter of cytomegalovirus ($P_{CMV\ IE}$) for protein expression and the SV40 origin for replication in mammalian cells expressing the SV40 T-antigen. The SV40 early promoter ($P_{SV40}$) provides neomycin resistance gene ($Neo^r$) expression to select stably transfected eukaryotic cells using G418. B16 and B16 rho0 BFP positive cells were then examined by confocal microscope together with un-transfected B16 rho0 cells, which were used here as non-fluorescence control. The confocal images shown below document a successful transfection and the expression of BFP in the nuclei of the appropriate cell lines.

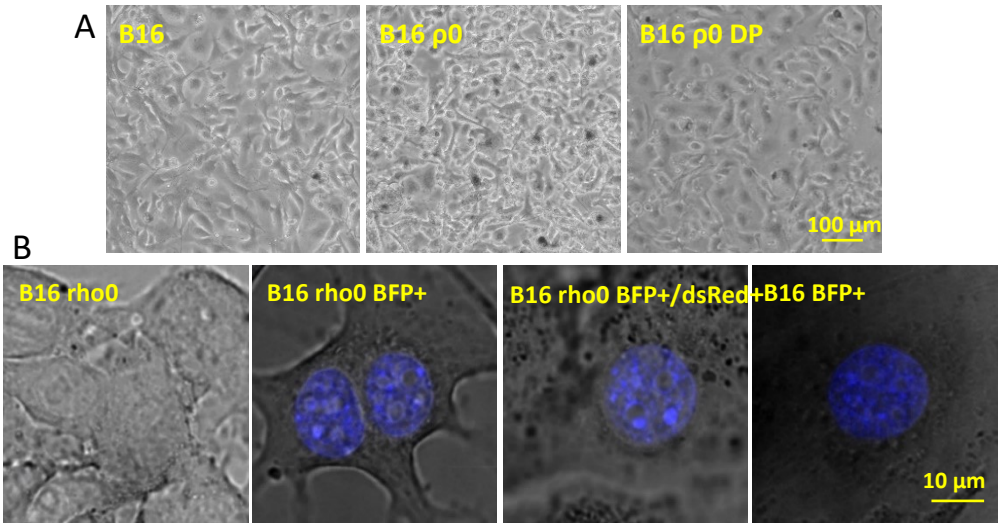


***FIGURE 5.1****.: Morphology of B16 parental cells and derived B16 rho0 and B16 rho0 DP cell lines was observed by Leica DMIL LED microscope and the images were processed in LAS v4.5 software (A). The transfected cells were observed in FluoroBrite™ DMEM Medium using Leica TCS SP5 AOBS Tandem confocal microscope (Obj. HCX PL APO 63x/1,30 GLYC CORR.) equipped with the LAS AF software (B). Figure 5.1. – B shows deconvolved images of one plane.*

### 5.1.2. Transfer of mitochondria from donor cells to recipient B16 rho0 cells *in vivo*

Transgenic C57BL/6Nsu9-DsRed2 mice with dsRed fluorescent mitochondria were used to observe the transfer of mitochondria *in vivo*. B16 rho0 cells were transfected with a plasmid expressing blue fluorescent protein targeting nuclei (nBFP) and subsequently injected s.c. into C57BL/6Nsu9$^{DsRed2}$ mice. 11 days later the mice were sacrificed, and the pre-tumour lesion was isolated. The tumour tissue was enzymatically disintegrated into single cell suspension which was then sorted for the double positive (DP) cell population. The DP B16 rho0 cell population reported both fluorescence signals – BFP signal from the recipient cell nucleus and dsRed signal from the host cell mitochondria. In the tumour single cell suspension, 0.52% were formed by the double-positive (BFP+/dsRed+) cell population. The sorted DP B16 rho0 cells were immediately allowed to attach and inspected by confocal microscope several hours later. The microscopy results shown in 5.2 document the transfer of mitochondria from host somatic cells to tumour cells with depleted mtDNA, showing both fluorescent signals (BFP and dsRed) within a single B16 rho0 cell.

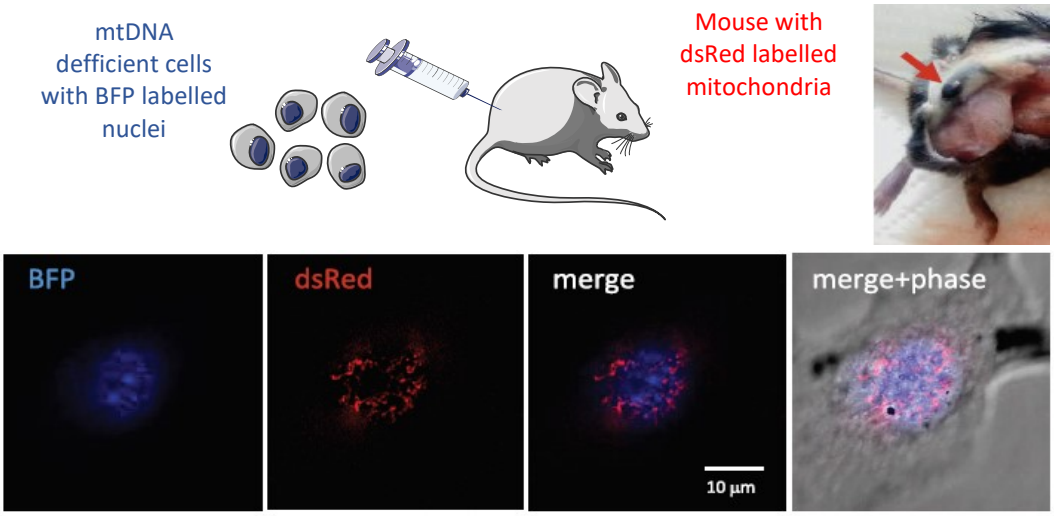


***FIGURE 5.2: In vivo detection of mitochondrial transfer from donor MSC cells to recipient B16 rho0 cells.*** *Transgenic mice with dsRed labelled mitochondria were s.c. injected with $10^6$ B16 rho0 cells, that stably expressing nBFP. 11 days later a mouse was sacrificed, the tumour tissue was digested into a single-cell population and sorted for DP cells, containing blue fluorescent nuclei and red fluorescent mitochondria. The sorted cells were allowed to attach and subsequently observed by confocal microscope. The image was acquired on Leica TCS SP5 AOBS Tandem confocal microscope (Obj. HC PL APO 63x/1,40 OIL, CS2) equipped with the LAS AF software. and shows maximum intensity Z-projection of a representative DP cell. These data were published by Dong et al., 2017.*

### 5.1.3. Tumour formation capacity of parental B16 and B16 rho0 cells

B16 parental, rho0 and the tumour derived rho0 DP cells were grafted s.c. into syngeneic mice to investigate the capacity of the individual cell-lines to form tumours. The rho0 cells started to form the tumours with almost 3-week delay compared with parental cells, while the rho0 DP cells were much more aggressive and formed tumours at the same time interval as the parental cells. The tumours (FUJIFILM VisualSonics).

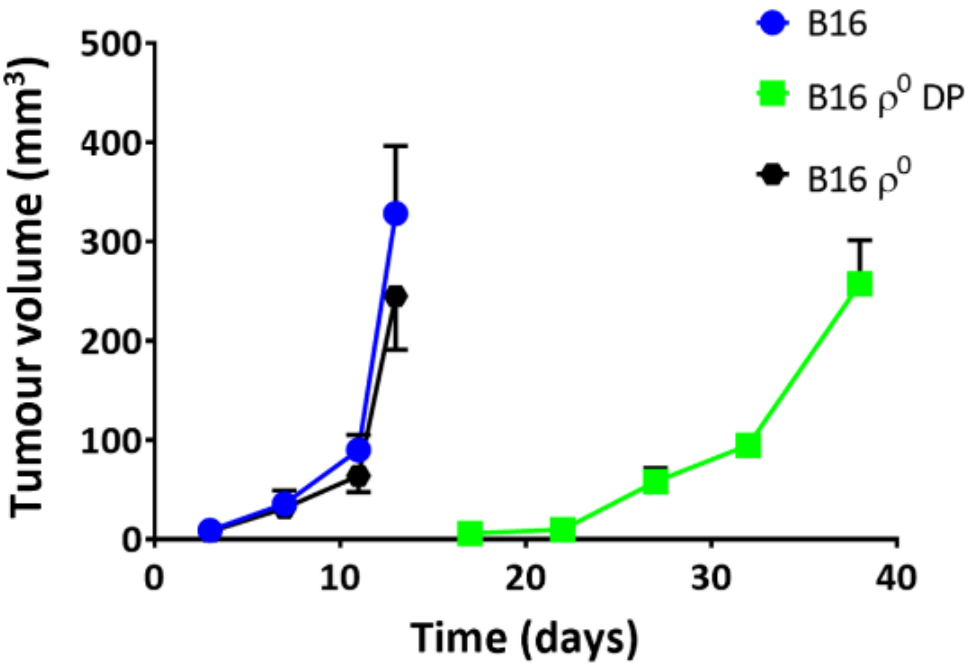


***FIGURE 5.3: Comparison of growth curves of tumours derived from parental, rho0 and rho0 DP B16 melanoma cancer cells.*** *B16 cells and their rho0 and rho0 DP counterparts were grafted s.c. into syngeneic mice. The graph shows data from three independent measurements and the results are expressed as mean ± SEM. The tumour growth curves were published by Dong et. al, 2017*

### 5.1.4. Evaluation of ATP levels in B16 sub-lines

B16 sub-lines were analysed for ATP levels in the absence and presence of 50 mM 2DG in glucose containing DMEM medium (4.5 g/L glucose) supplemented with 50 mg/ml uridine and 1 mM pyruvate using a luciferase-based ATP detection kit and a microplate reader. The results were normalized to the total protein level in cell lysates. The results shown in Figure 5.4 indicate that glycolysis contributed to ATP generation with 50% in parental and rho0 DP cells, where mitochondrial transfer predated, whereas in rho0 cells glycolysis contributed to ATP generation by 100%, since these cells provide no OXPHOS.

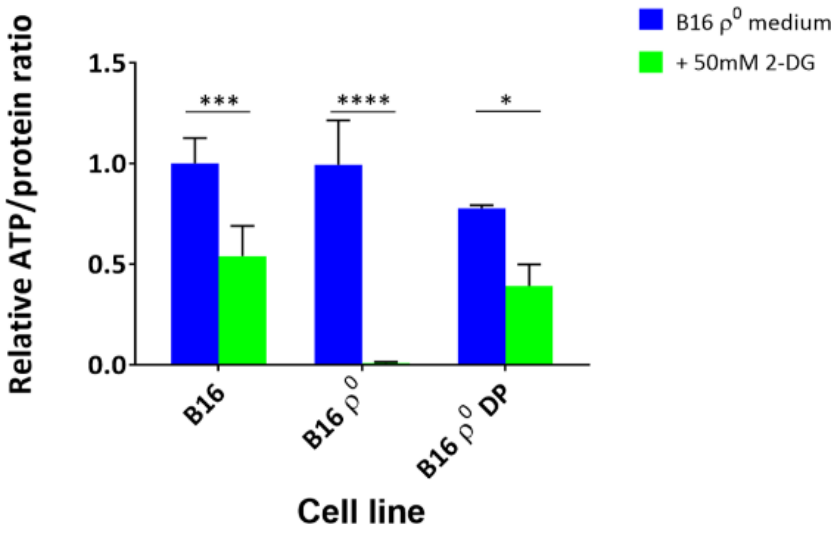


***FIGURE 5.4: ATP level was determined in B16 sub-lines****. B16, B16 rho0 and B16 rho0 DP cells were seeded each at a concentration of $10^4$ per 100 ul per well in white walled 96-well plates using a luciferase-based assay. Tecan Infinitive M200 microplate reader was used to measure luminescence. The graph shows data from three independent measurements and the results are expressed as mean ± SEM (Adjusted P values – '*' = 0,0118; '***' = 0,0008; '****' <0,0001)*

### 5.1.5. Determination of mtDNA content in B16 sub-lines by STED microscopy

B16, B16 rho0 and the established B16 rho0 DP cell lines were immunostained for DNA and mitochondrial transcription factor A (TFAM) or mitochondrial import receptor subunit (TOMM20) and observed by STED microscopy to determine the content of mtDNA in form of mitochondrial nucleoids. The results shown in representative micrographs below support the previous results showing similar levels of mtDNA in both – parental and rho0 DP cells, while no mitochondrial DNA as well as TFAM signal could be detected in B16 rho0 cells. The STED images also confirm the localisation of mitochondrial nucleoids within the mitochondria and their co-localisation with the TFAM protein, which binds to mitochondrial DNA and which is involved in maintenance and processing of mtDNA as well as packaging of mtDNA into mt-nucleoids.

A

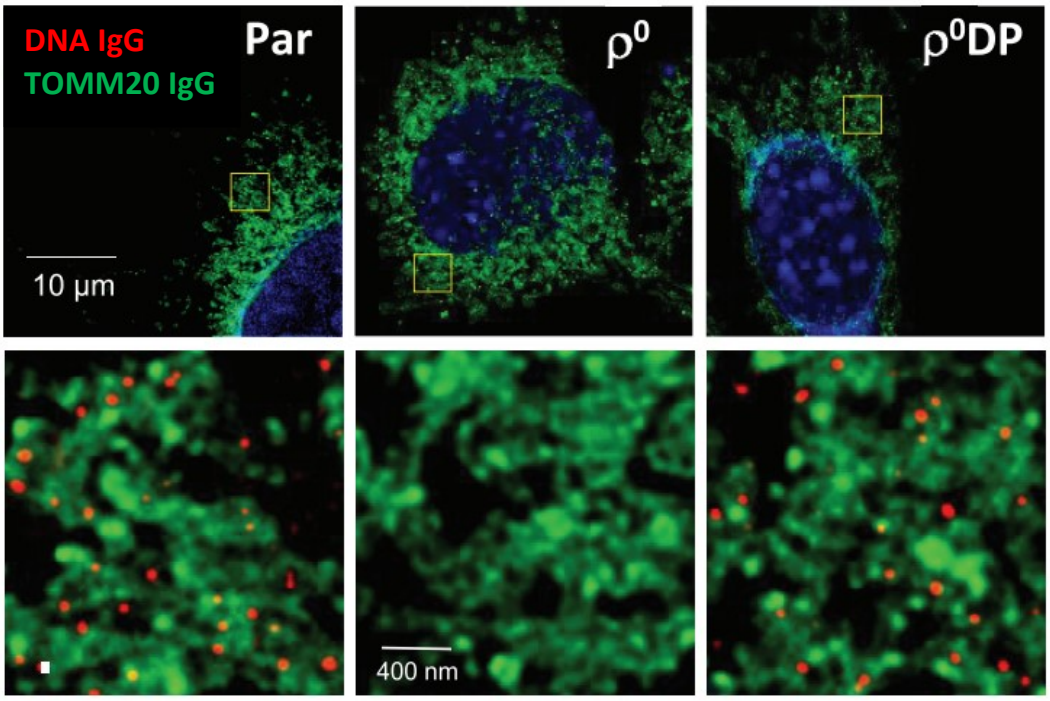

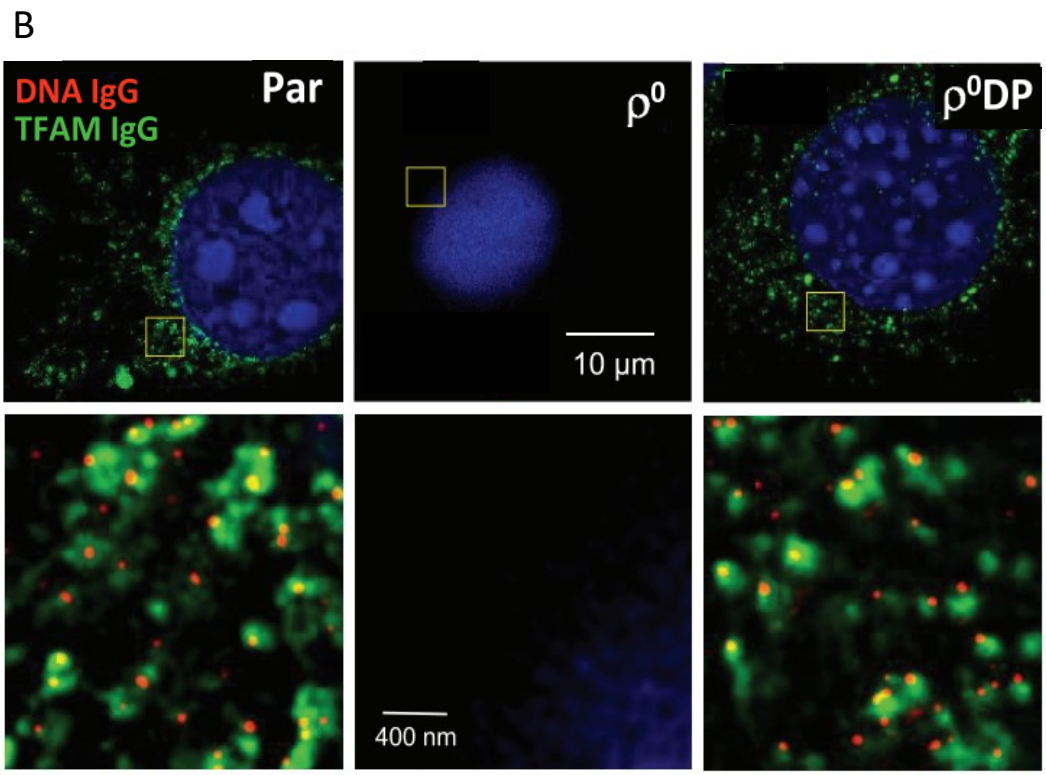


***FIGURE 5.5: Distribution of mitochondrial nucleoids in B16 sub-lines.*** *B16, B16 rho0 and B16 rho0 DP cells were co-stained for mitochondrial DNA (shown in red) and TOMM20 (A) or TFAM (B) protein (shown in green). The upper panels show the majority of individual cells while the lower panels represent a higher magnification of the region of interest indicated by the yellow boxes. TOMM20 and TFAM were stained with Alexa Fluor488 goat anti-rabbit IgG secondary antibody and DNA was stained with Alexa Fluor555 goat anti-mouse IgM secondary antibody. The cell nuclei were labelled with Hoechst 33342. The samples were visualized using Leica TCS SP8 STED 3X microscope equipped with 660 nm depletion laser and the LAS X 64 bit package software with LAS AF SP8 Dye Finder. These micrographs were published by Dong et al., 2017.*

## 5.2. Characterisation of the initial phase of primary tumour formation

To characterise the period of the initial tumour growth dormancy, the cells isolated at different time points from the primary tumours formed from the original rho0 cells were investigated in detail. The relevant experiments were carried out using 4T1 derived sub-lines.

4T1 rho0 cells were grafted s.c. into Balb/c mice in a concentration of $10^6$ cells per 100 ul PBS per mouse. The formed tumours were excised on days 5, 10, 15, 20, 25 and 60, whereby 5-6 animals were used in each time point. The cancer cells were subsequently isolated from the primary tumour tissue and cultivated in the presence of 6-TG as described by Tan et al. 2015 (Tan et al. 2015).

### 5.2.1. Tumour formation capacity of parental 4T1 and 4T1 rho0 cells

4T1 parental and the derived rho0 cells were grafted s.c. into syngeneic mice. The rho0 cells started to form the tumours with a with a lag of 3 week compared to the parental cells, with noticeable tumours appearing on day 20–25. The tumours were monitored, and their volume calculated using the USI device Vevo770 (FUJIFILM VisualSonics) (Figure 5.6 – B). The experiments were terminated when the tumour volume reached a size of about 1 000 $mm^3$. Delayed tumour formation suggests that the preceding mitochondrial transfer and the subsequent restoration of mitochondrial functions are essential for tumour formation initiation.

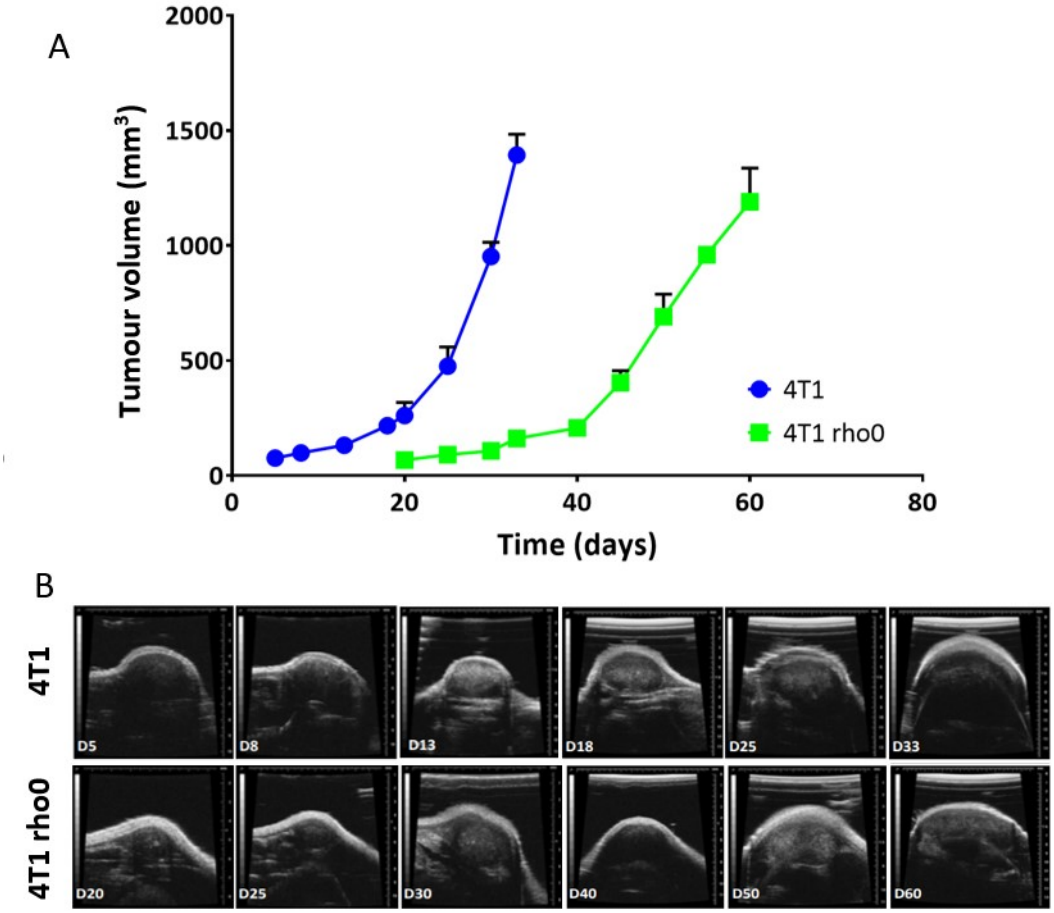


***FIGURE 5.6: Tumour formation ability of 4T1 parental and rho0 breast cancer cells.*** *4T1 cells and their and their rho0 derived sub-line were grafted into Balb/c mice and the tumour growth was monitored by Vevo770 USI (B). The above graph of tumour growth curves (A) shows data from three independent measurements and the results are expressed as mean ± SEM. The curves of tumour growth were published by Bajzikova et al., 2019.*

### 5.2.2. Evaluation of cell proliferation in tumour tissue

Parental 4T1 and 4T1 rho0 derived tumours were fixed with PFA and embedded in paraffin blocks. Subsequently, immunohistochemical tissue sections stained for Ki67 were prepared. Figure 5.7 shows gradually increasing Ki67 signal linked to cell proliferation between rho0 D5 and rho0 D15 tumours and a similar proliferation rate in rho0 D20 and rho0 D25 tumours as observed for the parental 4T1 tumours. These data correspond with the delay in tumour formation shown in Figure 5.6.

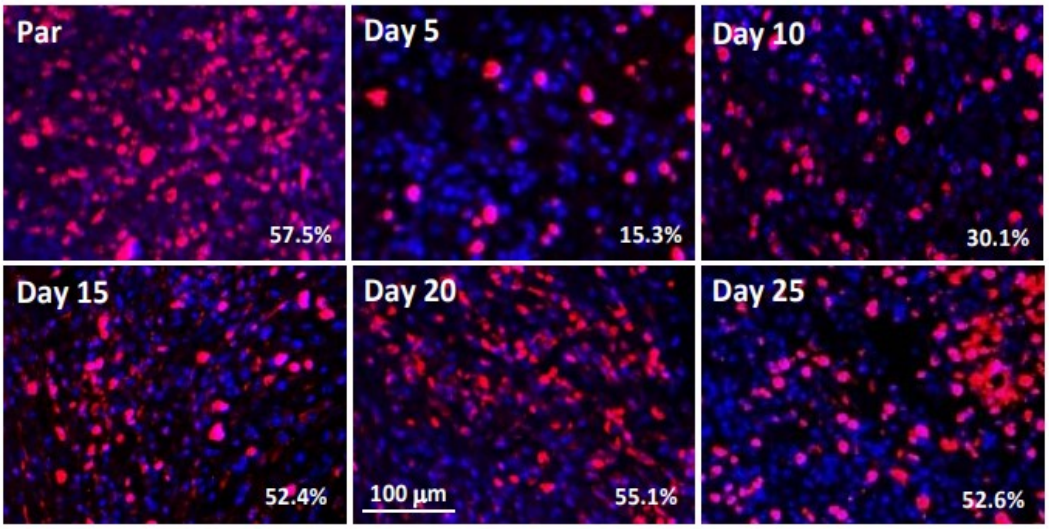


***FIGURE 5.7: Proliferating cells in 4T1 derived tumour tissue sections visualised by Ki-67 primary and AlexaFluor 594 secondary antibody.*** *The samples were observed with fluorescence microscope Nikon Eclipse E400 (CFI PL APO DM40X OIL). The numbers in the right bottom corner indicate percentage of Ki67-positive cells in each sub-line. The presented fluorescence images are representative of three micrographs. These data were published by Bajzikova et al. 2019.*

### 5.2.3. Morphology and growth of 4T1 sub-lines in normal medium and medium supplemented with 2-DG

Parental 4T1 cells and cells derived from primary 4T1 rho0 tumours at different time points were cultivated for 24 h in medium supplemented with 50 mM 2-DG. 2-DG is a glycolytic inhibitor. The results documented in fig. 5.8 indicate that rho0 cells and the derived cells with lower mtDNA content are more sensitive to the effects of 2-DG in contrast to the parental 4T1 cells and cells with higher mtDNA content. These data correspond with the mtDNA levels measured by Bajzíková et al (Bajzikova et al. 2019).

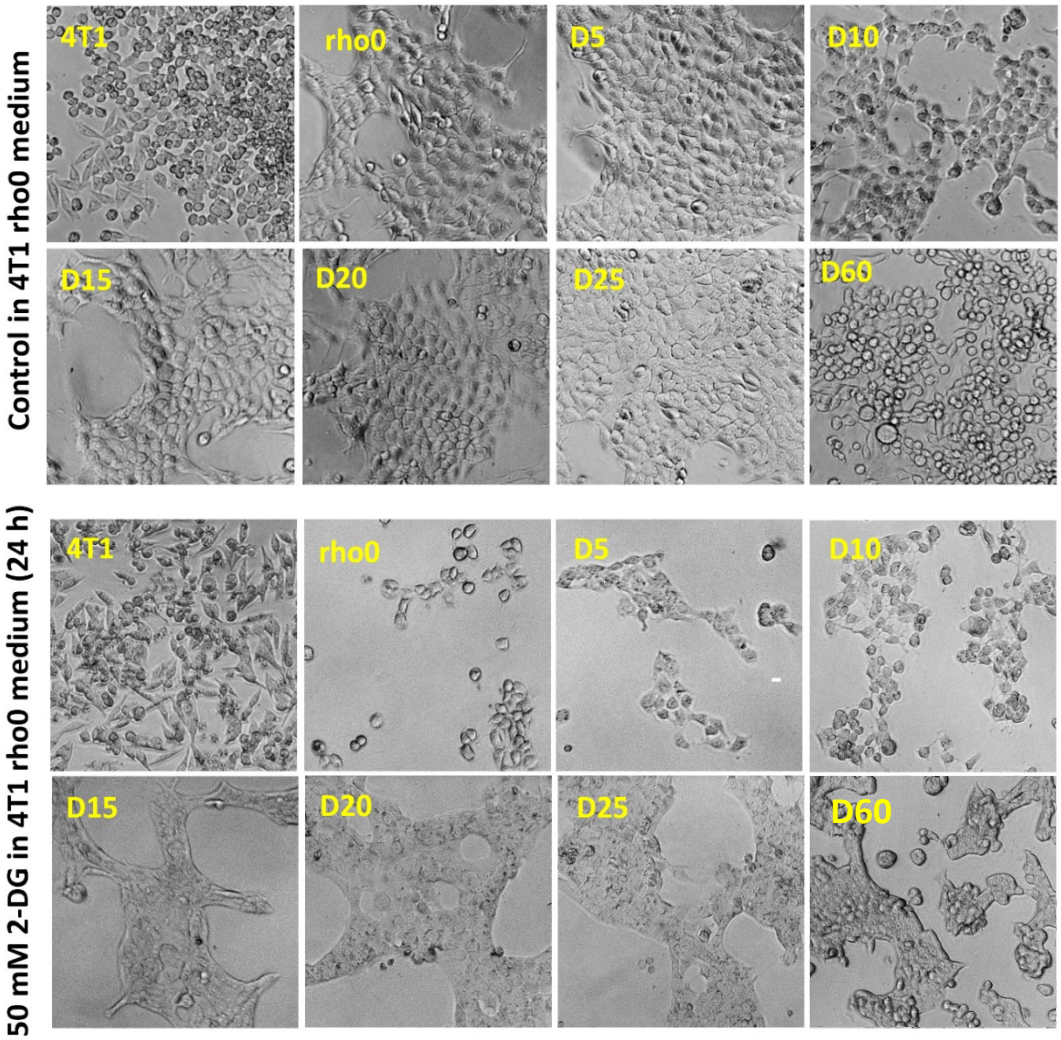


***FIGURE 5.8: Comparison of cellular morphology of cells cultivated in standard 4T1 rho0 medium and in 4T1 rho0 medium supplemented with 50 mM 2-DG.***

*The 4T1 sub-lines (4T1, 4T1 rho0 and 4T1 rho0 D5-D60) were cultivated for 24 h either in 4T1 rho0 medium or in 4T1 rho0 medium supplemented with 2-DG and subsequently live cell images were obtained by Leica DMIL LED microscope and the images were processed in LAS v4.5 software. The presented images are representative of three.*

### 5.2.4. Evaluation of ATP levels an NADH/NAD⁺ ratio in tumour derived 4T1 sub-lines

Individual tumour derived cell lines were evaluated for ATP levels in in medium containing 50 mM 2DG at 4.5 g/L glucose, supplemented with 50 mg/ml uridine and 1 mM pyruvate, and the results were expressed relative to total ATP in parental cells. The results presented in Fig. 5.9 are relative to total ATP/protein ratio in parental 4T1 cells and they document that glycolysis contributed to ATP generation by ≈30% in parental and 90% in D0–D10 cells.

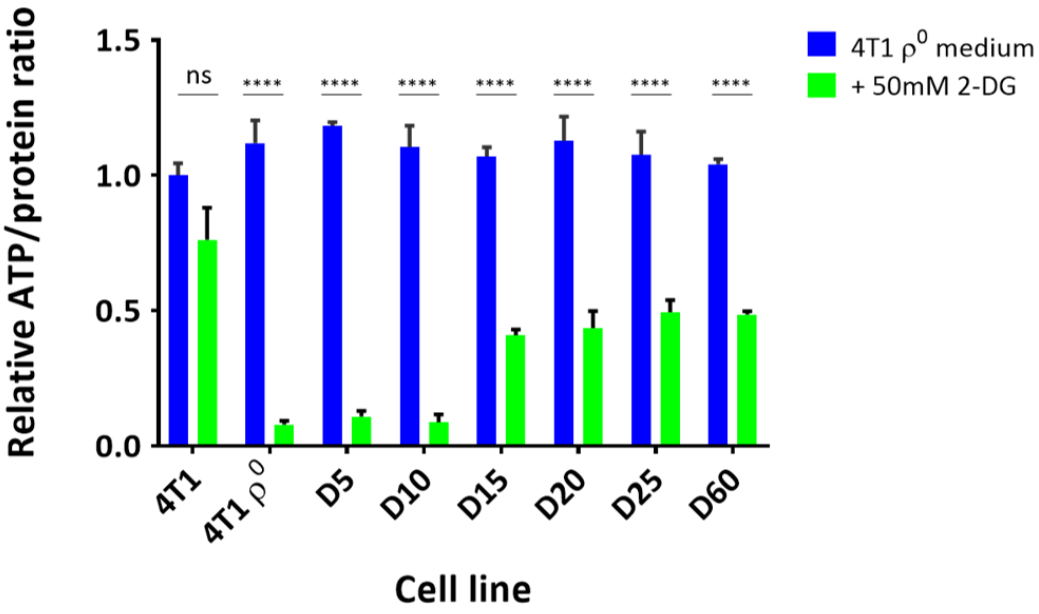


***FIGURE 5.9: Relative ATP/protein ratio was determined in the 4T1 sub-lines*** *seeded at a concentration of $10^4$ cells per 100 ul and well in white walled 96-well plates using a luciferase-based assay. Tecan Infinitive M200 microplate reader was used to measure luminescence. The graph shows data from three independent measurements and the results are expressed as mean ± SEM (Adjusted P values –'****' <0,0001). These data were adapted from Bajzikova et al., 2019.*

Oxidized and reduced nicotinamide adenine dinucleotides (NAD+ and NADH) were assessed in the 4T1 tumour-derived cell lines by a commercial luciferase-based assay and a microplate reader. The NADH/NAD⁺ ratios measured in the individual tumour-derived 4T1 sub-lines confirmed the tendency of the cells to return to basal respiration levels as measured for the parental 4T1 cells. These data correspond with the respiration levels measured by Bajzíková et al (Bajzikova et al. 2019).

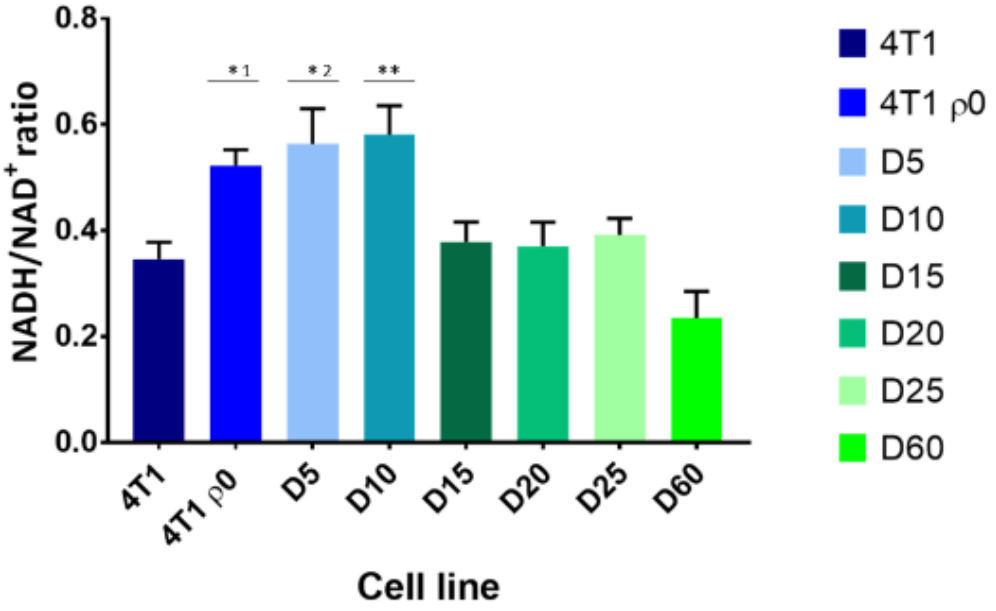


***FIGURE 5.10: NADH/NAD⁺ ratio was investigated*** *in 4T1 sub-lines using a luminescence-based assay and a Tecan Infinite M200 microplate reader was used to measure luminescence. The graph shows data from three independent experiments and the results are expressed as mean ± SEM (Adjusted P values – '* 1' = 0,0288; '* 2' = 0,0181; '**' = 0,0097). These data were published by Bajzikova et al., 2019.*

### 5.2.5. Visualisation of mtDNA distribution in form of mt-nucleoids in the analysed 4T1 sub-lines by STED microscopy

The individual sub-lines derived at different time points from the primary tumours grown from the 4T1 rho0 cells were further studied for their mtDNA distribution. The cells were immunostained for DNA and mitochondrial transcription factor A (TFAM) or DNA and mitochondrial import receptor subunit (TOMM20) and inspected by STED microscopy to determine the content of mtDNA in mitochondrial nucleoids. Representative micrographs shown in Fig. 5.11 support the above described results. The number of mt-nucleoids is gradually increasing from rho0 D5 to rho0 D15 cells. Cells isolated from rho0 D20 – rho0 D60 tumours provide a comparable level of mt-nucleoids as documented for the parental 4T1 cells. As expected, the 4T1 rho0 cells do not contain mtDNA and thus they show reduced levels of TFAM protein, which cannot bind to mtDNA.

A

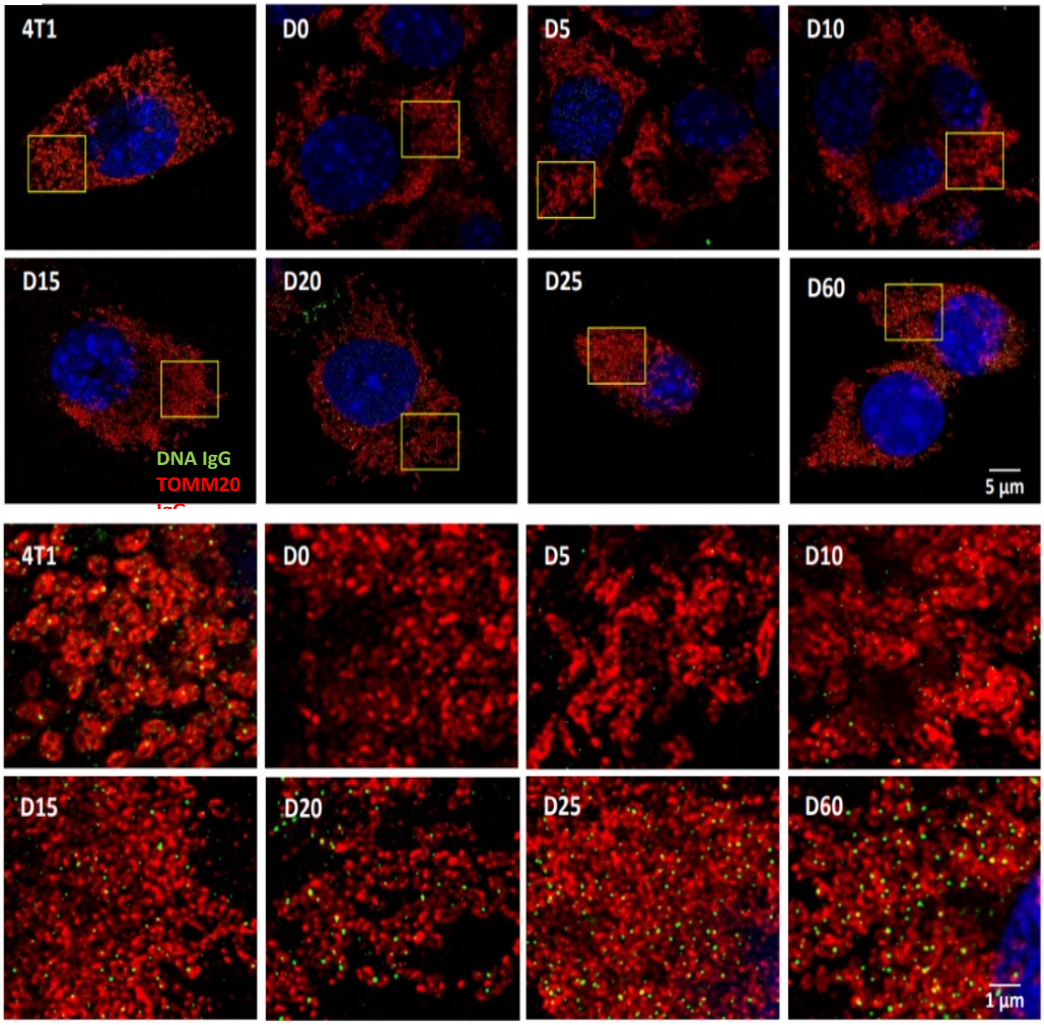

B

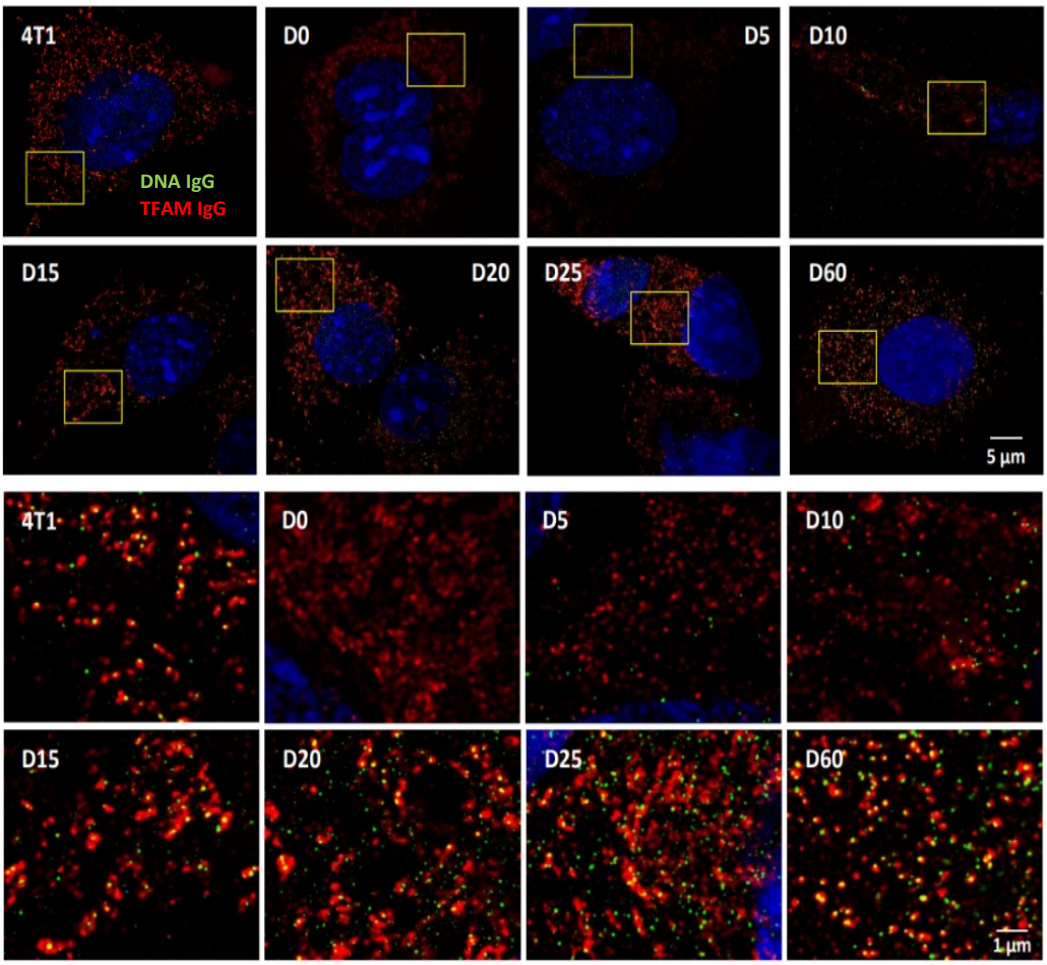


***FIGURE 5.11: Distribution of mitochondrial nucleoids in 4T1 sub-lines****. Mitochondrial proteins TOMM20 (A) and TFAM (B) were stained by immunofluorescence and the representative micrographs above show the co-localization with DNA staining, which represents the mtDNA of mitochondrial nucleoids. The upper panels show the majority of individual cells while the lower panels represent a higher magnification of the region of interest indicated by the yellow boxes. TOMM20 and TFAM were stained with Abberior STAR 580 goat ant-rabbit IgG secondary antibody and DNA was stained with Abberior STAR RED goat anti-mouse IgG. Nuclei were labelled with Hoechst 33342. Labelled samples were illuminated by pulsed 561 nm and 640 nm lasers and depleted by pulsed 775 nm STED depletion laser of 2D donut, using Abberior Instruments STED microscope. The maximal intensity projection of 500 nm Z-stack is shown. These micrographs were published by Bajzikova et al., 2019.*

## 5.3. Intercellular transfer of intact mitochondria

### 5.3.1. Mitochondrial transfer mediated through TNTs studied in a in vitro co-culture system

The stably transfected 4T1 rho0 cells expressing GFP in plasma membrane and BFP in nuclei were co-cultivated with MSCs expressing dsRed protein in mitochondria for 24 h. The cells were subsequently fixed with 4% PFA, permeabilised and stained for alpha-tubulin. The representative confocal image shown in Fig. 5.12 documents the transfer of intact mitochondria mediated by the TNT structure interconnecting the rho0 cell that expresses GFP (green) in its plasma membrane and BFP in cell nucleus with a MSC, which expresses dsRed fluorescent protein in its mitochondria (red). The yellow box represents a higher magnification of the region of interest, showing a TNT section containing tubulin fibres with aligned dsRed fluorescent mitochondria. This indicates the possible role of microtubules in mitochondrial transfer. Most importantly, the dsRed positive mitochondria can also be detected in the original 4T1 rho0 cell stably expressing GFP in its plasma membrane and BFP in the nucleus. The observed phenomenon documents the transfer of mitochondria from a MSC into a rho0 cell.

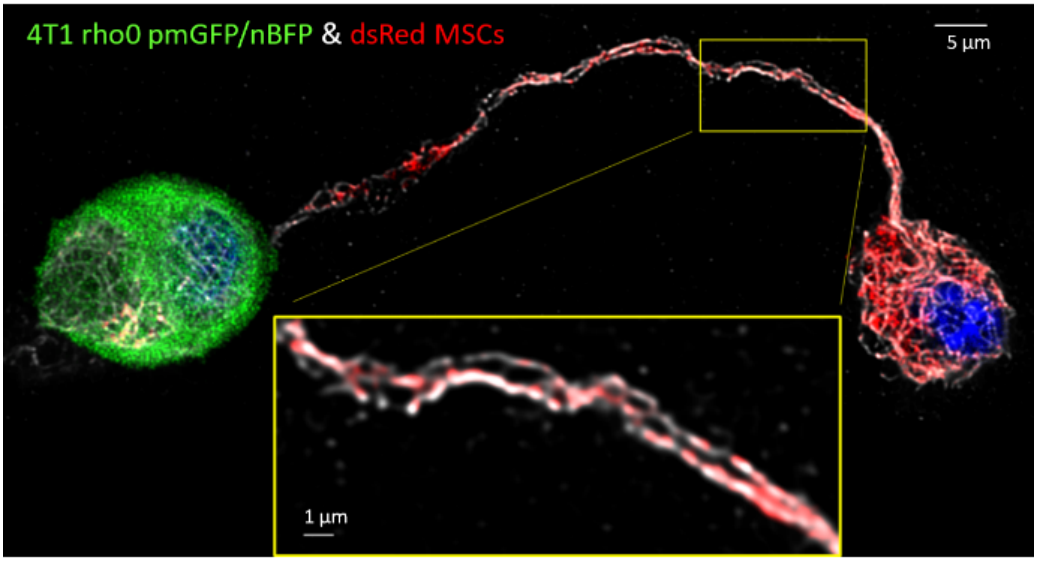


***FIGURE 5.12: Mitochondrial transfer in co-culture of 4T1 rho0 pmGFP/nBFP and dsRed MSCs.*** *The cells were fixed and permeabilised and alpha tubulin was visualised using an Anti-alpha-tubulin primary antibody and the appropriate AlexaFluor 647 secondary antibody (gray). The nuclei were stained with Hoechst 33342 (blue). The co-culture was observed by Leica SP8 SMD-FLIM confocal microscope using (Obj. HC PL APO CS2 63x OIL). The image shows maximal intensity projection (MIP) and was deconvolved using the Huygens Professional software - version software 17.04 (Scientific Volume Imaging). One representative image of three independent experiments is shown.*

### 5.3.2. Mitochondrial transfer by TNTs in co-cultures using microfluidic PDMS chip

In a co-culture system consisting of two different cell types an enormous disorder predominates. To get control over the system and to be able to easily detect TNTs formed between the two cell types a special microfluidic PDMS stamp was developed consisting of two channels separated by an inter-channel space.

4T1 rho0 cells stably expressing diffuse GFP in their cytoplasm were seeded at 1,5 x $10^4$ cells/µl in one channel of the microfluidic device while MSCs expressing dsRed fluorescent protein in their mitochondria were seeded in the second channel at the same concentration. The cells were allowed to attach to the coverslip surface overnight, then the device was removed and the cells, separated by the chip, were co-cultivated for further 24 h. The cells in the separated channel area as well as the inter-channel space were subsequently inspected for TNTs formed between both cell types. Fig. 5.13 documents the separation of the two different cell lines in two distinct channels in the PDMS stamp. The image does not show the inter-channel area with inter-connecting TNTs formed between the two different cell lines, since the developed co-culture device was at that time not fully operational and an optimalisation was required. This could not be achieved here due to the limited time of the diploma thesis.

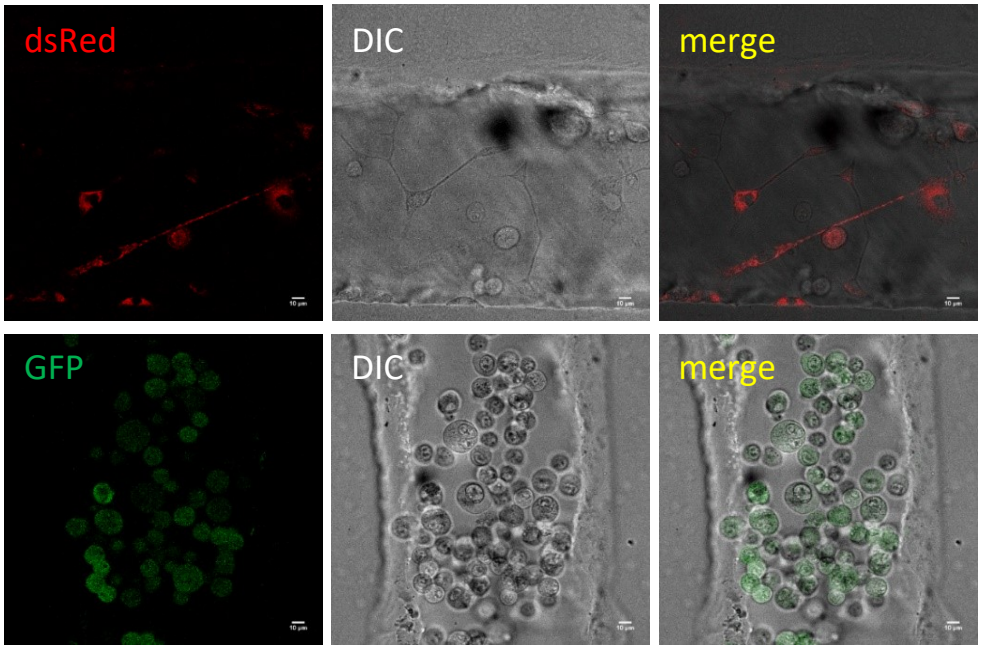


***FIGURE 5.13: Controlled co-culture of dsRed fluorescent MSCs and 4T1 rho0 cells expressing GFP in cytoplasm seeded in a PDMS microfluidic device.*** *The image shows the two separated channels in the microfluidic stamp device either with attached MSCs (red) or with 4T1 rho0 cells (green). The inter-channel area is not shown here. Representative image of three was acquired by Leica SP8 SMD-FLIM confocal microscope (Obj. HC PL APO CS2 63x WI) and shows the maximal intensity projection of a 500 nm Z-stack.*

### 5.3.3. Reconstruction of 3D structure of TNTs by CLEM/FIB-SEM

The next part of the work focused on the analysis of the 3D structure of a TNT formed between rho0 cancer cell and MSC. CLEM/FIB-SEM should also provide information about the mechanism and regulation of mitochondrial transfer, whether mitochondria are transported only in one way, i.e. from MSC towards rho0 cell, or whether the transport proceeds in both directions. It should also obvious, whether the mitochondria within the analysed part of TNT contain cristae or not and weather they have prolonged or rounded shape and if they are localised on tubulin fibres during transfer.

Since the PDMS co-culturing device was not completely established so far, the preliminary data were obtained using an MSC monoculture.

The MSCs were cultivated in glass bottom MatTek dish with grid for 24 hours. Subsequently, living cells were stained with the fluorescence dyes SiR-Tubulin (for 1 hour) and MitoTracker (for 30 minutes) and observed by confocal microscope. Then the cells were fixed with 2,5% GA and 1% PFA and again inspected by confocal microscope, as documented in Figures 5.14 and 5.15 – A. The area of interest showing two MSCs interconnected by a TNT is highlighted in DIC Tile-scan image (yellow box), in Figure 5.14. Figure 5.15 – A represents a micrograph with mitochondria fluorescently labelled by MitoTracker DeepRed (MTDR) (green) and alpha-tubulin fluorescently labelled by SiR-Tubulin (red) after fixation.

Subsequently, the cells were post-fixed by osmium tetroxide, contrasted by uranyl acetate and dehydrated in ethanol series. Then the cells were embedded in epoxy resin, mounted on a SEM stub and a trench was removed in front of the area of interest. Finally, the specimen was milled with FIB and imaged with SEM in a sequential manner as long as the tomographic dataset was acquired, as displayed in Figure 4.4. Figure 5.15 – B represents the stacked image of a part of tunnelling nanotube shown in Figure 5.15 – A indicated in a yellow box. The yellow box in Figure 5.15 – B represents a cross-section of the TNT at the level of the mitochondrion no. 1, highlighted by the yellow arrow and number 1. Figure 5.15 – C represents a 3D reconstruction of the inner structure of the particular part of TNT. This image was generated by Amira 6 software using Volren function, that allows a volume rendering of the acquired data based on the density differentiation of individual structures. In contrast to Figure 5.15 – B, Figure 5.15 – C is rotated by 90%, so that it can be viewed in the same orientation as the confocal microscope

image 5.15 – A. The black and yellow arrows with numbers in Figure 5.15 – A and – C indicate individual mitochondria in the particular TNT section. The results obtained by this experiment confirmed the presence of alpha-tubulin in the TNT structure formed between two MSCs. The data obtained by the FIB-SEM method were subsequently post-processed by Amira software and based on different densities, the 3D reconstruction of the selected TNT part was enabled.

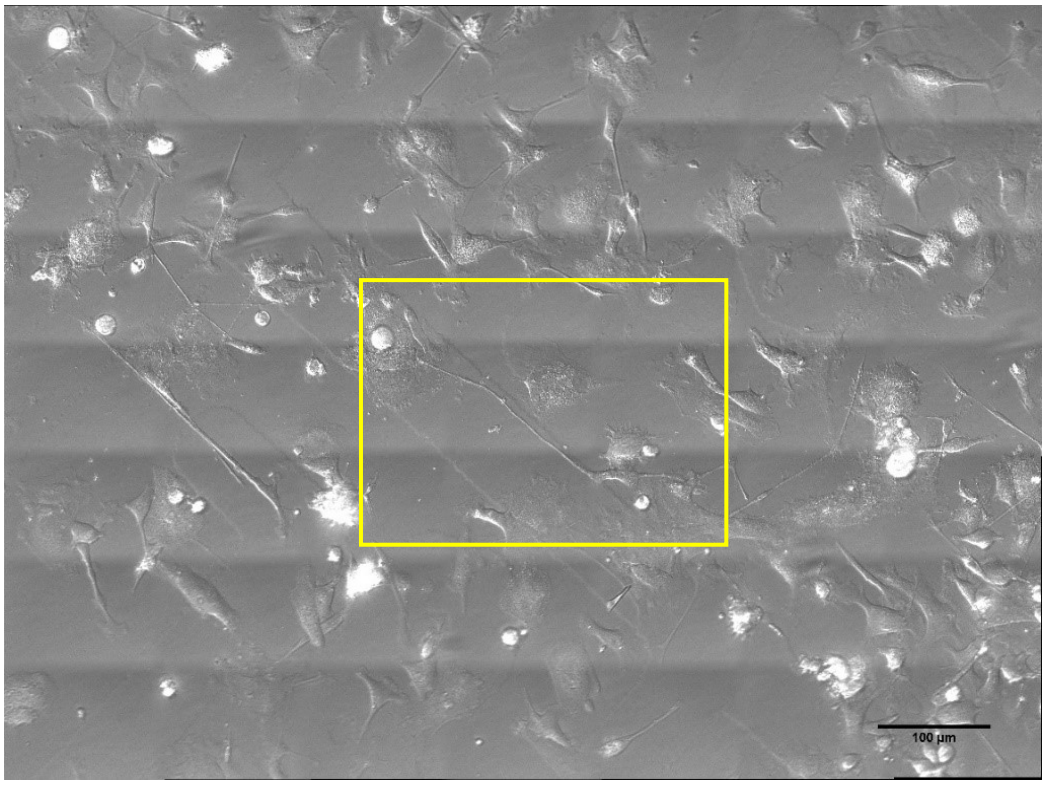


***FIGURE 5.14: Confocal DIC tile-scan image of MSC monoculture showing the selected region of interest highlighted by yellow box.*** *The image was acquired after fixation with 2,5% GA and 1% PFA by Leica SP8 SMD-FLIM confocal microscope (Obj. HC PL APO CS2 63x WI)*

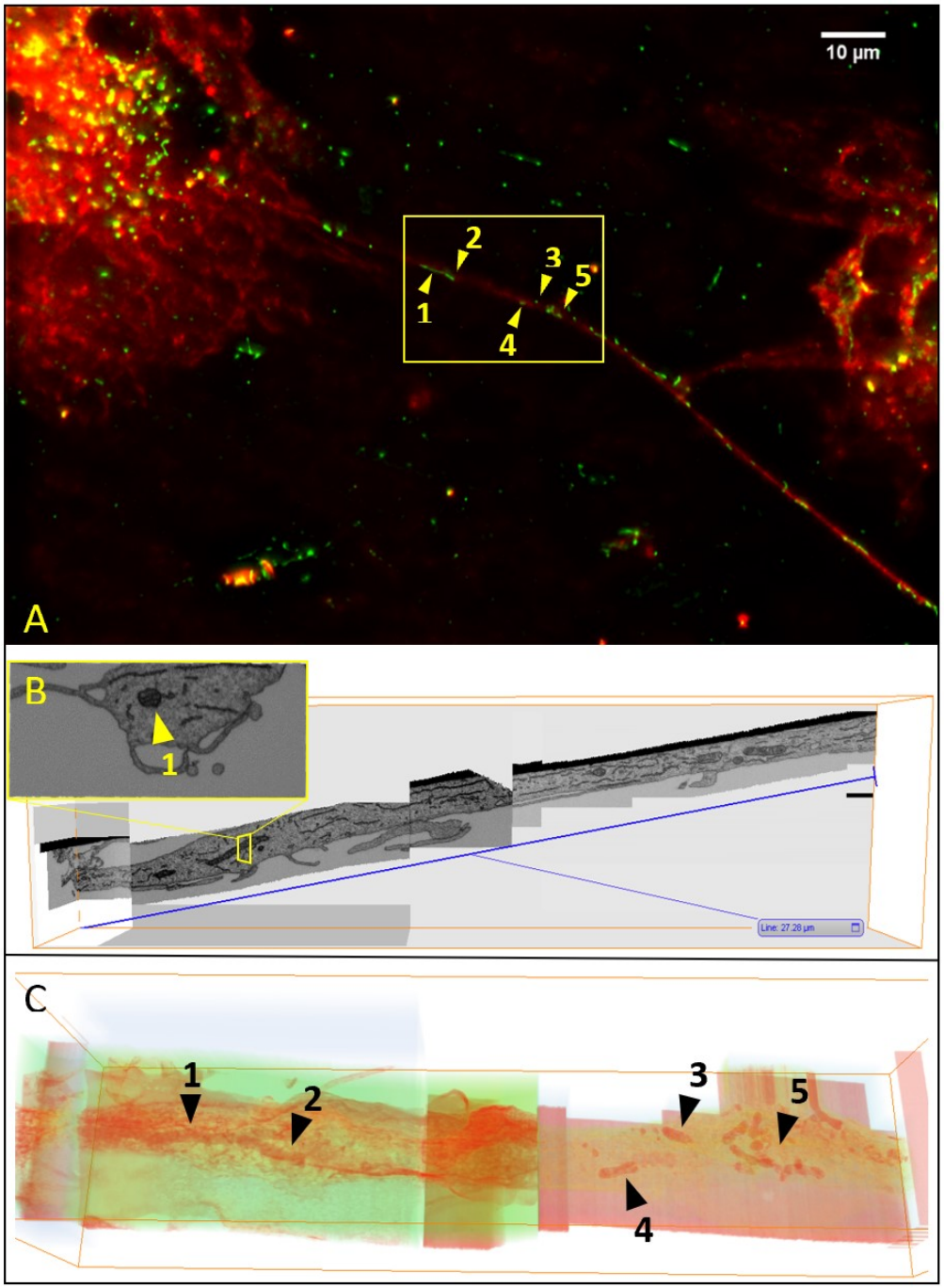


***FIGURE 5.15: Analysis of mitochondrial transfer mediated by TNT using CLEM/FIB-SEM.*** *The image obtained by confocal microscopy shows MTDR labelled mitochondria (red) and SiR-Tubulin labelled alpha-tubulin (red) (A). The composed image of a part of TNT was acquired by FIB-SEM, the yellow box represents a cross-section at the level of mitochondrion no.1, highlighted by the yellow arrow (B). 3D-reconsturction of the inner structure of the specific TNT part was created by the Volren function in Amira 6 software (C). The fluorescence microscopy was performed on the confocal microscope Leica TCS SP8 WLL SMD-FLIM (Obj. HC PL APO CS2 63x WI), the acquired confocal images were deconvolved using Huygens Professional version software 17.04 (Scientific Volume Imaging) and their maximal intensity projection was combined with FIB-SEM data acquired by FEI Helios NanoLab 660 G3 UC. Amira 6 was used for post-processing of the FIB-SEM data. All presented images show one representative image of three independent experiments.*

# 6. Discussion

In last decades genome mutations and instability became one of the ten hallmarks of cancer since the understanding of the role of mutations in nuclear DNA in neoplastic diseases deepened thanks to whole-genome approaches (Khurana et al. 2013, Hanahan and Weinberg 2011). Standard mammalian cells additionally contain thousands of copies of mitochondrial genome, which are organized in mtDNA-protein complexes known as mitochondrial nucleoids (Kukat et al. 2015).

Several mechanisms maintain the integrity of mitochondria and mitochondrial genome in post-mitotic cells. Constant cycles of fusion and fission promote the mixing and the homogenization of mtDNA between discrete organelles within the same cell (Mishra and Chan 2014). Therefore, the mtDNA copies in the cells can be identical (homoplasmy) or may vary (heteroplasmy). Although it was generally assumed that healthy individuals exhibit homoplasmy for a single mtDNA genotype, next-generation sequencing revealed the presence of low-level heteroplasmy in most tissues from healthy individuals and the heteroplasmic mtDNA mutations present in the cancer cells help to deregulate the cellular bioenergetics (He et al. 2010, Payne et al. 2013). Although, cells can tolerate a heavy load of pathogenic mutations, these can lead to disease when the mutation load surpasses a tolerable threshold (Wallace 2013).

As described by Tseng et al. mtDNA mutations and low amounts of mtDNA copy numbers are associated with increased metastasis and poor prognosis in breast cancer (Tseng et al. 2006). Low mtDNA copy numbers seem to be also the promoting factor of EMT via mitochondrial retrograde signaling (Guha and Avadhani 2013), the cells with deleterious mtDNA mutations fail in tumor formation and mutations in the genes encoding proteins of OXPHOS restrain tumorigenesis (Weinberg et al. 2010, Park et al. 2009) .

In this work 4T1 and B16 rho0 cells were used as an extreme model of mtDNA damage. The mtDNA/nDNA ratio and oxygen consumption were characterized in these cells and significant differences were estimated. Unlike the parental cells, rho0 cells do not contain mtDNA and do not respire through mitochondrial respiratory complexes (Dong et al. 2017, Tan et al. 2015). Transmission electron microscopy (TEM) revealed, differences in mitochondrial morphology between parental and rho0 cells, whereby 4T1 rho0 cells contain almost no cristae, when compared with their parental counterparts (Tan et al. 2015). Similar mitochondrial morphology

was also observed for B16 cell sub-lines. Mitochondria of parental B16 and rho0 DP cells contain fully formed mitochondrial cristae, whereas rho0 cells show almost no cristae (Dong et al. 2017).

The results from experiments on metastatic murine tumor models, shown in Figure 5.4 and 5.7, confirmed the findings of Tan et al. Rho0 cell lines with depleted mtDNA exhibited delayed tumor formation in both B16 rho0 melanoma cells grafted s.c. into syngeneic C57BL/6 and in 4T1 rho0 breast cancer cells injected s.c. into Balb/c mice. Tan et al. further confirmed that delayed tumor growth was associated with mtDNA acquisition via mitochondrial transfer from host stromal cells. They demonstrated that tumors grown from B16 rho0 and 4T1 rho0 cells were positive for cytochrome b (Cytb), a gene that is encoded by mtDNA. Also, mitochondrial protein synthesis was shown to be functional in cell lines derived from tumors formed from B16 rho0 and 4T1 rho0 cells by the presence of an mtDNA-encoded cytochrome c oxidase subunit 1 protein (COI). (Tan et al. 2015).

To further explore the link between OXPHOS function and tumor formation a unique experimental model was developed. Tumors were excised from the mice in different time points – between 0-60 days, and the isolated cancer cells were subsequently characterized. The derived 4T1 rho0 sub-lines (D5-D60) were stable in cell culture over time, and their biological properties, such as the level of mtDNA, respiration, or ETC assembly, did not change with time, when cultivated in the cell culture media supplemented uridine/pyruvate.

To find another evidence for mitochondrial DNA transfer in cells isolated from rho0 cell-derived tumors, further experiments were designed. STED microscopy confirmed co-localization of mtDNA with mitochondrial proteins TOM20 and TFAM in B16 rho0 DP cells as well as increasing levels of mtDNA in 4T1 rho0 cell sub-lines D5-D60, as documented by Figure 5.6 and 5.12.

The metabolic state of the rho0 cells and cells derived from rho0 tumors was established by a commercial assay measuring ATP levels in the cell sub-lines, shown in Figure 5.5 and 5.10. The results indicate similar bioenergetics between B16 rho0 DP and parental B16 cells. Both cell types produced 50% ATP by glycolysis, whereas in B16 rho0 cells the entire ATP was generated through glycolysis. Corresponding results were observed for the 4T1 cell sub-lines. The sub-lines isolated from 4T1 rho0 derived tumors showed high production of ATP by glycolysis in D5 and D10 cells and increased levels of OXPHOS in the other derived sub-lines. 4T1 rho0

produced all the ATP by glycolysis, whereas 30% of ATP were produced by glycolysis in parental 4T1 cells. These results also correspond with the delayed tumor formation of 4T1 rho0 cells, as shown in Figure 5.7.

The B16 rho0 cells seem to have higher requirements for the respiration recovery connected with tumor formation. The bioenergy threshold, which is apparently lower for 4T1 rho0 cells, might be caused by higher routine respiration of B16 cells (~100 pmol $O_2$/s/$10^6$ cells), while 4T1 cells provide five times lower routine respiration (~20 pmol $O_2$/s/$10^6$ cells) (Dong et al. 2017, Tan et al. 2015). In addition, the bioenergetic deregulation might also be the result of different genetic mutations in both B16 and 4T1 cell lines. It is still not clear, whether there is a link between these mutations and the need for respiration adjustment required for tumor initiation.

Interesting results, related to the above-mentioned ATP levels, were observed when 4T1 sub-lines were cultivated in medium supplemented with 50mM 2-deoxy-D-glucose, as displayed in Figure 5.9. Rho0 cells as well as the cells with lower content of mtDNA (i.e. D5 and D10), were significantly more sensitive to the effects of 2DG, in comparison with the parental 4T1 cells and sub-lines with higher content of mtDNA (D15-D60). No differences were observed between all the tested sub-lines cultivated in 4T1 rho0 medium without additional 2DG. All these results correspond with the outcomes from NADH/$NAD^+$ ratio measurements, which confirmed the respiration recovery linked to the tumor growth, shown in Figure 5.11. The same trend was documented by using the cell proliferation marker Ki-67 and immunohistochemical staining, as documented by Figure 5.8.

Additionally, to the above-mentioned experiments, the aspects of OXPHOS function, which is essential for the initiation of tumorigenesis, were investigated. Surprisingly 4T1 cells deficient in ATP synthase (ATP5β KO) were able to form tumors, when s.c. grafted into syngeneic mice. This finding points to the fact that production of ATP by ATP synthase, is not a limiting factor for tumorigenesis (Bajzikova et al. 2019).

While ATP production was not essential, OXPHOS-related de novo pyrimidine synthesis, which is driven by respiration via DHODH was proven to be crucial for tumor formation. As described in Figure 1.6, there is a link between OXPHOS system and DHODH in the point of CoQ redox-cycling (Grégoire et al. 1984, Ayer, Macdonald and Stocker 2015). In healthy and fully respiring cells electrons are supplied to coenzyme Q through the CI, CII, and DHOH. From CoQ the electrons are transferred

to CIII, which forwards them to complex IV. Complexes I, III and IV increase the proton-motive force, that drives the ATP formation catalyzed by CV – ATP synthase. In the case of extremely damaged mtDNA, when a cancer cell is disabled to assemble functional complexes of ETC, there is no CIII activity and therefore the CoQ redox-cycle is disrupted, whereby DHODH is not able to convert DHO into orotate.

The importance of the link between OXPHOS and pyrimidine *de novo* synthesis was demonstrated on DHODH deficient cancer cells (DHODH KO), that failed in tumor formation, despite the fact that these cells provided the otherwise fully functional OXPHOS and normal ATP levels (Bajzikova et al. 2019).

Taking together, these results confirm mitochondrial transfer *in vivo* and its importance for the tumorigenesis. On the other hand, a question arises, how mtDNA is acquired. Since no mechanism of mtDNA transfer through the outer and inner mitochondrial membranes and across the plasma membrane to another cell has been described in mammalian cells so far, the only possible ways for mitochondrial transfer are the transfer of intact mitochondria between two cells or mitochondria transmission by fusion of two cells. Recent literature describes both ways of mitochondrial transfer, selective transport of mitochondria (Tan et al. 2015, Dong et al. 2017) and cell fusion (Vitale et al. 2011). Mitochondrial transfer has been previously described *in vitro* (Spees et al. 2006, Gerdes and Carvalho 2008, Gurke et al. 2008, Cho et al. 2012) and *in vivo* in a murine model of acute lung injury (Islam et al. 2012).

The most interesting evidence for *in vivo* mitochondrial transmission, which at the same time partially answers the previously formulated question about how mtDNA is acquired, is documented by the experiment, where B16 rho0 cells with BFP-labeled nuclei were grafted into C57BL/6Nsu9$^{DsRed2}$ mice expressing dsRed protein in mitochondria of somatic cells, shown in Figure 5.2. The mentioned experiment was designed to bring the evidence that intact mitochondria are transferred between somatic cells of host organism and grafted cancer cells with depleted mtDNA. This hypothesis of intact mitochondria transfer was verified by this experiment as well as by other experiments confirming long-term respiration recovery. Furthermore, mitoChIP analysis showed that the mitochondrial DNA polymerase subunit gamma (POLG1) binds strongly to the D-LOOP region of mtDNA in B16 rho0 DP cells as well as in parental B16 (Dong et al. 2017).

The transient nature of dsRed fluorescence affirms the fact that the intact mitochondria are transferred from the host cells. Since the dsRed protein is encoded by nuclear DNA of the donor cell, it cannot be replenished by *de novo* synthesis in the recipient cancer cell. The fluorescent signal of dsRed protein therefore depends on the fluorescence life-time of the protein and is gradually lost after the cell isolation from tumor. In case of cell fusion, the dsRed fluorescent signal would be stable.

The next aim of this work was to explore the mechanism by which are mitochondria transferred between cells. Since tunneling nanotubes seem to be a plausible form of intercellular transfer of organelles (Rustom et al. 2004, Rustom 2016, Rogers and Bhattacharya 2013) the diploma thesis also focuses on this mechanism. The experimental tools here were represented by 4T1 rho0 cells, an experimental model of bioenergetically deregulated acceptor cancer cells and MSCs, the donator somatic cells with functional mitochondrial bioenergetics. MSCs have been described previously as donors of mitochondria in range of experiments using models of mitochondrial damage (Spees et al. 2006, Li et al. 2014, He et al. 2011, Liu et al. 2014, Plotnikov et al. 2010, Oh et al. 2003, Islam et al. 2012, Acquistapace et al. 2011).

One of the possible ways, how to explore intercellular mitochondrial transfer is the usage of advanced imaging techniques including confocal, STED and FIB-SEM microscopy. In these experiments MSCs, expressing dsRed fluorescent protein in mitochondria, were co-cultivated with 4T1 rho0 cells expressing diffuse GFP in cytoplasm, plasmatic membrane or in mitochondria. Mesenchymal stem cells tend to form rich protrusions *in vitro* and they cross-link with rho0 cancer cells through their protrusions – tunneling nanotubes in a co-culture, as shown in Figure 5.13.

Recent literature is not uniform in the view of cytoskeletal equipment of TNTs (Ariazi et al. 2017, Resnik et al. 2018). Confocal microscopy used in this work confirms, that the TNTs formed between MSCs and rho0 cancer cells are tubulin-based. Furthermore, co-localization of alpha-tubulin and dsRed labeled mitochondria assumes that mitochondrial transfer is mediated by the movement of molecular motors along microtubule fibers. The transferred dsRed mitochondria can also be found in recipient GFP labeled 4T1 rho0 cell as documented in Figure 5.13.

The complication of co-culture experiments represents the uncontrollable orientation in the cell types mixture. Therefore, this work introduces a new co-

cultivation system. It makes use of a PDMS microfluidic chip, where two cell types are seeded separately, shown in Figure 5.14. After removing the PDMS stamp the cells remain attached to the glass surface in precisely defined lines with clearly defined spacing between the two cells lines. Subsequently the formation of TNTs formed between the two separated cell types can be investigated more easily. This method of co-cultivation seems to be a promising tool to clarify the structure and properties of TNTs formation. It should also clarify, whether TNTs are primary products of the cancer cell with damaged mitochondria, or whether they are products of donor cells. This method should also shed light on the direction of mitochondrial transfer via TNTs, whether it is uni- or bi-directional.

Total internal reflection fluorescence (TIRF) microscopy can be used to elucidate the direction an velocity of the mitochondrial movement through the TNTs. This method allows separate mapping of fluorescently labeled structures moving in different directions and subsequent evaluation of the direction and speed of their motion. Kymographic analysis of mitochondrial transfer will subsequently show if the movement of fluorescently labeled mitochondria between the cells is unidirectional or bidirectional. The result of kymographic analysis is graphic record – kymogram, from which the velocity of moving particles can be calculated.

Pilot kymographic analysis of data sets obtained by measurement on Nikon Ti-E H-TIRF microscope examined mitochondrial movement between dsRed labeled MSCs. The results showed the approximate velocity of mitochondria of 0.5 μm/s (unpublished data by Luděk Štěpánek PhD).

The co-cultures separated by PDMS microfluidic chip can also be used for CLEM/FIB-SEM microscopy analysis of inner arrangement of the tunneling nanotube.

Correlative light-electron microscopy (CLEM) is a method combining fluorescence microscopy with electron microscopy. By combining these two methods, the information about fluorescence labeled particle is obtained, while the localization context of the particle in the internal cell structure is not lost due to subsequent electron microscopy analysis (de Boer, Hoogenboom and Giepmans 2015). Various ultrastructural techniques are established for 3D-reconstruction of biological specimens, however focused ion beam scanning electron microscopy (FIB-SEM) allows larger volumes and a higher z-axis resolution is provided, than by cryo-TEM or array tomography (Luckner and Wanner 2018).

The preliminary data were obtained by CLEM/FIB-SEM in a homogenous culture of MSCs. Mitochondria in living cells were stained with MitoTracker DeepRed (MTDR). Tubulin fibers were labeled with SiR-Tubulin. The data obtained by confocal microscopy document the co-localization of transported mitochondria and tubulin fibers within the TNT structure. FIB-SEM data correspond with those from the confocal microscope, showing 3D-structure of mitochondria in the lumen of TNT. Internal mitochondrial structure with cristae was clearly visible in both longitudinal- and cross-sections. The FIB-SEM data were acquired by FEI Helios NanoLab 660 G3 UC and were combined with the fluorescence microscopy data provided by Leica TCS SP8 WLL SMD-FLIM.

As mentioned in the introduction, TNTs play an important role in the development, immune response and in various pathophysiological states. Under physiological conditions, TNTs mediate cell contact during the development and play a role in stem cell differentiation and repair of damaged tissues. They also participate in distant cell communications, and in the exchange of organelles between cells. Under pathophysiological conditions, TNTs can have a disease-promoting function, e.g. in the restoration of mitochondrial functions in deregulated cancer cells, as discussed in the present work. On the other hand, TNTs may have rescuing-functions as transporting healthy mitochondria to cells damaged by ischemic reperfusion.

*In vitro* evidence exists that intracellular transmission of various signals and cargos takes place mediated through TNTs. TNT formation is widespread among a variety of cell types. There is no steady opinion on the cytoskeletal nature of TNTs as well as on the selectivity of organelles and the direction of their movement in the context to cytoskeletal equipment.

The experimental model described in chapter 5.3.1. documents, intercellular mitochondria transport between the acceptor mtDNA depleted cancer cell and the donor somatic mesenchymal stem cells. Used advanced imaging could help to determine whether the mitochondrial transfer between the two cell types is uni- or bi-directional. The transport of mitochondria with depleted mtDNA from cancer cells to somatic cells would mean that it is important for cancer cells to ensure a more balanced ratio of healthy and non-functional mitochondria to achieve a more balanced mitochondrial heteroplasmy.

Along with a better understanding of the cytoskeletal equipment of TNTs, as well as their morphology and internal ordering of the various components they contain, it

will be necessary to standardize the terminology in this field of study, to provide a broader definition of TNTs and possibly to delineate different subtypes.

Another and equally important aspect of research in the field of TNTs is, what factors are involved in the induction of tunneling nanotubes and to find out the biomarker of TNTs will be also beneficial. Different triggering factors as various pathogen, metabolic stress, e.g. it seems to be responsible for the TNTs formation. For the intercellular transfer of mitochondria, it appears to be one of the key factors the production of ROS by the cells that have somehow damaged mitochondria (Babenko et al. 2018). In contrast, axonal mitochondrial transport has been shown to have a specific deterioration in mitochondrial transport associated with ROS production, causing an imbalance in $Ca^{2+}$ homeostasis and JNK pathway activation (Liao, Tandarich and Hollenbeck 2017). Debattisti et al. also investigated mitochondrial motility inhibition and found out, that it is induced by physiologically relevant doses of $H_2O_2$ and is rapidly reversed by removal of $H_2O_2$. This supports the idea that ROS might work as a physiological regulator of mitochondrial distribution, temporally decelerating the organelles when and where it is required (Debattisti et al. 2017). Anyway, the nature of ROS is very transient, and it is possible that the TNT formation pathway is Akt-dependent and cross-talks with signaling complexes from the lysosome and the mitochondria. Increased oxidative stress, through increased ROS formation from aggregates within the cytosol or from lysosomal aggregation of protein, can cause mitochondrial dysfunction and lysosomal dysfunction, which act in a feedback loop to create increased ROS, which are believed to be responsible for TNT formation through the Akt pathway (Rustom 2016, Victoria and Zurzolo 2017).

Next research can also target the regulation, induction and suppression of TNTs production and use TNTs in therapy, or on the contrary, synthesize inhibitors of key TNT-drivers. One of the possible uses for therapeutic purposes would be also the targeted delivery of drugs to damaged cells through TNTs.

# 7. Conclusion

Restoration of mtDNA mediated by the transfer of intact mitochondria was confirmed in B16 rho0 cells stably expressing BFP in nuclei, s.c. injected into C57BL/6Nsu9$^{DsRed2}$ mice. Subsequent analysis of the formed pre-tumour lesions excised 11 days later, confirmed the presence of dsRed fluorescent host cell mitochondria in the recipient B16 rho0 cells expressing BFP in nuclei. Further analysis of the established sub-line (B16 rho0 DP cells) confirmed a comparable metabolic state as in the parental B16 cells and STED microscopy analysis documented a similar distribution of mitochondrial nucleoids in both B16 counterparts. The B16 rho0 DP cells formed tumours with a similar efficacy as the parental B16 cells.

Analogous results were obtained with the 4T1 cell line. Additionally, tumours derived from 4T1 rho0 cells were excised in defined time points and analysed subsequently for the aspects of metabolic state and mtDNA content as well as for the proliferation rate. The results document gradual increase in ATP production mediated by OXPHOS. The measured NADH/NAD$^+$ ratios also confirmed the recovery of the parental phenotype in the 4T1 rho0 D15-D60 sub-lines. These data are in accordance with the increasing levels of mtDNA in the analysed 4T1 sub-lines, observed by STED microscopy as well as with the increasing cell proliferation rates estimated by the Ki-67 test.

Microscopy experiments focused on intercellular mitochondrial transfer between mtDNA depleted cancer cells and mice derived MSCs mediated by TNTs brought interesting results as well as a lot of questions. The data obtained by confocal microscopy proved the formation of TNTs between the two cell types and transfer of mitochondria from MSCs into 4T1 rho0 cells. Presence of alpha-tubulin in TNTs and its co-localization with donor cell mitochondria was also documented.

Future direction of this research will include CLEM/FIB-SEM microscopy and TIRF microscopy and will benefit from the use of the PDMS microfluidic device.

This approach will help to understand the nature of TNTs and the principles of the mediated mitochondrial transfer.

# 8. List of publications

1. Bajzikova, M., J. Kovarova, A. R. Coelho, S. Boukalova, S. Oh, K. Rohlenova, D. Svec, S. Hubackova, B. Endaya, K. Judasova, A. Bezawork-Geleta, K. Kluckova, L. Chatre, R. Zobalova, **A. Novakova**, K. Vanova, Z. Ezrova, G. J. Maghzal, S. Magalhaes Novais, M. Olsinova, L. Krobova, Y. J. An, E. Davidova, Z. Nahacka, M. Sobol, T. Cunha-Oliveira, C. Sandoval-Acuña, H. Strnad, T. Zhang, T. Huynh, T. L. Serafim, P. Hozak, V. A. Sardao, W. J. H. Koopman, M. Ricchetti, P. J. Oliveira, F. Kolar, M. Kubista, J. Truksa, K. Dvorakova-Hortova, K. Pacak, R. Gurlich, R. Stocker, Y. Zhou, M. V. Berridge, S. Park, L. Dong, J. Rohlena & J. Neuzil (2019) Reactivation of Dihydroorotate Dehydrogenase-Driven Pyrimidine Biosynthesis Restores Tumour Growth of Respiration-Deficient Cancer Cells. *Cell Metab*, 29, 399-416.e10.

2. Dong, L. F., J. Kovarova, M. Bajzikova, A. Bezawork-Geleta, D. Svec, B. Endaya, K. Sachaphibulkij, A. R. Coelho, N. Sebkova, **A. Ruzickova**, A. S. Tan, K. Kluckova, K. Judasova, K. Zamecnikova, Z. Rychtarcikova, V. Gopalan, L. Andera, M. Sobol, B. Yan, B. Pattnaik, N. Bhatraju, J. Truksa, P. Stopka, P. Hozak, A. K. Lam, R. Sedlacek, P. J. Oliveira, M. Kubista, A. Agrawal, K. Dvorakova-Hortova, J. Rohlena, M. V. Berridge & J. Neuzil (2017) Horizontal transfer of whole mitochondria restores tumourigenic potential in mitochondrial DNA-deficient cancer cells. *Elife*, 6.

# 9. References


Abounit, S., E. Delage & C. Zurzolo (2015) Identification and Characterization of Tunneling Nanotubes for Intercellular Trafficking. *Curr Protoc Cell Biol,* 67**,** 12.10.1-21.

Achkova, D. & J. Maher (2016) Role of the colony-stimulating factor (CSF)/CSF-1 receptor axis in cancer. *Biochem Soc Trans,* 44**,** 333-41.

Acquistapace, A., T. Bru, P.-F. Lesault, F. Figeac, A. E. Coudert, O. le Coz, C. Christov, X. Baudin, F. Auber, R. Yiou, J.-L. Dubois-Randé & A.-M. Rodriguez (2011) Human mesenchymal stem cells reprogram adult cardiomyocytes toward a progenitor-like state through partial cell fusion and mitochondria transfer. *Stem cells (Dayton, Ohio),* 29**,** 812-824.

Ady, J. W., S. Desir, V. Thayanithy, R. I. Vogel, A. L. Moreira, R. J. Downey, Y. Fong, K. Manova-Todorova, M. A. S. Moore & E. Lou (2014) Intercellular communication in malignant pleural mesothelioma: properties of tunneling nanotubes. *Frontiers in physiology,* 5**,** 400-400.

Ahmad, T., S. Mukherjee, B. Pattnaik, M. Kumar, S. Singh, R. Rehman, B. K. Tiwari, K. A. Jha, A. P. Barhanpurkar, M. R. Wani, S. S. Roy, U. Mabalirajan, B. Ghosh & A. Agrawal (2014) Miro1 regulates intercellular mitochondrial transport & enhances mesenchymal stem cell rescue efficacy. *EMBO J,* 33**,** 994-1010.

Almuhaideb, A., N. Papathanasiou & J. Bomanji (2011) 18F-FDG PET/CT imaging in oncology. *Ann Saudi Med,* 31**,** 3-13.

Amelio, I. & G. Melino (2015) The p53 family and the hypoxia-inducible factors (HIFs): determinants of cancer progression. *Trends Biochem Sci,* 40**,** 425-34.

Anderson, K. G., I. M. Stromnes & P. D. Greenberg (2017) Obstacles Posed by the Tumor Microenvironment to T cell Activity: A Case for Synergistic Therapies. *Cancer cell,* 31**,** 311-325.

Antanavičiūtė, I., K. Rysevaitė, V. Liutkevičius, A. Marandykina, L. Rimkutė, R. Sveikatienė, V. Uloza & V. A. Skeberdis (2014) Long-distance communication between laryngeal carcinoma cells. *PLoS One,* 9**,** e99196.

Ariazi, J., A. Benowitz, V. De Biasi, M. L. Den Boer, S. Cherqui, H. Cui, N. Douillet, E. A. Eugenin, D. Favre, S. Goodman, K. Gousset, D. Hanein, D. I. Israel, S. Kimura, R. B. Kirkpatrick, N. Kuhn, C. Jeong, E. Lou, R. Mailliard, S. Maio, G. Okafo, M. Osswald, J. Pasquier, R. Polak, G. Pradel, B. de Rooij, P. Schaeffer, V. A. Skeberdis, I. F. Smith, A. Tanveer, N. Volkmann, Z. Wu & C. Zurzolo (2017) Tunneling Nanotubes and Gap Junctions-Their Role in Long-Range Intercellular Communication during Development, Health, and Disease Conditions. *Frontiers in molecular neuroscience,* 10**,** 333-333.

Babenko, V. A., D. N. Silachev, V. A. Popkov, L. D. Zorova, I. B. Pevzner, E. Y. Plotnikov, G. T. Sukhikh & D. B. Zorov (2018) Miro1 Enhances Mitochondria Transfer from Multipotent Mesenchymal Stem Cells (MMSC) to Neural Cells and Improves the Efficacy of Cell Recovery. *Molecules (Basel, Switzerland),* 23**,** 687.

Bajzikova, M., J. Kovarova, A. R. Coelho, S. Boukalova, S. Oh, K. Rohlenova, D. Svec, S. Hubackova, B. Endaya, K. Judasova, A. Bezawork-Geleta, K. Kluckova, L. Chatre, R. Zobalova, A. Novakova, K. Vanova, Z. Ezrova, G. J. Maghzal, S. Magalhaes Novais, M. Olsinova, L. Krobova, Y. J. An, E. Davidova, Z. Nahacka, M. Sobol, T. Cunha-Oliveira, C. Sandoval-Acuña, H. Strnad, T. Zhang, T. Huynh, T. L. Serafim, P. Hozak, V. A. Sardao, W. J. H. Koopman, M. Ricchetti, P. J. Oliveira, F. Kolar, M. Kubista, J. Truksa, K. Dvorakova-Hortova, K. Pacak, R. Gurlich, R. Stocker, Y. Zhou, M. V. Berridge, S. Park, L. Dong, J. Rohlena & J. Neuzil (2019) Reactivation of Dihydroorotate Dehydrogenase-Driven Pyrimidine Biosynthesis Restores Tumor Growth of Respiration-Deficient Cancer Cells. *Cell Metab,* 29**,** 399-416.e10.

Balkwill, F. R., M. Capasso & T. Hagemann (2012) The tumor microenvironment at a glance. *J Cell Sci,* 125**,** 5591-6.

Barcellos-de-Souza, P., V. Gori, F. Bambi & P. Chiarugi (2013) Tumor microenvironment: bone marrow-mesenchymal stem cells as key players. *Biochim Biophys Acta,* 1836**,** 321-35.

Bates, G. J., S. B. Fox, C. Han, R. D. Leek, J. F. Garcia, A. L. Harris & A. H. Banham (2006) Quantification of regulatory T cells enables the identification of high-risk breast cancer patients and those at risk of late relapse. *J Clin Oncol,* 24**,** 5373-80.

Baysal, B. E., R. E. Ferrell, J. E. Willett-Brozick, E. C. Lawrence, D. Myssiorek, A. Bosch, A. van der Mey, P. E. Taschner, W. S. Rubinstein, E. N. Myers, C. W. Richard, C. J. Cornelisse, P. Devilee & B. Devlin (2000) Mutations in SDHD, a mitochondrial complex II gene, in hereditary paraganglioma. *Science,* 287**,** 848-51.

Becht, E., N. A. Giraldo, M. C. Dieu-Nosjean, C. Sautès-Fridman & W. H. Fridman (2016) Cancer immune contexture and immunotherapy. *Curr Opin Immunol,* 39**,** 7-13.

Berridge, M. V., M. J. McConnell, C. Grasso, M. Bajzikova, J. Kovarova & J. Neuzil (2016) Horizontal transfer of mitochondria between mammalian cells: beyond co-culture approaches. *Curr Opin Genet Dev,* 38**,** 75-82.

Bingle, L., N. J. Brown & C. E. Lewis (2002) The role of tumour-associated macrophages in tumour progression: implications for new anticancer therapies. *J Pathol,* 196**,** 254-65.

Brickley, K., M. J. Smith, M. Beck & F. A. Stephenson (2005) GRIF-1 and OIP106, members of a novel gene family of coiled-coil domain proteins: association in vivo and in vitro with kinesin. *J Biol Chem,* 280**,** 14723-32.

Brücher, B. L. & I. S. Jamall (2014) Cell-cell communication in the tumor microenvironment, carcinogenesis, and anticancer treatment. *Cell Physiol Biochem,* 34**,** 213-43.

Bukoreshtliev, N. V., X. Wang, E. Hodneland, S. Gurke, J. F. Barroso & H. H. Gerdes (2009) Selective block of tunneling nanotube (TNT) formation inhibits intercellular organelle transfer between PC12 cells. *FEBS Lett,* 583**,** 1481-8.

Caicedo, A., V. Fritz, J.-M. Brondello, M. Ayala, I. Dennemont, N. Abdellaoui, F. de Fraipont, A. Moisan, C. A. Prouteau, H. Boukhaddaoui, C. Jorgensen & M.-L. Vignais (2015) MitoCeption as a new tool to assess the effects of mesenchymal stem/stromal cell mitochondria on cancer cell metabolism and function. *Scientific reports,* 5**,** 9073-9073.

Carmeliet, P. & R. K. Jain (2011) Molecular mechanisms and clinical applications of angiogenesis. *Nature,* 473**,** 298-307.

Chan, D. A., P. D. Sutphin, P. Nguyen, S. Turcotte, E. W. Lai, A. Banh, G. E. Reynolds, J. T. Chi, J. Wu, D. E. Solow-Cordero, M. Bonnet, J. U. Flanagan, D. M. Bouley, E. E. Graves, W. A. Denny, M. P. Hay & A. J. Giaccia (2011) Targeting GLUT1 and the Warburg effect in renal cell carcinoma by chemical synthetic lethality. *Sci Transl Med,* 3**,** 94ra70.

Cho, Y. M., J. H. Kim, M. Kim, S. J. Park, S. H. Koh, H. S. Ahn, G. H. Kang, J. B. Lee, K. S. Park & H. K. Lee (2012) Mesenchymal stem cells transfer mitochondria to the cells with virtually no mitochondrial function but not with pathogenic mtDNA mutations. *PLoS One,* 7**,** e32778.

Chuang, D. M., C. Hough & V. V. Senatorov (2005) Glyceraldehyde-3-phosphate dehydrogenase, apoptosis, and neurodegenerative diseases. *Annu Rev Pharmacol Toxicol,* 45**,** 269-90.

Colell, A., D. R. Green & J. E. Ricci (2009) Novel roles for GAPDH in cell death and carcinogenesis. *Cell Death Differ,* 16**,** 1573-81.

Colombo, M. P., A. Modesti, G. Parmiani & G. Forni (1992) Local cytokine availability elicits tumor rejection and systemic immunity through granulocyte-T-lymphocyte cross-talk. *Cancer Res,* 52**,** 4853-7.

Condeelis, J. & J. W. Pollard (2006) Macrophages: obligate partners for tumor cell migration, invasion, and metastasis. *Cell,* 124**,** 263-6.

Cooke, V. G., V. S. LeBleu, D. Keskin, Z. Khan, J. T. O'Connell, Y. Teng, M. B. Duncan, L. Xie, G. Maeda, S. Vong, H. Sugimoto, R. M. Rocha, A. Damascena, R. R. Brentani & R. Kalluri (2012) Pericyte depletion results in hypoxia-associated epithelial-to-mesenchymal transition and metastasis mediated by met signaling pathway. *Cancer cell,* 21**,** 66-81.

Coronella, J. A., P. Telleman, G. A. Kingsbury, T. D. Truong, S. Hays & R. P. Junghans (2001) Evidence for an antigen-driven humoral immune response in medullary ductal breast cancer. *Cancer Res,* 61**,** 7889-99.

Curiel, T. J., G. Coukos, L. Zou, X. Alvarez, P. Cheng, P. Mottram, M. Evdemon-Hogan, J. R. Conejo-Garcia, L. Zhang, M. Burow, Y. Zhu, S. Wei, I. Kryczek, B. Daniel, A. Gordon, L. Myers, A. Lackner, M. L. Disis, K. L. Knutson, L. Chen & W. Zou (2004) Specific recruitment of regulatory T cells in ovarian carcinoma fosters immune privilege and predicts reduced survival. *Nat Med,* 10**,** 942-9.

D'Aloia, A., G. Berruti, B. Costa, C. Schiller, R. Ambrosini, V. Pastori, E. Martegani & M. Ceriani (2018) RalGPS2 is involved in tunneling nanotubes formation in 5637 bladder cancer cells. *Exp Cell Res,* 362**,** 349-361.

Danial, N. N., C. F. Gramm, L. Scorrano, C. Y. Zhang, S. Krauss, A. M. Ranger, S. R. Datta, M. E. Greenberg, L. J. Licklider, B. B. Lowell, S. P. Gygi & S. J. Korsmeyer (2003) BAD and glucokinase reside in a mitochondrial complex that integrates glycolysis and apoptosis. *Nature,* 424**,** 952-6.

Dastoor, Z. & J. L. Dreyer (2001) Potential role of nuclear translocation of glyceraldehyde-3-phosphate dehydrogenase in apoptosis and oxidative stress. *J Cell Sci,* 114**,** 1643-53.

de Boer, P., J. P. Hoogenboom & B. N. Giepmans (2015) Correlated light and electron microscopy: ultrastructure lights up! *Nat Methods,* 12**,** 503-13.

De Larco, J. E., B. R. Wuertz & L. T. Furcht (2004) The potential role of neutrophils in promoting the metastatic phenotype of tumors releasing interleukin-8. *Clin Cancer Res,* 10**,** 4895-900.

de Padua, M. C., G. Delodi, M. Vučetić, J. Durivault, V. Vial, P. Bayer, G. R. Noleto, N. M. Mazure, M. Ždralević & J. Pouysségur (2017) Disrupting glucose-6-phosphate isomerase fully suppresses the "Warburg effect" and activates OXPHOS with minimal impact on tumor growth except in hypoxia. *Oncotarget,* 8**,** 87623-87637.

Debattisti, V., A. A. Gerencser, M. Saotome, S. Das & G. Hajnóczky (2017) ROS Control Mitochondrial Motility through p38 and the Motor Adaptor Miro/Trak. *Cell reports,* 21**,** 1667-1680.

Domhan, S., L. Ma, A. Tai, Z. Anaya, A. Beheshti, M. Zeier, L. Hlatky & A. Abdollahi (2011) Intercellular communication by exchange of cytoplasmic material via tunneling nano-tube like structures in primary human renal epithelial cells. *PLoS One,* 6**,** e21283.

Dong, G., Q. Mao, W. Xia, Y. Xu, J. Wang, L. Xu & F. Jiang (2016) PKM2 and cancer: The function of PKM2 beyond glycolysis. *Oncology letters,* 11**,** 1980-1986.

Dong, L. F., J. Kovarova, M. Bajzikova, A. Bezawork-Geleta, D. Svec, B. Endaya, K. Sachaphibulkij, A. R. Coelho, N. Sebkova, A. Ruzickova, A. S. Tan, K. Kluckova, K. Judasova, K. Zamecnikova, Z. Rychtarcikova, V. Gopalan, L. Andera, M. Sobol, B. Yan, B. Pattnaik, N. Bhatraju, J. Truksa, P. Stopka, P. Hozak, A. K. Lam, R. Sedlacek, P. J. Oliveira, M. Kubista, A. Agrawal, K. Dvorakova-Hortova, J. Rohlena, M. V. Berridge & J. Neuzil (2017) Horizontal transfer of whole mitochondria restores tumorigenic potential in mitochondrial DNA-deficient cancer cells. *Elife,* 6.

Donnelly, J. M., A. Engevik, R. Feng, C. Xiao, G. P. Boivin, J. Li, J. Houghton & Y. Zavros (2014) Mesenchymal stem cells induce epithelial proliferation within the inflamed stomach. *American journal of physiology. Gastrointestinal and liver physiology,* 306**,** G1075-G1088.

Dwyer, A. R., E. L. Greenland & F. J. Pixley (2017) Promotion of Tumor Invasion by Tumor-Associated Macrophages: The Role of CSF-1-Activated Phosphatidylinositol 3 Kinase and Src Family Kinase Motility Signaling. *Cancers,* 9**,** 68.

Erez, N., M. Truitt, P. Olson, S. T. Arron & D. Hanahan (2010) Cancer-Associated Fibroblasts Are Activated in Incipient Neoplasia to Orchestrate Tumor-Promoting Inflammation in an NF-kappaB-Dependent Manner. *Cancer Cell,* 17**,** 135-47.

Erler, J. T., K. L. Bennewith, T. R. Cox, G. Lang, D. Bird, A. Koong, Q. T. Le & A. J. Giaccia (2009) Hypoxia-induced lysyl oxidase is a critical mediator of bone marrow cell recruitment to form the premetastatic niche. *Cancer Cell,* 15**,** 35-44.

Farhood, B., M. Najafi & K. Mortezaee (2019) Cancer-associated fibroblasts: Secretions, interactions, and therapy. *J Cell Biochem,* 120**,** 2791-2800.

Feo, S., D. Arcuri, E. Piddini, R. Passantino & A. Giallongo (2000) ENO1 gene product binds to the c-myc promoter and acts as a transcriptional repressor: relationship with Myc promoter-binding protein 1 (MBP-1). *FEBS Lett,* 473**,** 47-52.

Fransson, S., A. Ruusala & P. Aspenström (2006) The atypical Rho GTPases Miro-1 and Miro-2 have essential roles in mitochondrial trafficking. *Biochem Biophys Res Commun,* 344**,** 500-10.

Fridman, W. H., F. Pagès, C. Sautès-Fridman & J. Galon (2012) The immune contexture in human tumours: impact on clinical outcome. *Nat Rev Cancer,* 12**,** 298-306.

Futreal, P. A., L. Coin, M. Marshall, T. Down, T. Hubbard, R. Wooster, N. Rahman & M. R. Stratton (2004) A census of human cancer genes. *Nat Rev Cancer,* 4**,** 177-83.

Gallardo-Pérez, J. C., N. A. Rivero-Segura, A. Marín-Hernández, R. Moreno-Sánchez & S. Rodríguez-Enríquez (2014) GPI/AMF inhibition blocks the development of the metastatic phenotype of mature multi-cellular tumor spheroids. *Biochim Biophys Acta,* 1843**,** 1043-53.

Galluzzi, L., E. Morselli, O. Kepp, I. Vitale, A. Rigoni, E. Vacchelli, M. Michaud, H. Zischka, M. Castedo & G. Kroemer (2010) Mitochondrial gateways to cancer. *Mol Aspects Med,* 31**,** 1-20.

Gentric, G., V. Mieulet & F. Mechta-Grigoriou (2017) Heterogeneity in Cancer Metabolism: New Concepts in an Old Field. *Antioxid Redox Signal,* 26**,** 462-485.

Gerdes, H. H. & R. N. Carvalho (2008) Intercellular transfer mediated by tunneling nanotubes. *Curr Opin Cell Biol,* 20**,** 470-5.

Giampazolias, E. & S. W. Tait (2016) Mitochondria and the hallmarks of cancer. *FEBS J,* 283**,** 803-14.

Glater, E. E., L. J. Megeath, R. S. Stowers & T. L. Schwarz (2006) Axonal transport of mitochondria requires milton to recruit kinesin heavy chain and is light chain independent. *J Cell Biol,* 173**,** 545-57.

Gousset, K., E. Schiff, C. Langevin, Z. Marijanovic, A. Caputo, D. T. Browman, N. Chenouard, F. de Chaumont, A. Martino, J. Enninga, J. C. Olivo-Marin, D. Männel & C. Zurzolo (2009) Prions hijack tunnelling nanotubes for intercellular spread. *Nat Cell Biol,* 11**,** 328-36.

Guan, J. & J. Chen (2013) Mesenchymal stem cells in the tumor microenvironment. *Biomed Rep,* 1**,** 517-521.

Guertin, D. A. & D. M. Sabatini (2007) Defining the role of mTOR in cancer. *Cancer Cell,* 12**,** 9-22.

Guha, M. & N. G. Avadhani (2013) Mitochondrial retrograde signaling at the crossroads of tumor bioenergetics, genetics and epigenetics. *Mitochondrion,* 13**,** 577-591.

Guo, X., G. T. Macleod, A. Wellington, F. Hu, S. Panchumarthi, M. Schoenfield, L. Marin, M. P. Charlton, H. L. Atwood & K. E. Zinsmaier (2005) The GTPase dMiro is required for axonal transport of mitochondria to Drosophila synapses. *Neuron,* 47**,** 379-93.

Gurke, S., J. F. Barroso, E. Hodneland, N. V. Bukoreshtliev, O. Schlicker & H. H. Gerdes (2008) Tunneling nanotube (TNT)-like structures facilitate a constitutive, actomyosin-dependent exchange of endocytic organelles between normal rat kidney cells. *Exp Cell Res,* 314**,** 3669-83.

Han, Z., Y. Jing, Y. Xia, S. Zhang, J. Hou, Y. Meng, F. Yu, X. Liu, M. Wu, P. Zhang & L. Wei (2014) Mesenchymal stem cells contribute to the chemoresistance of hepatocellular carcinoma cells in inflammatory environment by inducing autophagy. *Cell & bioscience,* 4**,** 22-22.

Hanahan, D. & R. A. Weinberg (2000) The hallmarks of cancer. *Cell,* 100**,** 57-70.

--- (2011) Hallmarks of cancer: the next generation. *Cell,* 144**,** 646-74.

Hashimoto, M., F. Bhuyan, M. Hiyoshi, O. Noyori, H. Nasser, M. Miyazaki, T. Saito, Y. Kondoh, H. Osada, S. Kimura, K. Hase, H. Ohno & S. Suzu (2016) Potential Role of the Formation of Tunneling Nanotubes in HIV-1 Spread in Macrophages. *J Immunol,* 196**,** 1832-41.

Hasuwa, H., Y. Muro, M. Ikawa, N. Kato, Y. Tsujimoto & M. Okabe (2010) Transgenic Mouse Sperm that Have Green Acrosome and Red Mitochondria Allow Visualization of Sperm and Their Acrosome Reaction in Vivo. *Experimental Animals,* 59**,** 105-107.

He, K., X. Shi, X. Zhang, S. Dang, X. Ma, F. Liu, M. Xu, Z. Lv, D. Han, X. Fang & Y. Zhang (2011) Long-distance intercellular connectivity between cardiomyocytes and cardiofibroblasts mediated by membrane nanotubes. *Cardiovasc Res,* 92**,** 39-47.

He, Y., J. Wu, D. C. Dressman, C. Iacobuzio-Donahue, S. D. Markowitz, V. E. Velculescu, L. A. Diaz, Jr., K. W. Kinzler, B. Vogelstein & N. Papadopoulos (2010) Heteroplasmic mitochondrial DNA mutations in normal and tumour cells. *Nature,* 464**,** 610-614.

Hekmatshoar, Y., J. Nakhle, M. Galloni & M. L. Vignais (2018) The role of metabolism and tunneling nanotube-mediated intercellular mitochondria exchange in cancer drug resistance. *Biochem J,* 475**,** 2305-2328.

Hicks, A. M., G. Riedlinger, M. C. Willingham, M. A. Alexander-Miller, C. Von Kap-Herr, M. J. Pettenati, A. M. Sanders, H. M. Weir, W. Du, J. Kim, A. J. Simpson, L. J. Old & Z. Cui (2006) Transferable anticancer innate immunity in spontaneous regression/complete resistance mice. *Proc Natl Acad Sci U S A,* 103**,** 7753-8.

Hiraoka, N., K. Onozato, T. Kosuge & S. Hirohashi (2006) Prevalence of FOXP3+ regulatory T cells increases during the progression of pancreatic ductal adenocarcinoma and its premalignant lesions. *Clin Cancer Res,* 12**,** 5423-34.

Ho, I. A., H. C. Toh, W. H. Ng, Y. L. Teo, C. M. Guo, K. M. Hui & P. Y. Lam (2013) Human bone marrow-derived mesenchymal stem cells suppress human glioma growth through inhibition of angiogenesis. *Stem Cells,* 31**,** 146-55.

Hong, B., H. Li, M. Zhang, J. Xu, Y. Lu, Y. Zheng, J. Qian, J. T. Chang, J. Yang & Q. Yi (2015) p38 MAPK inhibits breast cancer metastasis through regulation of stromal expansion. *International journal of cancer,* 136**,** 34-43.

Hsu, P. P. & D. M. Sabatini (2008) Cancer cell metabolism: Warburg and beyond. *Cell,* 134**,** 703-7.

Hurt, B., R. Schulick, B. Edil, K. C. El Kasmi & C. Barnett (2017) Cancer-promoting mechanisms of tumor-associated neutrophils. *Am J Surg,* 214**,** 938-944.

Islam, M. N., S. R. Das, M. T. Emin, M. Wei, L. Sun, K. Westphalen, D. J. Rowlands, S. K. Quadri, S. Bhattacharya & J. Bhattacharya (2012) Mitochondrial transfer from bone-marrow-derived stromal cells to pulmonary alveoli protects against acute lung injury. *Nat Med,* 18**,** 759-65.

Jansens, R. J. J., W. Van den Broeck, S. De Pelsmaeker, J. A. S. Lamote, C. Van Waesberghe, L. Couck & H. W. Favoreel (2017) Pseudorabies virus US3-induced tunneling nanotubes contain stabilized microtubules, interact with neighbouring cells via cadherins and allow intercellular molecular communication. *Journal of virology,* 91**,** e00749-17.

Jin, H. J., Y. K. Bae, M. Kim, S.-J. Kwon, H. B. Jeon, S. J. Choi, S. W. Kim, Y. S. Yang, W. Oh & J. W. Chang (2013) Comparative analysis of human mesenchymal stem cells from bone marrow, adipose tissue, and umbilical cord blood as sources of cell therapy. *International journal of molecular sciences,* 14**,** 17986-18001.

Jose, C., N. Bellance & R. Rossignol (2011) Choosing between glycolysis and oxidative phosphorylation: a tumor's dilemma? *Biochim Biophys Acta,* 1807**,** 552-61.

Khakoo, A. Y., S. Pati, S. A. Anderson, W. Reid, M. F. Elshal, I. I. Rovira, A. T. Nguyen, D. Malide, C. A. Combs, G. Hall, J. Zhang, M. Raffeld, T. B. Rogers, W. Stetler-Stevenson, J. A. Frank, M. Reitz & T. Finkel (2006) Human mesenchymal stem cells exert potent antitumorigenic effects in a model of Kaposi's sarcoma. *The Journal of experimental medicine,* 203**,** 1235-1247.

Khurana, E., Y. Fu, V. Colonna, X. J. Mu, H. M. Kang, T. Lappalainen, A. Sboner, L. Lochovsky, J. Chen, A. Harmanci, J. Das, A. Abyzov, S. Balasubramanian, K. Beal, D. Chakravarty, D. Challis, Y. Chen, D. Clarke, L. Clarke, F. Cunningham, U. S. Evani, P. Flicek, R. Fragoza, E. Garrison, R. Gibbs, Z. H. Gümüş, J. Herrero, N. Kitabayashi, Y. Kong, K. Lage, V. Liluashvili, S. M. Lipkin, D. G. MacArthur, G. Marth, D. Muzny, T. H. Pers, G. R. S. Ritchie, J. A. Rosenfeld, C. Sisu, X. Wei, M. Wilson, Y. Xue, F. Yu, C. Genomes Project, E. T. Dermitzakis, H. Yu, M. A. Rubin, C. Tyler-Smith & M. Gerstein (2013) Integrative annotation of variants from 1092 humans: application to cancer genomics. *Science (New York, N.Y.),* 342**,** 1235587-1235587.

Kirk, E., L. S. Chin & L. Li (2006) GRIF1 binds Hrs and is a new regulator of endosomal trafficking. *J Cell Sci,* 119**,** 4689-701.

Kitajima, Y. & K. Miyazaki (2013) The Critical Impact of HIF-1a on Gastric Cancer Biology. *Cancers (Basel),* 5**,** 15-26.

Kondoh, H., M. E. Lleonart, Y. Nakashima, M. Yokode, M. Tanaka, D. Bernard, J. Gil & D. Beach (2007) A high glycolytic flux supports the proliferative potential of murine embryonic stem cells. *Antioxid Redox Signal,* 9**,** 293-9.

Koppenol, W. H., P. L. Bounds & C. V. Dang (2011) Otto Warburg's contributions to current concepts of cancer metabolism. *Nat Rev Cancer,* 11**,** 325-37.

Koyanagi, M., R. P. Brandes, J. Haendeler, A. M. Zeiher & S. Dimmeler (2005) Cell-to-cell connection of endothelial progenitor cells with cardiac myocytes by nanotubes: a novel mechanism for cell fate changes? *Circ Res,* 96**,** 1039-41.

Kroemer, G. & J. Pouyssegur (2008) Tumor cell metabolism: cancer's Achilles' heel. *Cancer Cell,* 13**,** 472-82.

Kucerova, L., S. Skolekova, L. Demkova, R. Bohovic & M. Matuskova (2014) Long-term efficiency of mesenchymal stromal cell-mediated CD-MSC/5FC therapy in human melanoma xenograft model. *Gene Ther,* 21**,** 874-87.

Kukat, C., K. M. Davies, C. A. Wurm, H. Spåhr, N. A. Bonekamp, I. Kühl, F. Joos, P. L. Polosa, C. B. Park, V. Posse, M. Falkenberg, S. Jakobs, W. Kühlbrandt & N.-G. Larsson (2015) Cross-strand binding of TFAM to a single mtDNA molecule forms the mitochondrial nucleoid. *Proceedings of the National Academy of Sciences of the United States of America,* 112**,** 11288-11293.

Kumar, A., J. H. Kim, P. Ranjan, M. G. Metcalfe, W. Cao, M. Mishina, S. Gangappa, Z. Guo, E. S. Boyden, S. Zaki, I. York, A. García-Sastre, M. Shaw & S. Sambhara (2017) Influenza virus exploits tunneling nanotubes for cell-to-cell spread. *Scientific reports,* 7**,** 40360-40360.

Kumari, S. & R. Malla (2015) New Insight on the Role of Plasminogen Receptor in Cancer Progression. *Cancer growth and metastasis,* 8**,** 35-42.

Li, X., Y. Zhang, S. C. Yeung, Y. Liang, X. Liang, Y. Ding, M. S. Ip, H. F. Tse, J. C. Mak & Q. Lian (2014) Mitochondrial transfer of induced pluripotent stem cell-derived mesenchymal stem cells to airway epithelial cells attenuates cigarette smoke-induced damage. *Am J Respir Cell Mol Biol,* 51**,** 455-65.

Li, X., Y. Zheng & Z. Lu (2016) PGK1 is a new member of the protein kinome. *Cell cycle (Georgetown, Tex.),* 15**,** 1803-1804.

Liao, P.-C., L. C. Tandarich & P. J. Hollenbeck (2017) ROS regulation of axonal mitochondrial transport is mediated by Ca2+ and JNK in Drosophila. *PloS one,* 12**,** e0178105-e0178105.

Liao, Y.-X., Z.-Z. Fu, C.-H. Zhou, L.-C. Shan, Z.-Y. Wang, F. Yin, L.-P. Zheng, Y.-Q. Hua & Z.-D. Cai (2015) AMD3100 reduces CXCR4-mediated survival and metastasis of osteosarcoma by inhibiting JNK and Akt, but not p38 or Erk1/2, pathways in in vitro and mouse experiments. *Oncology reports,* 34**,** 33-42.

Lin, E. Y., J. F. Li, L. Gnatovskiy, Y. Deng, L. Zhu, D. A. Grzesik, H. Qian, X. N. Xue & J. W. Pollard (2006) Macrophages regulate the angiogenic switch in a mouse model of breast cancer. *Cancer Res,* 66**,** 11238-46.

Lin, E. Y., A. V. Nguyen, R. G. Russell & J. W. Pollard (2001) Colony-stimulating factor 1 promotes progression of mammary tumors to malignancy. *J Exp Med,* 193**,** 727-40.

Lin, H. Y., C. W. Liou, S. D. Chen, T. Y. Hsu, J. H. Chuang, P. W. Wang, S. T. Huang, M. M. Tiao, J. B. Chen, T. K. Lin & Y. C. Chuang (2015) Mitochondrial transfer from Wharton's jelly-derived mesenchymal

stem cells to mitochondria-defective cells recaptures impaired mitochondrial function. *Mitochondrion,* 22**,** 31-44.

Liu, J., C. Zhang, W. Hu & Z. Feng (2015) Tumor suppressor p53 and its mutants in cancer metabolism. *Cancer letters,* 356**,** 197-203.

Liu, K., K. Ji, L. Guo, W. Wu, H. Lu, P. Shan & C. Yan (2014) Mesenchymal stem cells rescue injured endothelial cells in an in vitro ischemia-reperfusion model via tunneling nanotube like structure-mediated mitochondrial transfer. *Microvasc Res,* 92**,** 10-8.

LoRusso, P. M. (2016) Inhibition of the PI3K/AKT/mTOR Pathway in Solid Tumors. *J Clin Oncol,* 34**,** 3803-3815.

Lou, E., S. Fujisawa, A. Morozov, A. Barlas, Y. Romin, Y. Dogan, S. Gholami, A. L. Moreira, K. Manova-Todorova & M. A. Moore (2012) Tunneling nanotubes provide a unique conduit for intercellular transfer of cellular contents in human malignant pleural mesothelioma. *PLoS One,* 7**,** e33093.

Lovas, J. R. & X. Wang (2013) The meaning of mitochondrial movement to a neuron's life. *Biochimica et biophysica acta,* 1833**,** 184-194.

Lu, J., X. Zheng, F. Li, Y. Yu, Z. Chen, Z. Liu, Z. Wang, H. Xu & W. Yang (2017) Tunneling nanotubes promote intercellular mitochondria transfer followed by increased invasiveness in bladder cancer cells. *Oncotarget,* 8**,** 15539-15552.

Luckner, M. & G. Wanner (2018) Precise and economic FIB/SEM for CLEM: with 2 nm voxels through mitosis. *Histochemistry and cell biology,* 150**,** 149-170.

Luo, W. & G. L. Semenza (2012) Emerging roles of PKM2 in cell metabolism and cancer progression. *Trends Endocrinol Metab,* 23**,** 560-6.

Löffler, M., L. D. Fairbanks, E. Zameitat, A. M. Marinaki & H. A. Simmonds (2005) Pyrimidine pathways in health and disease. *Trends Mol Med,* 11**,** 430-7.

MacAskill, A. F. & J. T. Kittler (2010) Control of mitochondrial transport and localization in neurons. *Trends Cell Biol,* 20**,** 102-12.

Macaskill, A. F., J. E. Rinholm, A. E. Twelvetrees, I. L. Arancibia-Carcamo, J. Muir, A. Fransson, P. Aspenstrom, D. Attwell & J. T. Kittler (2009) Miro1 is a calcium sensor for glutamate receptor-dependent localization of mitochondria at synapses. *Neuron,* 61**,** 541-55.

Maddocks, O. D. & K. H. Vousden (2011) Metabolic regulation by p53. *J Mol Med (Berl),* 89**,** 237-45.

Majewski, N., V. Nogueira, R. B. Robey & N. Hay (2004) Akt inhibits apoptosis downstream of BID cleavage via a glucose-dependent mechanism involving mitochondrial hexokinases. *Molecular and cellular biology,* 24**,** 730-740.

Mantovani, A., T. Schioppa, C. Porta, P. Allavena & A. Sica (2006) Role of tumor-associated macrophages in tumor progression and invasion. *Cancer Metastasis Rev,* 25**,** 315-22.

Margolin, D. A., T. Myers, X. Zhang, D. M. Bertoni, B. A. Reuter, I. Obokhare, T. Borgovan, C. Grimes, H. Green, T. Driscoll, C. G. Lee, N. K. Davis & L. Li (2015) The critical roles of tumor-initiating cells and the lymph node stromal microenvironment in human colorectal cancer extranodal metastasis using a unique humanized orthotopic mouse model. *FASEB J,* 29**,** 3571-81.

Mathupala, S. P., Y. H. Ko & P. L. Pedersen (2006) Hexokinase II: cancer's double-edged sword acting as both facilitator and gatekeeper of malignancy when bound to mitochondria. *Oncogene,* 25**,** 4777-86.

Milne, K., M. Köbel, S. E. Kalloger, R. O. Barnes, D. Gao, C. B. Gilks, P. H. Watson & B. H. Nelson (2009) Systematic analysis of immune infiltrates in high-grade serous ovarian cancer reveals CD20, FoxP3 and TIA-1 as positive prognostic factors. *PLoS One,* 4**,** e6412.

Mishra, P. & D. C. Chan (2014) Mitochondrial dynamics and inheritance during cell division, development and disease. *Nature reviews. Molecular cell biology,* 15**,** 634-646.

Mishra, P. J., P. J. Mishra, R. Humeniuk, D. J. Medina, G. Alexe, J. P. Mesirov, S. Ganesan, J. W. Glod & D. Banerjee (2008) Carcinoma-associated fibroblast-like differentiation of human mesenchymal stem cells. *Cancer research,* 68**,** 4331-4339.

Mittal, K., J. Ebos & B. Rini (2014) Angiogenesis and the tumor microenvironment: vascular endothelial growth factor and beyond. *Semin Oncol,* 41**,** 235-51.

Mueller, M. M. & N. E. Fusenig (2004) Friends or foes - bipolar effects of the tumour stroma in cancer. *Nat Rev Cancer,* 4**,** 839-49.

Murdoch, C., A. Giannoudis & C. E. Lewis (2004) Mechanisms regulating the recruitment of macrophages into hypoxic areas of tumors and other ischemic tissues. *Blood,* 104**,** 2224-34.

Mühlethaler-Mottet, A., J. Liberman, K. Ascenção, M. Flahaut, K. Balmas Bourloud, P. Yan, N. Jauquier, N. Gross & J.-M. Joseph (2015) The CXCR4/CXCR7/CXCL12 Axis Is Involved in a Secondary but Complex Control of Neuroblastoma Metastatic Cell Homing. *PloS one,* 10**,** e0125616-e0125616.

Nieman, K. M., H. A. Kenny, C. V. Penicka, A. Ladanyi, R. Buell-Gutbrod, M. R. Zillhardt, I. L. Romero, M. S. Carey, G. B. Mills, G. S. Hotamisligil, S. D. Yamada, M. E. Peter, K. Gwin & E. Lengyel (2011) Adipocytes promote ovarian cancer metastasis and provide energy for rapid tumor growth. *Nat Med,* 17**,** 1498-503.

Niinaka, Y., S. Paku, A. Haga, H. Watanabe & A. Raz (1998) Expression and secretion of neuroleukin/phosphohexose isomerase/maturation factor as autocrine motility factor by tumor cells. *Cancer Res,* 58**,** 2667-74.

Nozawa, H., C. Chiu & D. Hanahan (2006) Infiltrating neutrophils mediate the initial angiogenic switch in a mouse model of multistage carcinogenesis. *Proc Natl Acad Sci U S A,* 103**,** 12493-8.

Nwabo Kamdje, A. H., P. T. Kamga, R. T. Simo, L. Vecchio, P. F. Seke Etet, J. M. Muller, G. Bassi, E. Lukong, R. K. Goel, J. M. Amvene & M. Krampera (2017) Mesenchymal stromal cells' role in tumor microenvironment: involvement of signaling pathways. *Cancer biology & medicine,* 14**,** 129-141.

Nwabo Kamdje, A. H., F. Mosna, F. Bifari, V. Lisi, G. Bassi, G. Malpeli, M. Ricciardi, O. Perbellini, M. T. Scupoli, G. Pizzolo & M. Krampera (2011) Notch-3 and Notch-4 signaling rescue from apoptosis human B-ALL cells in contact with human bone marrow-derived mesenchymal stromal cells. *Blood,* 118**,** 380-9.

Oh, H., S. B. Bradfute, T. D. Gallardo, T. Nakamura, V. Gaussin, Y. Mishina, J. Pocius, L. H. Michael, R. R. Behringer, D. J. Garry, M. L. Entman & M. D. Schneider (2003) Cardiac progenitor cells from adult myocardium: homing, differentiation, and fusion after infarction. *Proc Natl Acad Sci U S A,* 100**,** 12313-8.

Olkhanud, P. B., B. Damdinsuren, M. Bodogai, R. E. Gress, R. Sen, K. Wejksza, E. Malchinkhuu, R. P. Wersto & A. Biragyn (2011) Tumor-evoked regulatory B cells promote breast cancer metastasis by converting resting $CD4^+$ T cells to T-regulatory cells. *Cancer Res,* 71**,** 3505-15.

Onfelt, B., S. Nedvetzki, R. K. Benninger, M. A. Purbhoo, S. Sowinski, A. N. Hume, M. C. Seabra, M. A. Neil, P. M. French & D. M. Davis (2006) Structurally distinct membrane nanotubes between human macrophages support long-distance vesicular traffic or surfing of bacteria. *J Immunol,* 177**,** 8476-83.

Osswald, M., E. Jung, F. Sahm, G. Solecki, V. Venkataramani, J. Blaes, S. Weil, H. Horstmann, B. Wiestler, M. Syed, L. Huang, M. Ratliff, K. Karimian Jazi, F. T. Kurz, T. Schmenger, D. Lemke, M. Gömmel, M. Pauli, Y. Liao, P. Häring, S. Pusch, V. Herl, C. Steinhäuser, D. Krunic, M. Jarahian, H. Miletic, A. S. Berghoff, O. Griesbeck, G. Kalamakis, O. Garaschuk, M. Preusser, S. Weiss, H. Liu, S. Heiland, M. Platten, P. E. Huber, T. Kuner, A. von Deimling, W. Wick & F. Winkler (2015) Brain tumour cells interconnect to a functional and resistant network. *Nature,* 528**,** 93-8.

Osteikoetxea-Molnár, A., E. Szabó-Meleg, E. A. Tóth, Á. Oszvald, E. Izsépi, M. Kremlitzka, B. Biri, L. Nyitray, T. Bozó, P. Németh, M. Kellermayer, M. Nyitrai & J. Matko (2016) The growth determinants and transport properties of tunneling nanotube networks between B lymphocytes. *Cell Mol Life Sci,* 73**,** 4531-4545.

Otsu, K., S. Das, S. D. Houser, S. K. Quadri, S. Bhattacharya & J. Bhattacharya (2009) Concentration-dependent inhibition of angiogenesis by mesenchymal stem cells. *Blood,* 113**,** 4197-4205.

Panasiuk, M., M. Rychłowski, N. Derewońko & K. Bieńkowska-Szewczyk (2018) Tunneling Nanotubes as a Novel Route of Cell-to-Cell Spread of Herpesviruses. *Journal of virology,* 92**,** e00090-18.

Pang, R. W. C. & R. T. P. Poon (2006) Clinical implications of angiogenesis in cancers. *Vascular health and risk management,* 2**,** 97-108.

Park, J. S., L. K. Sharma, H. Li, R. Xiang, D. Holstein, J. Wu, J. Lechleiter, S. L. Naylor, J. J. Deng, J. Lu & Y. Bai (2009) A heteroplasmic, not homoplasmic, mitochondrial DNA mutation promotes tumorigenesis via alteration in reactive oxygen species generation and apoptosis. *Human molecular genetics,* 18**,** 1578-1589.

Pasquier, J., B. S. Guerrouahen, H. Al Thawadi, P. Ghiabi, M. Maleki, N. Abu-Kaoud, A. Jacob, M. Mirshahi, L. Galas, S. Rafii, F. Le Foll & A. Rafii (2013) Preferential transfer of mitochondria from endothelial to cancer cells through tunneling nanotubes modulates chemoresistance. *Journal of translational medicine,* 11**,** 94-94.

Pastorino, J. G. & J. B. Hoek (2003) Hexokinase II: the integration of energy metabolism and control of apoptosis. *Curr Med Chem,* 10**,** 1535-51.

Pastorino, J. G., N. Shulga & J. B. Hoek (2002) Mitochondrial binding of hexokinase II inhibits Bax-induced cytochrome c release and apoptosis. *J Biol Chem,* 277**,** 7610-8.

Pavlova, N. N. & C. B. Thompson (2016) The Emerging Hallmarks of Cancer Metabolism. *Cell Metab,* 23**,** 27-47.

Payne, B. A. I., I. J. Wilson, P. Yu-Wai-Man, J. Coxhead, D. Deehan, R. Horvath, R. W. Taylor, D. C. Samuels, M. Santibanez-Koref & P. F. Chinnery (2013) Universal heteroplasmy of human mitochondrial DNA. *Human molecular genetics,* 22**,** 384-390.

Peters, D. T., L. Kay, J. Eswaran, J. H. Lakey & M. Soundararajan (2018) Human Miro Proteins Act as NTP Hydrolases through a Novel, Non-Canonical Catalytic Mechanism. *International journal of molecular sciences,* 19**,** 3839.

Phinney, D. G., M. Di Giuseppe, J. Njah, E. Sala, S. Shiva, C. M. St Croix, D. B. Stolz, S. C. Watkins, Y. P. Di, G. D. Leikauf, J. Kolls, D. W. H. Riches, G. Deiuliis, N. Kaminski, S. V. Boregowda, D. H. McKenna & L. A. Ortiz (2015) Mesenchymal stem cells use extracellular vesicles to outsource mitophagy and shuttle microRNAs. *Nature communications,* 6**,** 8472-8472.

Plotnikov, E. Y., T. G. Khryapenkova, S. I. Galkina, G. T. Sukhikh & D. B. Zorov (2010) Cytoplasm and organelle transfer between mesenchymal multipotent stromal cells and renal tubular cells in co-culture. *Exp Cell Res,* 316**,** 2447-55.

Plotnikov, E. Y., T. G. Khryapenkova, A. K. Vasileva, M. V. Marey, S. I. Galkina, N. K. Isaev, E. V. Sheval, V. Y. Polyakov, G. T. Sukhikh & D. B. Zorov (2008) Cell-to-cell cross-talk between mesenchymal stem cells and cardiomyocytes in co-culture. *J Cell Mol Med,* 12**,** 1622-31.

Pollard, J. W. (2004) Tumour-educated macrophages promote tumour progression and metastasis. *Nat Rev Cancer,* 4**,** 71-8.

Porta, C., A. Sica & E. Riboldi (2018) Tumor-associated myeloid cells: new understandings on their metabolic regulation and their influence in cancer immunotherapy. *FEBS J,* 285**,** 717-733.

Prockop, D. J., C. A. Gregory & J. L. Spees (2003) One strategy for cell and gene therapy: harnessing the power of adult stem cells to repair tissues. *Proceedings of the National Academy of Sciences of the United States of America,* 100 Suppl 1**,** 11917-11923.

Pusapati, R. V., A. Daemen, C. Wilson, W. Sandoval, M. Gao, B. Haley, A. R. Baudy, G. Hatzivassiliou, M. Evangelista & J. Settleman (2016) mTORC1-Dependent Metabolic Reprogramming Underlies Escape from Glycolysis Addiction in Cancer Cells. *Cancer Cell,* 29**,** 548-562.

Qian, B.-Z. & J. W. Pollard (2010) Macrophage diversity enhances tumor progression and metastasis. *Cell,* 141**,** 39-51.

Qin, Z., G. Richter, T. Schüler, S. Ibe, X. Cao & T. Blankenstein (1998) B cells inhibit induction of T cell-dependent tumor immunity. *Nat Med,* 4**,** 627-30.

Rathmell, J. C., C. J. Fox, D. R. Plas, P. S. Hammerman, R. M. Cinalli & C. B. Thompson (2003) Akt-directed glucose metabolism can prevent Bax conformation change and promote growth factor-independent survival. *Molecular and cellular biology,* 23**,** 7315-7328.

Rebbeck, C. A., A. M. Leroi & A. Burt (2011) Mitochondrial capture by a transmissible cancer. *Science,* 331**,** 303.

Resnik, N., T. Prezelj, G. M. R. De Luca, E. Manders, R. Polishchuk, P. Veranič & M. E. Kreft (2018) Helical organization of microtubules occurs in a minority of tunneling membrane nanotubes in normal and cancer urothelial cells. *Scientific reports,* 8**,** 17133-17133.

Rogers, R. S. & J. Bhattacharya (2013) When cells become organelle donors. *Physiology (Bethesda),* 28**,** 414-22.

Romero-Brey, I. & R. Bartenschlager (2015) Viral Infection at High Magnification: 3D Electron Microscopy Methods to Analyze the Architecture of Infected Cells. *Viruses,* 7**,** 6316-6345.

Rustom, A. (2016) The missing link: does tunnelling nanotube-based supercellularity provide a new understanding of chronic and lifestyle diseases? *Open biology,* 6**,** 160057.

Rustom, A., R. Saffrich, I. Markovic, P. Walther & H. H. Gerdes (2004) Nanotubular highways for intercellular organelle transport. *Science,* 303**,** 1007-10.

Saotome, M., D. Safiulina, G. Szabadkai, S. Das, A. Fransson, P. Aspenstrom, R. Rizzuto & G. Hajnóczky (2008) Bidirectional Ca2+-dependent control of mitochondrial dynamics by the Miro GTPase. *Proc Natl Acad Sci U S A,* 105**,** 20728-33.

Sarvaria, A., J. A. Madrigal & A. Saudemont (2017) B cell regulation in cancer and anti-tumor immunity. *Cellular & molecular immunology,* 14**,** 662-674.

Schioppa, T., R. Moore, R. G. Thompson, E. C. Rosser, H. Kulbe, S. Nedospasov, C. Mauri, L. M. Coussens & F. R. Balkwill (2011) B regulatory cells and the tumor-promoting actions of TNF-α during squamous carcinogenesis. *Proceedings of the National Academy of Sciences of the United States of America,* 108**,** 10662-10667.

Secchiero, P., S. Zorzet, C. Tripodo, F. Corallini, E. Melloni, L. Caruso, R. Bosco, S. Ingrao, B. Zavan & G. Zauli (2010) Human bone marrow mesenchymal stem cells display anti-cancer activity in SCID mice bearing disseminated non-Hodgkin's lymphoma xenografts. *PloS one,* 5**,** e11140-e11140.

Semenza, G. L. (2013) HIF-1 mediates metabolic responses to intratumoral hypoxia and oncogenic mutations. *The Journal of clinical investigation,* 123**,** 3664-3671.

Shackelford, D. B. & R. J. Shaw (2009) The LKB1-AMPK pathway: metabolism and growth control in tumour suppression. *Nat Rev Cancer,* 9**,** 563-75.

Sinha, P., V. K. Clements, S. K. Bunt, S. M. Albelda & S. Ostrand-Rosenberg (2007) Cross-talk between myeloid-derived suppressor cells and macrophages subverts tumor immunity toward a type 2 response. *J Immunol,* 179**,** 977-83.

Sinha, P., M. N. Islam, S. Bhattacharya & J. Bhattacharya (2016) Intercellular mitochondrial transfer: bioenergetic crosstalk between cells. *Curr Opin Genet Dev,* 38**,** 97-101.

Smith, I. F., J. Shuai & I. Parker (2011) Active generation and propagation of Ca2+ signals within tunneling membrane nanotubes. *Biophys J,* 100**,** L37-9.

Som, P., H. L. Atkins, D. Bandoypadhyay, J. S. Fowler, R. R. MacGregor, K. Matsui, Z. H. Oster, D. F. Sacker, C. Y. Shiue, H. Turner, C. N. Wan, A. P. Wolf & S. V. Zabinski (1980) A fluorinated glucose analog, 2-fluoro-2-deoxy-D-glucose (F-18): nontoxic tracer for rapid tumor detection. *J Nucl Med,* 21**,** 670-5.

Spees, J. L., S. D. Olson, M. J. Whitney & D. J. Prockop (2006) Mitochondrial transfer between cells can rescue aerobic respiration. *Proc Natl Acad Sci U S A,* 103**,** 1283-8.

Strakova, A., M. Ní Leathlobhair, G. D. Wang, T. T. Yin, I. Airikkala-Otter, J. L. Allen, K. M. Allum, L. Bansse-Issa, J. L. Bisson, A. Castillo Domracheva, K. F. de Castro, A. M. Corrigan, H. R. Cran, J. T. Crawford, S. M. Cutter, L. Delgadillo Keenan, E. M. Donelan, I. A. Faramade, E. Flores Reynoso, E. Fotopoulou, S. N. Fruean, F. Gallardo-Arrieta, O. Glebova, R. F. Häfelin Manrique, J. J. Henriques, N. Ignatenko, D. Koenig, M. Lanza-Perea, R. Lobetti, A. M. Lopez Quintana, T. Losfelt, G. Marino, I. Martincorena, S. Martínez Castañeda, M. F. Martínez-López, M. Meyer, B. Nakanwagi, A. B. De Nardi, W. Neunzig, S. J. Nixon, M. M. Onsare, A. Ortega-Pacheco, M. C. Peleteiro, R. J. Pye, J. F. Reece, J. Rojas Gutierrez, H. Sadia, S. K. Schmeling, O. Shamanova, R. K. Ssuna, A. E. Steenland-Smit, A. Svitich, I. Thoya Ngoka, B. A. Viţălaru, A. P. de Vos, J. P. de Vos, O. Walkinton, D. C. Wedge, A. S. Wehrle-Martinez, M. G. van der Wel, S. A. Widdowson & E. P. Murchison (2016) Mitochondrial genetic diversity, selection and recombination in a canine transmissible cancer. *Elife,* 5.

Subramanian, A. & D. M. Miller (2000) Structural analysis of alpha-enolase. Mapping the functional domains involved in down-regulation of the c-myc protooncogene. *J Biol Chem,* 275**,** 5958-65.

Sugihara, H., T. Ishimoto, T. Yasuda, D. Izumi, K. Eto, H. Sawayama, K. Miyake, J. Kurashige, Y. Imamura, Y. Hiyoshi, M. Iwatsuki, S. Iwagami, Y. Baba, Y. Sakamoto, Y. Miyamoto, N. Yoshida, M. Watanabe, H. Takamori & H. Baba (2015) Cancer-associated fibroblast-derived CXCL12 causes tumor progression in adenocarcinoma of the esophagogastric junction. *Med Oncol,* 32**,** 618.

Sáenz-de-Santa-María, I., C. Bernardo-Castiñeira, E. Enciso, I. García-Moreno, J. L. Chiara, C. Suarez & M.-D. Chiara (2017) Control of long-distance cell-to-cell communication and autophagosome transfer in squamous cell carcinoma via tunneling nanotubes. *Oncotarget,* 8**,** 20939-20960.

Tan, A. S., J. W. Baty, L. F. Dong, A. Bezawork-Geleta, B. Endaya, J. Goodwin, M. Bajzikova, J. Kovarova, M. Peterka, B. Yan, E. A. Pesdar, M. Sobol, A. Filimonenko, S. Stuart, M. Vondrusova, K. Kluckova, K. Sachaphibulkij, J. Rohlena, P. Hozak, J. Truksa, D. Eccles, L. M. Haupt, L. R. Griffiths, J. Neuzil & M. V. Berridge (2015) Mitochondrial genome acquisition restores respiratory function and tumorigenic potential of cancer cells without mitochondrial DNA. *Cell Metab,* 21**,** 81-94.

Tomlinson, I. P., N. A. Alam, A. J. Rowan, E. Barclay, E. E. Jaeger, D. Kelsell, I. Leigh, P. Gorman, H. Lamlum, S. Rahman, R. R. Roylance, S. Olpin, S. Bevan, K. Barker, N. Hearle, R. S. Houlston, M. Kiuru, R. Lehtonen, A. Karhu, S. Vilkki, P. Laiho, C. Eklund, O. Vierimaa, K. Aittomäki, M. Hietala, P. Sistonen, A. Paetau, R. Salovaara, R. Herva, V. Launonen, L. A. Aaltonen & M. L. Consortium (2002) Germline mutations in FH predispose to dominantly inherited uterine fibroids, skin leiomyomata and papillary renal cell cancer. *Nat Genet,* 30**,** 406-10.

Torralba, D., F. Baixauli & F. Sánchez-Madrid (2016) Mitochondria Know No Boundaries: Mechanisms and Functions of Intercellular Mitochondrial Transfer. *Front Cell Dev Biol,* 4**,** 107.

Tseng, L. M., P. H. Yin, C. W. Chi, C. Y. Hsu, C. W. Wu, L. M. Lee, Y. H. Wei & H. C. Lee (2006) Mitochondrial DNA mutations and mitochondrial DNA depletion in breast cancer. *Genes Chromosomes Cancer,* 45**,** 629-38.

Vander Heiden, M. G., L. C. Cantley & C. B. Thompson (2009) Understanding the Warburg effect: the metabolic requirements of cell proliferation. *Science,* 324**,** 1029-33.

Veranic, P., M. Lokar, G. J. Schütz, J. Weghuber, S. Wieser, H. Hägerstrand, V. Kralj-Iglic & A. Iglic (2008) Different types of cell-to-cell connections mediated by nanotubular structures. *Biophysical journal,* 95**,** 4416-4425.

Victoria, G. S. & C. Zurzolo (2017) The spread of prion-like proteins by lysosomes and tunneling nanotubes: Implications for neurodegenerative diseases. *The Journal of cell biology,* 216**,** 2633-2644.

Vignais, M.-L., A. Caicedo, J.-M. Brondello & C. Jorgensen (2017) Cell Connections by Tunneling Nanotubes: Effects of Mitochondrial Trafficking on Target Cell Metabolism, Homeostasis, and Response to Therapy. *Stem cells international,* 2017**,** 6917941-6917941.

Vitale, I., L. Galluzzi, L. Senovilla, A. Criollo, M. Jemaà, M. Castedo & G. Kroemer (2011) Illicit survival of cancer cells during polyploidization and depolyploidization. *Cell death and differentiation,* 18**,** 1403-1413.

Vona-Davis, L. & L. F. Gibson (2013) Adipocytes as a critical component of the tumor microenvironment. *Leukemia research,* 37**,** 483-484.

Wallace, D. C. (2005) A mitochondrial paradigm of metabolic and degenerative diseases, aging, and cancer: a dawn for evolutionary medicine. *Annu Rev Genet,* 39**,** 359-407.

--- (2013) A mitochondrial bioenergetic etiology of disease. *The Journal of clinical investigation,* 123**,** 1405-1412.

Wang, M. L., C. M. Pan, S. H. Chiou, W. H. Chen, H. Y. Chang, O. K. Lee, H. S. Hsu & C. W. Wu (2012) Oncostatin m modulates the mesenchymal-epithelial transition of lung adenocarcinoma cells by a mesenchymal stem cell-mediated paracrine effect. *Cancer Res,* 72**,** 6051-64.

Wang, X. & H. H. Gerdes (2015a) Transfer of mitochondria via tunneling nanotubes rescues apoptotic PC12 cells. *Cell death and differentiation,* 22**,** 1181-1191.

--- (2015b) Transfer of mitochondria via tunneling nanotubes rescues apoptotic PC12 cells. *Cell Death Differ,* 22**,** 1181-91.

Wang, X. & T. L. Schwarz (2009) The mechanism of Ca2+ -dependent regulation of kinesin-mediated mitochondrial motility. *Cell,* 136**,** 163-74.

Wang, Y., J. Cui, X. Sun & Y. Zhang (2011) Tunneling-nanotube development in astrocytes depends on p53 activation. *Cell Death Differ,* 18**,** 732-42.

Ward, P. S. & C. B. Thompson (2012) Metabolic reprogramming: a cancer hallmark even warburg did not anticipate. *Cancer cell,* 21**,** 297-308.

Watanabe, H., K. Takehana, M. Date, T. Shinozaki & A. Raz (1996) Tumor cell autocrine motility factor is the neuroleukin/phosphohexose isomerase polypeptide. *Cancer Res,* 56**,** 2960-3.

Webber, E., L. Li & L. S. Chin (2008) Hypertonia-associated protein Trak1 is a novel regulator of endosome-to-lysosome trafficking. *J Mol Biol,* 382**,** 638-51.

Wei, H.-J., J. A. Nickoloff, W.-H. Chen, H.-Y. Liu, W.-C. Lo, Y.-T. Chang, P.-C. Yang, C.-W. Wu, D. F. Williams, J. G. Gelovani & W.-P. Deng (2014) FOXF1 mediates mesenchymal stem cell fusion-induced reprogramming of lung cancer cells. *Oncotarget,* 5**,** 9514-9529.

Weinberg, F., R. Hamanaka, W. W. Wheaton, S. Weinberg, J. Joseph, M. Lopez, B. Kalyanaraman, G. M. Mutlu, G. R. Budinger & N. S. Chandel (2010) Mitochondrial metabolism and ROS generation are essential for Kras-mediated tumorigenicity. *Proc Natl Acad Sci U S A,* 107**,** 8788-93.

White, J. R., R. A. Harris, S. R. Lee, M. H. Craigon, K. Binley, T. Price, G. L. Beard, C. R. Mundy & S. Naylor (2004) Genetic amplification of the transcriptional response to hypoxia as a novel means of identifying regulators of angiogenesis. *Genomics,* 83**,** 1-8.

Wittig, D., X. Wang, C. Walter, H. H. Gerdes, R. H. Funk & C. Roehlecke (2012) Multi-level communication of human retinal pigment epithelial cells via tunneling nanotubes. *PLoS One,* 7**,** e33195.

Yanagawa, T., T. Funasaka, S. Tsutsumi, H. Watanabe & A. Raz (2004) Novel roles of the autocrine motility factor/phosphoglucose isomerase in tumor malignancy. *Endocr Relat Cancer,* 11**,** 749-59.

Yang, Y., A. Otte & R. Hass (2015) Human mesenchymal stroma/stem cells exchange membrane proteins and alter functionality during interaction with different tumor cell lines. *Stem cells and development,* 24**,** 1205-1222.

Yasuda, K., A. Khandare, L. Burianovskyy, S. Maruyama, F. Zhang, A. Nasjletti & M. S. Goligorsky (2011) Tunneling nanotubes mediate rescue of prematurely senescent endothelial cells by endothelial progenitors: exchange of lysosomal pool. *Aging (Albany NY),* 3**,** 597-608.

Yi, M., D. Weaver & G. Hajnóczky (2004) Control of mitochondrial motility and distribution by the calcium signal: a homeostatic circuit. *The Journal of cell biology,* 167**,** 661-672.

Yu, Y., C. H. Xiao, L. D. Tan, Q. S. Wang, X. Q. Li & Y. M. Feng (2014) Cancer-associated fibroblasts induce epithelial-mesenchymal transition of breast cancer cells through paracrine TGF-β signalling. *British journal of cancer,* 110**,** 724-732.

Zhan, P., Y. Wang, S. Zhao, C. Liu, M. Wen, J. H. Mao, G. Wei & P. Zhang (2015) FBXW7 negatively regulates ENO1 expression and function in colorectal cancer. *Lab Invest,* 95**,** 995-1004.

Zhang, B., M. Li, T. McDonald, T. L. Holyoake, R. T. Moon, D. Campana, L. Shultz & R. Bhatia (2013a) Microenvironmental protection of CML stem and progenitor cells from tyrosine kinase inhibitors through N-cadherin and Wnt-β-catenin signaling. *Blood,* 121**,** 1824-1838.

Zhang, C., J. Liu, Y. Liang, R. Wu, Y. Zhao, X. Hong, M. Lin, H. Yu, L. Liu, A. J. Levine, W. Hu & Z. Feng (2013b) Tumour-associated mutant p53 drives the Warburg effect. *Nature communications,* 4**,** 2935-2935.

Zheng, J. (2012) Energy metabolism of cancer: Glycolysis versus oxidative phosphorylation (Review). *Oncol Lett,* 4**,** 1151-1157.

Zheng, L., R. G. Roeder & Y. Luo (2003) S phase activation of the histone H2B promoter by OCA-S, a coactivator complex that contains GAPDH as a key component. *Cell,* 114**,** 255-66.

Zumsteg, A. & G. Christofori (2009) Corrupt policemen: inflammatory cells promote tumor angiogenesis. *Curr Opin Oncol,* 21**,** 60-70.

pTagBFP-H2B vector Data sheet (pdf)
http://evrogen.com/vector-descriptions/pTagBFP-H2B/pTagBFP-H2B.pdf

Scheme of photolitography

http://biomechanicalregulation-lab.org/photolithography/